PhD-FSTC-2016-20
The Faculty of Sciences, Technology and Communication

DISSERTATION

Defense held on 14/06/2016 in Luxembourg

to obtain the degree of

DOCTEUR DE L'UNIVERSITÉ DU LUXEMBOURG

EN SCIENCES de L'INGÉNIEUR

by

Surena NESHVAD
Born on 22nd February 1976 in city of Teheran, (Iran)

TOPOLOGY AND PARAMETER ESTIMATION IN POWER SYSTEMS THROUGH INVERTER BASED BROADBAND STIMULATIONS

Dissertation defense committee

Dr Jürgen Sachau, dissertation supervisor
Professor, Université du Luxembourg

Dr Stijn Stevens
Technical manager and system architect, SMA Solar Technology, Niestetal, Germany

Dr Thomas Engel, Chairman
Professor, Université du Luxembourg

Dr Markus Jostock
Head of Information Technology, Arend Prozessautomation, Wittlich, Germany

Dr Symeon Chatzinotas, Vice Chairman
Research Scientist, Université du Luxembourg

University of Luxembourg

Doctoral Thesis

Topology and Parameter Estimation in Power Systems through Inverter Based Broadband Stimulations

Author:
Surena Neshvad

Supervisor:
Dr. Prof. Jürgen Sachau

A thesis submitted in fulfilment of the requirements for the degree of Doctor of Philosophy

in

Interdisciplinary Centre for Security, Reliability and Trust

June 2016

Declaration of Authorship

I, Surena Neshvad, declare that this thesis titled, 'Topology and Parameter Estimation in Power Systems through Inverter Based Broadband Stimulations' and the work presented in it are my own. I confirm that:

- This work was done wholly or mainly while in candidature for a research degree at this University.
- Where any part of this thesis has previously been submitted for a degree or any other qualification at this University or any other institution, this has been clearly stated.
- Where I have consulted the published work of others, this is always clearly attributed.
- Where I have quoted from the work of others, the source is always given. With the exception of such quotations, this thesis is entirely my own work.
- I have acknowledged all main sources of help.
- Where the thesis is based on work done by myself jointly with others, I have made clear exactly what was done by others and what I have contributed myself.

Signed: _____

Date: _____

UNIVERSITY OF LUXEMBOURG

Abstract

Faculty Name
Interdisciplinary Centre for Security, Reliability and Trust

Doctor of Philosophy

Topology and Parameter Estimation in Power Systems through Inverter Based Broadband Stimulations

by Surena NESHVAD

During the last decade, a substantial growth in renewable, distributed energy production has been observed in industrial countries. This phenomenon, coupled with the adoption of open energy markets has significantly complicated the powerflows on the distribution network, requiring advanced and intelligent system monitoring in order to optimize the efficiency, quality and reliability of the system.

This thesis proposes a solution several power network challenges encountered with increasing Distributed Generation (DG) penetration. The three problems that are addressed are islanding detection, online transmission line parameter identification and system topology identification. These tasks are performed by requesting the DGs to provide ancillary services to the network operator. A novel and intelligent method has been proposed for reprogramming the DGs Pulse Width Modulator, requesting each DG to inject a uniquely coded Pseudo-Random Binary Sequence along with the fundamental.

Islanding detection is obtained by measuring the equivalent Thevenin impedance at the inverters Point of Common Coupling, while system characterization is obtained by measuring the induced current frequencies at various locations in the grid. To process and evaluate the measured signals, a novel Weighed Least-Squares aggregation method is developed, through which measurements are combined and correlated in order to obtain an accurate snapshot of the power network parameters.

...

Acknowledgements

This work was conducted at the "Interdisciplinary Centre for Security, Reliability and Trust" (SnT) at the University of Luxembourg in collaboration with CREOS S.A., the Luxemburgish utility provider. It is supported by the National Research Fund, Luxembourg, under AFR Grant 4881120.

I would like to thank the University of Luxembourg's Interdisciplinary Center for Security, Reliability and Trust (SnT) who provided me the opportunity to conduct this research. In particular, I would like to thank my supervisor, Professor Jürgen Sachau, chair of system and control engineering, whose knowledge and innovative ideas had a significant impact on the quality of this work. I would also like to express my gratitude my other co-supervisors and members of my Dissertation Supervisory Committee for their kindness support. Thank you Dr. Symeon Chatzinotas and Professor Thomas Engel, I consider myself very lucky to have had the chance to research in the same faculty as you.

Additional support came from the Luxembourgish Electric Power utility provider CREOS. In particular, I am very thankful to Mr Nico Kaufmann for his support and guidance during this thesis, as well as Patrick Thill for the expertise that he provided and the depth of knowledge that he shared about CREOS's power system concepts.

Finally, I would like to express my gratitude to the Fonds National de la Recherche Luxembourgeoise (FNR) for having trusted in me and for funding this research. I am very grateful for the provided opportunity.

...

Contents

List of Figures

List of Tables

Abbreviations

VSI	**V**oltage **S**ource **I**nverter
DG	**D**istributed **G**enerator
PCC	**P**oint of **C**ommon **C**oupling
PWM	**P**ulse **W**idth **M**odulation
PRBS	**P**seudo **R**andom **B**inary **S**equence
LFSR	**L**inear **F**eedback **S**hift **R**egister
DFT	**D**iscrete **F**ourier **T**ransform
PMU	**P**hasor **M**easurement **U**nit
SNR	**S**ignal to **N**oise **R**atio
ICT	**I**nformation and **C**ommunication **T**echnology
FRT	**F**ault **R**ight **T**hrough
IGBT	**I**nsulated **G**ate **B**ipoar **T**ransisitor
THD	**T**otal **H**armonic **D**istortion
MLE	**M**aximum **L**ikelihood **E**stimation
WLS	**W**eighed **L**east **S**quares
PDF	**P**robability **D**ensitiy **F**unction
HV	**H**igh **V**oltage
MV	**M**edium **V**oltage
LV	**L**ow **V**oltage
SIC	**S**uccessive **I**nterference **C**ancellation
EMS	**E**nergy **M**anagement **S**ystem
SE	**S**tate **E**stimation
MLS	**M**aximum **L**ength **S**equence
MM	**M**inimum **M**elting

TC	**T**otal **C**learing
DSP	**D**igital **S**ignal **P**rocessing
ASF	**A**ctive **S**hunt **F**ilter
ROCOF	**R**ate **O**f **C**hange **O**f **F**requency
MOSFET	**M**etal **O**xide **S**emiconductor **F**ield **E**ffect **T**ransistor
SMFS	**M**etal **O**xide **S**emiconductor
PLL	**P**hase **L**ocked **L**oop
GPIC	**G**eneral **P**urpose **I**nverter **C**ontrol
VI	**V**irtual **I**nstrument
DDS	**D**irect **D**igital **S**ynthesis
RMS	**R**oot **M**ean **S**quare
FIFO	**F**irst **I**n **F**irst **O**ut

Dedicated to
Darius, Adrian and Anusha ...

Chapter 1

Introduction

1.1 Background Problem and Defintion

In recent years, a substantial growth in renewable, distributed energy production has been observed. This has had a significant impact on the power system, and its traditional centralized configuration has been challenged. This trend has been stimulated by political regulations to combat global warning, subsidizing energy production by local homeowners and even by larger power plants. Besides, fossil fuels have had substantial price fluctuations, and high petrol prices have spurred the interest and technological development of alternative energy sources [1]. Many other factors have played a role, such as reduction in technology cost, instabilities in oil exporting countries, and also the liberalization of the energy market.

Homeowners in many countries around the world are connecting local energy generators, whose surplus production is being fed to the power network [2]. Medium sized generators have also been connected on the distribution network, even partially funded by the utility providers themselves. For the longest times, the utility providers have had a monopoly on the production and distribution of the electricity, the changes that happened for the aforementioned reasons have induced adjustments in methodologies and business models, and have brought with them a large number of challenges and technical complications to the power system infrastructure.

The power system is composed of three distinct structures. Large power plants that generate the electricity are connected to a high voltage network, that transmits

the energy to substations, which in turn distribute the electricity to the medium voltage network to broad geographical areas, where the load get consumed in or gets forwarded to low voltage networks. The architecture and network infrastructure has been designed with this framework in mind. Due to the development of distributed generation, this paradigm has been challenged. Small and medium sized generators are connected to the distribution network, they are referred to as Distributed Generators (DG). DGs have been used for a long time as backup or emergency energy sources, such as in hospitals. On the other hand, the implementation of modern DGs that are to operate as an integral part of the power system, support grid power and contribute to the daily power generation in conjunction with large power plants makes their role very different and considerably more complicated.

The increasing number of DG and their large variety in modes of operation presents new issues of concern. In the next years, the amount of DG on the network will keep rising and with the drop in technology cost, new markets will become financially available [3]. Thus the power grid of the future will need to be able to cope with this change of paradigm and be able to accommodate them, while providing the reliability and quality that is expected by the customers. The power network will have to operate differently from the current grid. Since the High Voltage (HV) network was meant to accommodate many energy sources, it was designed to be able to withstand all the effects that come with it. This is not the case for the distribution network, which has not been specified with power generation connection as its purpose.

As of now, most distribution networks have a radial structure from the power station, and assume that the powerflow will go only downstream, from the substation to the loads. The architecture, protection mechanism and dimensioning was not designed for power generation, but a small amount of DG can be incorporated, when care is taken of the operation mode of the DG, its dimensioning and energy production [4]. On the other hand, DGs have the ability to improve the general quality of the power transmission through voltage regulation, power quality improvement, and other ancillary services that they can be requested to provide by the utility provider.

The energy market in Europe is being redesigned in order to address this change in paradigm. Areas such as tariffing the DG production, power regulation grid codes and operating standards with the technical issues that arise are being redefined

[5]. DG interconnection standards are currently being developed and implemented by electric standard organizations In Europe and generally all countries around the world.

In making this shift to renewable energy, it is crucial to modernize the distribution network and add features allowing real-time control and monitoring of its relevant components. In fact, compared to the HV network, the visibility of the distribution network is relatively sparse, and having a real-time monitoring of its parameters will permit to adjust the supply, the protection devices and optimize the usage of the distributed generators.

1.2 Distribution Generation Challenges

The distribution grid was not originally designed to accommodate generators. On the other hand the transmission network was elaborated from the ground up to permit bi-directional flows on the lines, and larger amount of wide spread generation units. The initial purpose of the distribution grid was solely distribution, it was supposed receive the energy fro the upstream network and distribute it downstream to the low voltage network and the loads. The architecture, protection mechanisms and voltage control mechanisms, and observability components have been designed with this in mind. Thus the issues caused by DGs are being considered as they are getting connected, and are not based on the traditional paradigm of the power network [6].

The standardizations of DG have been sparse and lagging for a ling time. Particularly, the methods on connection, power quality regulations, fault behavior and tariffing have been solved in each country in a separate and individual manner. Some countries even lack well defined standards for many of the technical issues. While there is a drive for international standardization, the task is confronted with serious setbacks, due to the wide array of implementation, size and technology of DG that exists, coupled with the fact that the distribution network in each country presents itself with a different shape, structure and policies [7]. Thus universal standardization is a very difficult challenge, and this can hinder the quick development and cost reduction through mass production of DG. Nevertheless at a European level grid code guidelines are specified, but many countries have their own specific grid codes that take precedence.

Because of the lack of standardization, many grid operators determine their own rules based on what suits their network best. Thus manufacturers must build equipment that is able to operate with a wide range of specifications, or need to create specific components for each regulatory zone, as long as no unified standard is ratified. This in turn increases component prices and slows down the progress and development of new technologies.

One of the factors that hinders the development of DG is the structure of the power system and the diversity between the individual power systems. The other major setback is due to the fact that in the current utility usage model, the utility provider earns money on energy that is being fed over their lines. Thus a customer with his own DG installation profits form the utility infrastructure by selling his surplus to the network, and reduces his own energy consumption from the utility though his DG production. Therefore, local DGs are a big setback in the current energy business model for the utility providers, many of them trying to discourage homeowners by adding excessive connection fees for DG [8]. Through tariff reforms and subsidies and political intervention in the energy market, this issue is being addressed locally in each country, in order to initiate DG development.

The technical issues involved in extensive DG integration in the distribution grid are numerous. They impact most aspects of power delivery. In fact, DGs can cause power reverse flows on powerlines, thereby disturbing the protection schemes employed. They have an effect on voltage regulation, their impact can be positive since DGs might reduce voltage drop along the feeders, but they might also push the voltage beyond the permitted limits [9]. The fact that many DGs are based on solar and wind causes them to be very volatile and intermittent. They are a big challenge on many aspects of power system management control such as on power flow regulation, short circuit power availability, frequency regulation and voltage stability [10]. DGs also affect power quality by injecting harmonics. They are further increasingly being asked to provide ancillary services and to contribute to harmonic cleansing of the system through harmonics compensation. Finally, they have a serious impact during islanding, since an islanded system with DGs is dangerous, unpredictable, prone to cause extreme damages to the system if it happens without being detected.

1.3 Objective and Research Questions

As distributed generation is gaining importance on the power system, current modes of operations and grid structure are not fully adapted to handle the implementation of large amounts of generators on lower voltage networks. In order to complete the transition to future electricity supply, which will be more distributed and intermittent, the power system operation needs to be modernized, monitored and flexible. Especially the Medium Voltage (MV) and Low Voltage (LV) networks, which have been operating without extensive supervision need to be progressively redesigned [11]. Real-time knowledge of the power system parameters will be a key feature to adapt to the flexibility required, without sacrificing reliability and power quality. The research in this theses focuses on online power system parameter identification on a power network with substantial DG penetration. The work presents a possibility of monitoring the power network continuously by requesting ancillary services from DGs.

The objective in this thesis is online active power system identification, which will be applied to solve several power system problems that are becoming increasingly challenging with the advent energy production in distribution networks.

The first topic covered is islanding [12]. The concept of an island in power systems can be a positive feature, if it is operated intentionally and under control. In this case the island operates as a micro-grid, if the generators inside have the capability of supplying the loads and maintaining a stable frequency. It can also be a dangerous problem scenario to be accounted for if it happens unintentionally[13][14]. In either case it is very important for the grid operator and also for the DGs operating in the grid to be aware of islanding occurrences and react to it. For example DGs operating during line faults can damage standard power system components equipment such as auto-reclosers. They can also be a great danger to maintenance teams if they feed in power when the mains are off. Thus having a reliable and fail-safe method for islanding detection at the DG is a crucial feature. One objective of this thesis is to develop an innovative method that is dependable and which utilizes components already present in inverter based DGs to provide an accurate and reliable islanding detection algorithm.

Secondly, the technique is applied to obtain real-time and online parameters of the powerline. This information can be used by the grid operator to update their Energy Management System (EMS) tools with up-to-date values of line impedances

and obtain more accurate information from tools such as State Estimation (SE). The broadband characterization obtained will allow localization of resonance frequencies in the power network, and can also be applied for line temperature estimation, which in turn would allow advanced power systems control such as dynamic thermal rating [15]. The broad spectrum line parameter determination could be used for additional services to the power grid. For instance the reduction in power quality of the distribution network could be offset by requesting the DGs to compensate some of the harmonics and cleanse the harmonic pollution [16]. This ancillary service has been studied extensively and would be an important application of the proposed tool.

Finally, the proposed method is generalized in order to obtain a realtime snaphot of the distribution network while it is operational. The objective is the development of a monitoring system that will allow a smart management of the distribution network. The tool created in this research is obtained by expanding and reusing the DG based islanding detection mechanism developed in Chapter 4. This will allow online and continuous characterization of the power network. This in turn will enable the utility provider to have up to date knowledge of the status of its network. Line parameters and line capacities can be adapted continuously based on measurements [17]. Power system configuration alterations such as DG disconnecting, switch setting changes and other spurious modifications such as faults on the network can be detected, localized and diagnosed immediately.

1.4 Approach

To solve the aforementioned problems, the method developed in this research involves DG based ancillary services. It is assumed that in a network with deep DG penetration, DGs will be present on most feeders of the distribution network, and that in the future a large percentage of them will be inverter based. The Pulse Width Modulator (PWM) of the inverter switches transistors and produces a sine wave matching the fundamental of the grid frequency in order to feed in power. PWM and power transistors have an almost limitless capability for signal generation. This feature has been employed for other applications e.g. for harmonic compensation [18]. Reprogramming the Pulse Width Modulator drivers will allow us to create pilot signals at the DG, and overlay them on the fundamental while power is being fed. The stimulation signals employed in this thesis are Pseudo

Random Binary Sequences (PRBS) [19]. These sequences have been used for many years in system identification [20] and they combine spectral characteristics and correlation properties that allow them to efficiently characterize the system under study and be detected within large disturbances and interferences [21].

Injecting voltage signals and measuring the resulting broadband current allows the assessment of the impedance at the Point of Common Coupling (PCC). This is a very reliable islanding indicator. In fact, the inter-harmonics injected will not be influenced by powerflows on the power system, and the impedance measured on non-harmonic frequencies can be interpolated to the fundamental. The current signals can subsequently be detected and measured at the substation and at nearby DGs. A unique coded PRBS is allocated to each "participating" inverter on the distribution network. When the receivers detect the predefined code, they know which inverter it is originating from and taking this information into account, and taking the distortions of the received signal into account, they can infer the characteristics of the propagation path of the signal. The orthogonality of the PRBS sequences enables an efficient interference filtering and thus allows many concurrent injection to be present on the grid simultaneously.

The method of implementation, the employed architectures and algorithms will be detailed in the next Chapters.

1.5 List of Scientific Publications associated with this Thesis

1. S. Neshvad, S. Chatzinotas, J. Sachau, 'Online Determination of Grid Impedance Spectrum through Pseudo-Random Excitation of a Pulse Width Modulator', International Conference on Renewable Energies and Power Quality, April 2014 [22]

2. S. Neshvad, S. Chatzinotas, J. Sachau, 'Distribution Grid Monitoring through Pilot Injection and Successive Interference Cancellation', International Association for Energy Economics, October 2014 [23]

3. S. Neshvad, S. Chatzinotas, J. Sachau, 'Wideband Identification of Power Network Parameters Using Pseudo-Random Binary Sequences on Power Inverters', IEEE Transactions on Smart Grid, September 2015 [24]

4. U. Tewari, S. Neshvad, D. Goldbach, J. Sachau, 'Verification and Implementation of Pseudo-Random-Binary-Sequences for Online Determination of Grid Impedance Spectrum', International Conference on Renewable Energies and Power Quality, March 2015 [25]

5. S. Neshvad, H. Margossian, J. Sachau, Topology and Parameter Estimation in Power Systems through Inverter Based Broadband Stimulations, IET Generation, Transmission and Distribution, (accepted, waiting for publication) [26]

6. S. Neshvad, H. Margossian, J. Sachau, 'Estimation of Power Grid Topology Parameters through Pilot Signals', International Conference on Renewable Energies and Power Quality, Mai 2016 [27]

7. H. Margossian, S. Neshvad, J. Sachau, 'Adaptive Protection with Distribution Network Configuration and Distributed Generation Status Estimation', IEEE Transaction on Power Delivery, (under review)

1.6 Industrial Partner and Funding Institution

The research in this thesis has been performed within the framework with an AFR grant from FNR, number 445076. The project is pursued in collaboration with CREOS, the Luxembourgish utility provider, which were kind enough to provide data infrastructure and help for the process of this research.

1.7 Thesis Outline

Chapter 1: Introduction

The topic research in this thesis is power system parameter identification. Active identification methods are studied, and their application to an array of power system monitoring tools, from islanding detection to dynamic thermal rating are considered. Figure 1.1 shows the different areas of research covered. The dashed squares represent topics that are not treated, but that could be the topic of further research, since they could greatly benefit or be implemented based on the methods developed in this thesis.

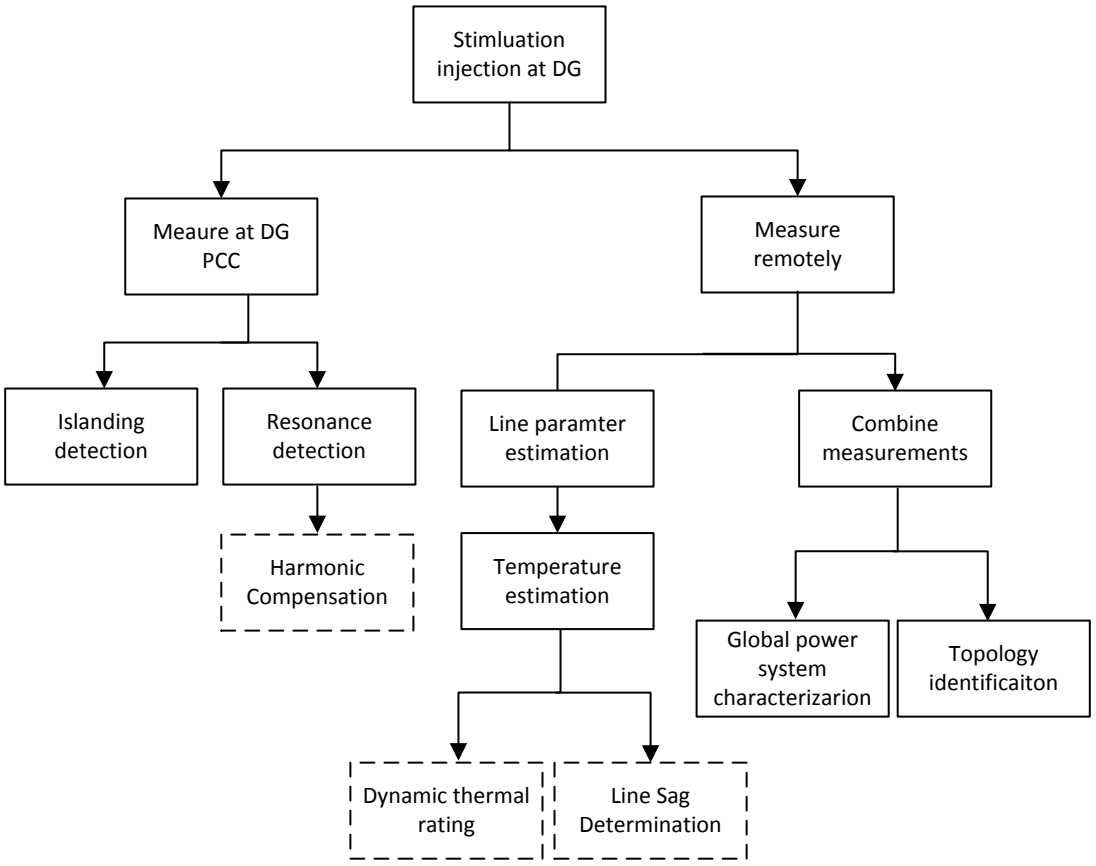

FIGURE 1.1: Thesis Outline

Chapter 2: Components of the Distribution Network

In this Section, an overview of main power system components in the distribution network is given, with emphasis on components relevant to the research in thesis. As a such, Inverter based grid-tie DG architecture and the properties and modeling of transmission lines are analyzed in detail.

Chapter 3: Pseudo-Random Binary Sequence Injection on Inverter

A description of PRBS sequences is given and their typical application in communications and system identification presented. Their properties and their implementation are depicted. Finally, several methods are proposed for injecting them through an inverter by overlapping them on the fundamental generated by

the PWM. The method exhibiting the best properties is then employed in further Chapters in order to provide power system ancillary services.

Chapter 4: Islanding Detection

An overview of islanding detection methods in the state-of-the-art is provided, before the proposed method based on injection of PRBS sequences is elaborated. The advantages and qualities of the method are highlighted, and simulations with realistic settings are performed.

Chapter 5: Power Line Parameter Identification

The research in this Chapter re-utilizes the generated stimulations for islanding detection and measures the generated current-harmonics at the substation. This method allows us to estimate power line parameters and the obtained information could be used for temperature estimation, harmonic power compensation on the powerline. An enhancement of the proposed algorithm based on Successive Interference Cancellation (SIC) is studied subsequently. This algorithm improves the obtained results when multiple current signals are present by reducing the near-far effect created when strong and weak signals cohabit.

Chapter 6: Power System Parameter Identification

In Chapter 6, a sub-grid containing several DGs emitting each a unique PRBS code is studied. The injection of multiple orthogonal patterns, and their reception at various locations in the grid is used for a complete parameter and topology identification of the sub-grid.

Chapter 7: Summary, Contributions and Recommendations

The outcomes of the research are summarized and conclusions on the result of the research are drawn. Recommendations for future research are given in order to improve the accuracy of the results, broaden the impact of the method to cover more services and validate the presented methodologies through extended laboratory experiments.

Chapter 2

Components of the Distribution Network

In this Chapter, an overview of relevant components of a distributed energy power system is given. The functionality of the most widespread distributed energy sources is explained, and a brief description of main electrical components of the distribution systems is given. Finally, since it is relevant to the research in this thesis, the architecture of inverter based DGs, focusing on the Pulse Width Modulator, are examined in detail.

The topic of this thesis is distribution network monitoring. While the high voltage grid is usually well controlled and observed, the distribution network, where typically a large amount of DG is feeding its energy, is sparsely monitored [28]. Replicating the HV infrastructure on the distribution network would require large investments. In addition, since the number of nodes on the distribution network is much larger, its complete coverage would require a large amount of measurements and data collection, rendering a system that is hard to manage and to maintain. Additionally, the distribution network is increasingly confronted to power quality and load-balancing issues due to the surge in nonlinear loads and intermittent renewable energy sources that are being connected.

In general, distribution networks in power systems as very different from each other and are adapted to the local geographical and economical specifications. Although power system standards are defined by institutions such as IEEE [29] and IEC [30], every power system can be considered as unique. The main two implementations are Northern American and European styles, with different countries having a

network model that implements a mix of both of these specifications. On the other hand, one common feature of the distribution network until recently has been its radial structure. This has enabled each load to be fed from a single power source. This architectural assumption has greatly simplified the protection system mechanisms in the network. Thus assuming a radial network and unidirectional powerflow has led to a simple and easily manageable distribution system.

With the advent of DG, and a large amount of power connected to the distribution network, these assumption will not be true anymore. Reverse powerflows happen regularly, and the protection mechanisms have already had to be updated, revised and ancillary services such as Fault Right Through (FRT) requested from the main DGs to make the protections mechanisms operate properly [31] [32]. In addition recent research on looped networks suggested that a non-radial distribution network would present many benefits regarding power flow management and voltage regulation, while it would render network protection very complicated [33].

In the rest of Chapter, we will cover the most relevant components present on the distribution network which will be utilized in the modeling of the system.

2.1 Distributed Generators on the Power Network

Distributed Generation is a vague term and subject to misunderstandings. The definition of Distributed Generator in this thesis is a power source connected to distribution network. Generators with limited size and power input are considered.

While DGs have been operational for a long time, their expansion has seen a big boost in last decade. In fact, the combination of governmental policies, reduction in cost of power electronics and rise of fossil energy price, have made smaller generators connected to the distribution grid viable [34]. For smaller wind power plants situated far from the transmission network, it is not financially reasonable to build lines connecting them to the transmission network.

DG don't necessarily have to be based on renewable energy and environmentally friendly (diesel based DG have been existing for a long time). In addition, the environmentally friendly characteristics depend on a large number of parameters

and this subject is out of the scope of this thesis. In the following paragraphs a quick description of the main DG energy sources is given.

- **Wind energy** has seen a significant growth in recent years. Countries such as Denmark have more than 40% of their electricity needs covered by wind. This growth has risen mainly due to political push by the Danish government to reduce their dependency on foreign energy [34]. On the other hand, the state of Texas has seen a huge rise in wind energy in recent years, without political backing and 36 million MWh of electricity have been produced by wind in 2014, amounting to 10% of the consumption [35]. Therefore, whether pushed by political or economical motives, the production of wind energy keeps growing as long as potent sites are available for windfarming. The next step for wind energy expansion is offshore, where the wind is more stable and large amount of exploitable surfaces are available. From a technological point of view, offshore wind farms are far more expensive to build and also much more complex to maintain. A lot of research in recent years has been invested in order to come up with effective and cost efficient methods to conquer the seas.

  The main advantage of wind energy is the fact that it is a renewable energy. Its fuel free and abundant. The drawback from the power system's point of view is their volatility. In fact, wind energy is not always present, and predicting it's fluctuations for 4-5 days in advance is very challenging [36]. Thus, as of now, windfarms need to have a traditional energy source as a backup for when the wind is not blowing.

- **Photovoltaic** generators convert light radiation energy to electrical energy. The power of these type of generators varies greatly and ranges from microwatt to megawatt. Currently, the most commonly used technology is polycristalline, although its efficiency is not the highest among photovoltaic technologies. While efficiencies over 20% have been obtained in laboratories, commercial models hover between 12 and 14%. Its production is relatively energy intensive, and it takes a couple of years of energy production for them to become energy neutral. Nevertheless polycristalline is made out of silicium, which is one of the most abundant elements on earth. Other compelling technologies exist, and the most prominent one are thin-film solar

cells. Those have lower efficiencies but are easier and less expensive to produce [37]. They are partially made of exotic and rare materials and therefore, as of now, the photovoltaic market is dominated by polycristalline.

Advantages of photovoltaic generators are their durability, they have been known to last 20 to 30 years in mild conditions. They also don't produce any noise and have no moving parts. Compared to other energy sources, they do produce a smaller amount of energy per covered ground surface, and the failing link in photovoltaic systems are mostly the converters which have a much shorter life cycle than the PV panels themselves. Solar has seen a massive surge in recent years, fueled by the cost reduction due to industrial streamlining, shift to production in low cost countries and government subsidies.

- **CHP** plant are combined heat and power plant produce both heat and electricity, typically with a ratio 60-30 %. These installations, are usually fossil fuel based, and have very high efficiencies. Models for residential and tertiary sectors are being proposed by vendors, the most common one being the Sterling model, and fuel cell based ones are starting to penetrate the market as well [38]. While the cost of these installations is still pretty high, they have seen a big surge in the adoption in Japan after Fukushima.

- **Hydropower** is a renewable energy source, but typically hydro plants are very large and present in small numbers and thus cannot be considered as DG. They do have many advantages. They can act as a a temporary storage, the energy produced can be precisely controlled and no fuel is needed. They can produce a large amount of energy, have a large capacity factor and are very dispatchable. Most large hydroplants have been around for many decades, and the construction of new ones requires very large investments and is sparsely authorized because of its substantial impact on the environment.

- **Other sources**: Other distributed energy sources exist such as biomass, geothermal, waste based energy production. But their relative contribution is still very low, and their impact on global European power systems rather insignificant.

- **Energy storage** will play an important role in the future. It is an asset that is not fully mature yet, but much research is done in order to integrate it in power systems. In fact, energy demand is not constant over time and

peak consumption requires expensive energy to be produced, through intermittent backup generators. Handling of peak loads will increasingly become a challenge for network operators [39]. This problem is exacerbated with the penetration of fluctuating DG generators. Energy production and demand can fluctuate greatly, and storage will be one contributing solution for renewable integration, since it will reduce the need of inefficient backup generators, and also reduce the curtailment of renewable energy sources due to the inflexibility of some traditional energy sources. The most promising technology for storage are batteries. As of now, since battery capacity is small and their costs are high, the main application of batteries are in island grids, where they have been successfully put to use for frequency stabilization [40].

2.2 Power Lines

The power network consists of mainly of AC overhead lines and underground cables. HDVC technology has seen a significant development for power transfer over long distances, but the technology is not mature enough yet for distribution networks [41]. Thus, the medium voltage network will operate in AC at 50 Hz in Europe for the foreseeable future.

The transmission cables are operated on three phases, and the line consists of three conductors, which are often composed of a bundle of thin conductors. Each cable represents one phase of the transmission line. In overhead lines, the lines are not isolated, and are suspended from towers hanging on insulators. A typical material used for the conductors is aluminum, which has excellent electrical properties, and a steel core inside the cable improves its mechanical properties [42].

As opposed to overhead lines, cables are underground or underwater. The conductors are not bare; they are electrically insulated and physically protected. Thus, power-cables are much more expensive, and are also more costly to maintain. While time between failure of a typical underground cable is longer, fault localization is more challenging, and access to the faulty sections can be time consuming and costly. Typically, cables are used for shorter distances and in urban areas. They have a larger capacitive effect, which can lower resonance frequencies of the system and thus contribute to harmonic current propagation in the system.

Whether it is overhead lines or cables, transmission lines are electrically characterized by a series resistance, series inductance and shunt capacity, per unit of length. These parameters determine how much energy the power line can transport (its capacity) and the voltage drop across line.

2.2.1 Power Line Resistance

The thermal limit of a power line indicates the load a line can transport before it starts to exhibit material damage. The temperature of the power line depends on external conditions (e.g. temperature, wind, humidity), and on the current flowing through it [43]. Currently the grid operators set a conservative limit on the current transmission of the line, to ensure that the thermal limit is never reached. This threshold can also take into account season weather estimations. On the other hand, dynamic calculation of this limit based on external conditions has been a topic of interest in order to maximize the capacity of powerlines [44].

The DC resistance of a conductor is expressed as a resistivity per length and cross sectional are :

$$R_{DC} = \frac{\rho l}{A} \tag{2.1}$$

where, ρ is the resistivity of the cable, l its length, and A its cross sectional surface [42].

The DC resistance of the power line increases linearly with temperature over normal ranges. If the DC resistance is known at a temperature, its relation to the resistance at another temperature is given by:

$$\rho_{T2} = \frac{M + T_2}{M + T_1}\rho_{T1} \tag{2.2}$$

Table 2.1: Material resistivity relationship to temperature

Material	**Res. ρ at 20°C [Ω.m]**	**Temp. Constant M [°C]**
Annealed copper	1.72E-08	234.5
Hard-drawn copper	1.77E-08	241.5
Aluminium	2.83E-08	228.1
Iron	1.00E-07	180
Silver	1.59E-08	243

The AC resistance is higher due to skin effect, which causes a higher amount of current to circulate at the outer borders of the conductor [42]. In order to optimize the current flow and limit the skin effect, thin conductors are bundled in a powerline, and the inner core of the powerline consists of a steel cable which improves its mechanical durability.

2.2.2 Power Line Inductance

The series inductance of the transmission line consists of two components: the internal and external inductances. They are caused by magnetic flux inside and outside the conductor. The inductance of power line is defined by the number of flux linkages produced for each ampere of current flowing through it [42]:

$$l = \frac{\lambda}{I} \tag{2.3}$$

The inductance of a single-phase transmission line is given by:

$$l = \frac{\mu}{\pi}\left(\frac{1}{4} + \ln\frac{D}{r}\right) \tag{2.4}$$

where r is the conductor radius, D the distance between cables, and μ the magnetic permeability $= 4\pi \cdot 10^{-7} H/m$. The units of the inductance of the power line are Henry's per meter. A conductor with a larger diameter will have a lower inductance. Bundling several conductors reduces corona loss, which is caused by air molecule ionization near the transmission line conductors.

For a three phased powerline, the larger the spacing between the phases, the greater the inductance of the line will be. Since higher voltage line phases must be further apart for insulation, HV lines exhibit higher inductances than low voltage lines. For cables that are insulated and buried in ground, the distance between cables is smaller, thus series inductance of cables is smaller than for overhead lines. Thus for short and lower voltage power lines, the resistive and inductive effect are in the same order of magnitudes. But for higher voltage networks and longer lines, the inductive effect is the dominant component of the series impedance.

2.2.3 Shunt Capacitance

The capacitance between two conductors is defined by the relationship between the conductor's charges and the voltage difference between the conductors [42].

$$c = \frac{q}{V} \tag{2.5}$$

For a single phase line, the capacitance is defined by:

$$C = \frac{2\pi\varepsilon}{\ln(\frac{D}{r})} \tag{2.6}$$

where r is the radius of the conductor, D the distance between cables, and ε the permittivity $= 8.85 \cdot 10^{-12} H/m$. The shunt-capacitance of powerlines is measured in Farads per meter. This capacitance is proportional to the surface area of the conductors and inversely proportional to the distance between the plates. For a transmission line, this means that a large space between phases will reduce its capacitance. Since high voltage overhead lines have to be far away from each other for insulation, they exhibit lower capacitance than low voltage lines. The distance between the phases of underground cables is small, thus their shunt capacitance is larger than overhead lines. The greater the radius of the powerline, the larger its surface will be and the higher its capacitance will be. Bundling increases the effective surface of the conductor and increases its capacitance.

Below are the most common models used in power systems for transmission line modeling. For shorter lines, lumped and simplified models are used in order to enable the representation of complex systems.

2.2.4 Short Line Model

In short overhead lines, shunt capacitance can be neglected, since its contribution to the dynamics of the powerline model are insignificant. The model used for overhead lines up to 100 km is shown in Figure 2.1.

The resistance and reactance of the powerline can be calculated as:

$$R = r \cdot d \tag{2.7}$$

$$X = x \cdot d \tag{2.8}$$

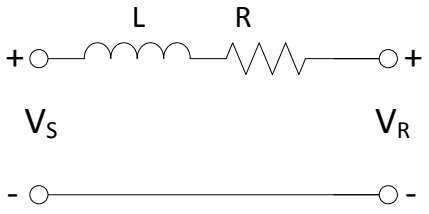

FIGURE 2.1: Short Power Line Model

where r, x are per unit resistance and reactance, and l is the length of transmission line. In short lines, with small reactances, the resistive heating is the factor delimiting the capacity of the line. In longer (more inductive) lines, feeding inductive loads (with a lagging power factor), it is the voltage drop at the end of the line which is the limiting factor.

2.2.5 Medium Length Line Model

When the line is long, or for underground cables of moderate length, the shunt admittance is considered. It is represented as 2 capacitors on each side of the powerline segment. This model is usually called the Pi-model.

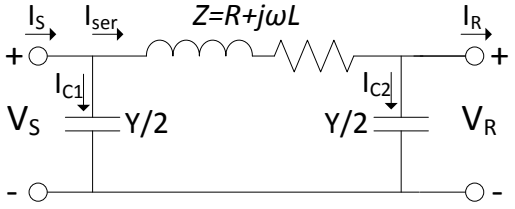

FIGURE 2.2: Medium Length Power Line Model

The total shunt admittance is given by:

$$Y = y \cdot l \tag{2.9}$$

where y is the admittance per length unit, and l is the length of the transmission line.

2.2.6 Long Line Model

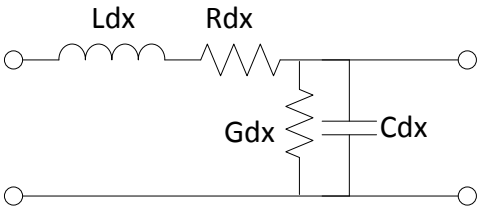

FIGURE 2.3: Long Power Line Model

For longer lines, shunt capacitance and series resistance and reactance are represented as distributed quantities along the powerline. Voltage and current values along the line are obtained by solving differential equations. For a lossless line, the second order steady-state equations provide the wave equations for the voltage and current.

$$\frac{\delta^2 V(x)}{\delta x^2} + \omega^2 LC \cdot V(x) = 0 \tag{2.10}$$

$$\frac{\delta^2 I(x)}{\delta x^2} + \omega^2 LC \cdot I(x) = 0 \tag{2.11}$$

Theses equations represent electromagnetic waves propagating along the transmissions line, and the reflected component of the wave interferes with the transmitted signal. For a lossy transmission line R and G must be taken into account [45], and the telegraphers equations can be written as:

$$\frac{\delta^2 V(x)}{\delta x^2} + \gamma^2 \cdot V(x) = 0 \tag{2.12}$$

$$\frac{\delta^2 I(x)}{\delta x^2} + \gamma^2 \cdot I(x) = 0 \tag{2.13}$$

where γ is the propagation constant:

$$\gamma = \sqrt{(R + j\omega L)(G + j\omega C)} \tag{2.14}$$

and the characteristic impedance is expressed as:

$$Z_0 = \sqrt{\frac{R + j\omega L}{G + j\omega C}} \tag{2.15}$$

the solution for $V(x)$ and $I(x)$ are given by:

$$V(x) = V^{+}e^{-\gamma x} - V^{-}e^{\gamma x} \tag{2.16}$$

$$I(x) = \frac{1}{Z_0}(V^{+}e^{-\gamma x} - V^{-}e^{\gamma x}) \tag{2.17}$$

The constant values V^{+}, V^{-}, I^{+} and I^{-} are determined by the boundary conditions of the signal propagation, depending for instance on the input impedances at both end of the line. Equations 2.16 and 2.17 represent a traveling wave with a reflective component for the current and for the voltage.

In order to simplify the calculations, it is possible to model a long transmission line as a Pi-model with a modified series impedance Z' and a modified shunt admittance Y'.

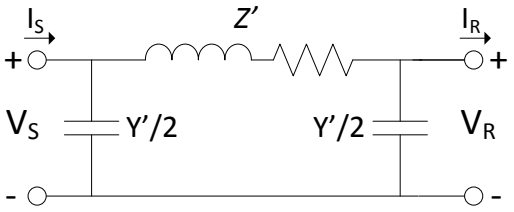

FIGURE 2.4: Long Power Line Model Simplified

Assuming that the conductance of the dielectric material is negligible, the analytical modified model for the transmission line is calculated as follows:

$$Z' = Z\frac{\sinh(\gamma d)}{\gamma d} \tag{2.18}$$

$$Y' = Y\frac{tanh(\frac{\gamma d}{2})}{\frac{\gamma d}{2}} \tag{2.19}$$

where the propagation constant is defined by:

$$\gamma = \sqrt{yz} \tag{2.20}$$

It is considered that wave-like behavior of signals traversing transmission lines are exhibited when the signal frequency attains 2 percent of the wavelength contained

in the line [46]. Given that the current waves propagate close to the light of speed in the conductors, the wavelength for a 50 Hz signal is

$$\lambda = \frac{c}{50} = 6000km \tag{2.21}$$

Thus below 120 km, a simple lumped model reproduces accurately the dynamics of the system. Given that the focus of the thesis on the distribution network in Luxembourg, the line lengths considered are short, usually less than 10 km. A simple or Pi-model can therefore be used for representing the power line.

2.3 Protective Elements

2.3.1 Fuses

Fuses are commonly used in distribution systems since they are less costly, and simpler than circuit breakers. The fuse is usually a short piece of metal that melts when excessive current flows through it and thus opens the circuit. Fuses are composed of materials having a low melting point and high conductivity, and if possible resistant to oxidation. Fuses are characterized by two main features: the Minimum Melting (MM) time and the Total Clearing (TC) time [47]. Both are determined by the amount of current passing through the fuse. For a given current, the MM time is the duration of time the fuse can handle such a current before it is damaged and has partially tripped. The TC time is the time it takes for the fuse to fully trip and clear a fault for a given current. Fuses with different TC and MM characteristics are used throughout a distribution system in order to coordinate tripping, so that the smallest possible section of the network in disconnected on line faults [48].

2.3.2 Relay and Circuit Breaker

Protective relays monitor electrical measurements on the powerline, for the purpose of triggering a circuit breaker to open in case of abnormality. Circuit breakers are used to disconnect faults from the system. The breakers are usually tripped by relays that detect faults through current transformers and voltage transformers. The circuit breaker is the electric component that is given the command to trip.

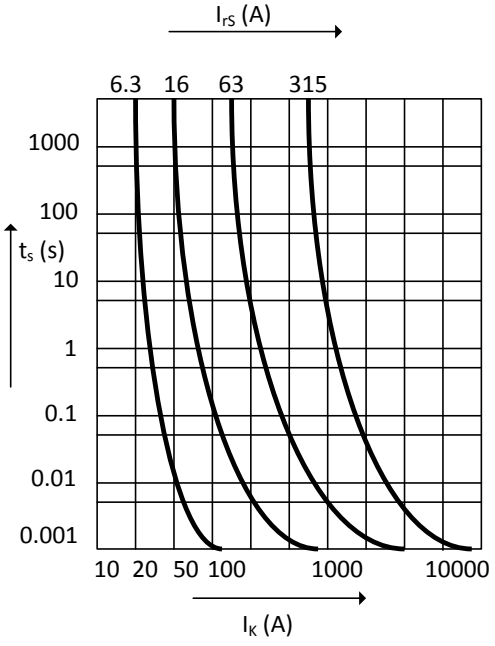

FIGURE 2.5: Time/Current Through Pass Lines of Fuses

2.3.3 Recloser and Sectionalizer

Reclosers provide a method for rapidly handling temporary faults on the line. In fact, two thirds of faults are temporary, e.g. due to arcing lines touching surrounding vegetation. If a fuse or circuit breaker trips, maintenance is called to the site in order to asses the fault and make the line operational again. Fuses have to be replaced once they have tripped, while circuit breakers, which are more expensive, degrade at a much slower rate. Reclosers are components of the power system whose purpose is to remove temporary faults quickly [47]. The idea is that when the faulty section is disconnected through the recloser, the produced arc deionizes and extinguishes. The line can then be reconnected again. Thus, the recloser disconnect and reconnects very quickly. If the fault is not cleared, it waits, and disconnects again for a longer time period and after several tries, the fault is assumed to be permanent an the fault section of the line is disconnected through a sectionalizer.

2.4 Transformers

Transformers are electrical components used in power systems to modify the voltage. Electricity transportation over transmission lines incurs losses and the power transmitted along a line is equal to the voltage times the current. Thus, higher voltages require lower the current to deliver the same power. Since heating losses are proportional to the currents traversing the conductor, higher voltage are used for long transmission lines. This requires less current for the same amount of power,and reduces resistive losses on transmission lines. However, high voltages are dangerous and too difficult to handle for loads and consumers [48].

The equivalent electrical circuit of a single-phase transformer is shown in Figure 2.6. In Figure 2.6(A), R_{eq} is the resistive core loss and the magnetizing reactance is represented by X_m. The leakage inductance of the transformer is X_{eq} and, and finally R_{eq} denotes transformer's winding resistance. All the quantities are represented on the primary side. The turns ratio of the transformer is given by N1 : N2.

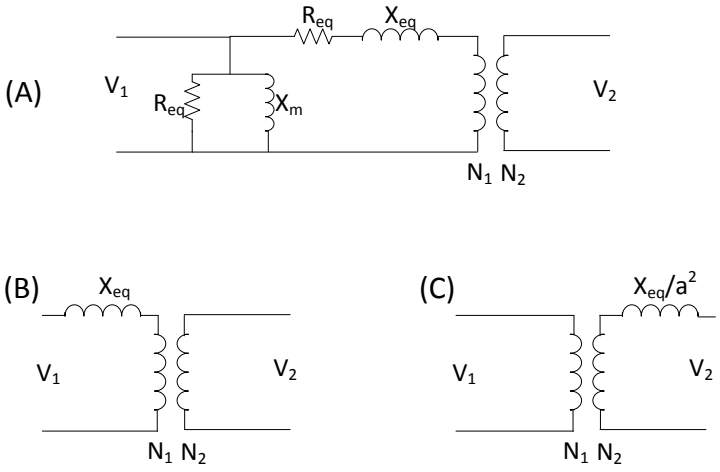

FIGURE 2.6: Transformer Electrical Model

Normally, the impedance of the shunt branch is much larger compared to that of the series branch and can be neglected X_m. In power systems models, the resistive component is much smaller than the inductive component and can be neglected as well. Thus, the transformer inductance is typically represented by its leakage reactance X_{eq}. The equivalent circuit can be established on the primary

side or on the secondary side. Both of which as pictured in Figure 2.6(B) and 2.6(C), the leakage inductance on the secondary side model being multiplied by the transformer ratio a where

$$a = \frac{N_1}{N_2} \tag{2.22}$$

2.5 Inverter based DGs

In modern photovoltaic generators, and increasingly in other distributed generators as well, the electrical power is converted to a mode where it is able to interface with a utility line through the use of power electronics. Inverters take DC and convert to AC. Inverters based on a Pulse Width Modulator are commonly utilized nowadays. The inverter contains many electrical components, but its main functional entities are shown in Figure 2.7.

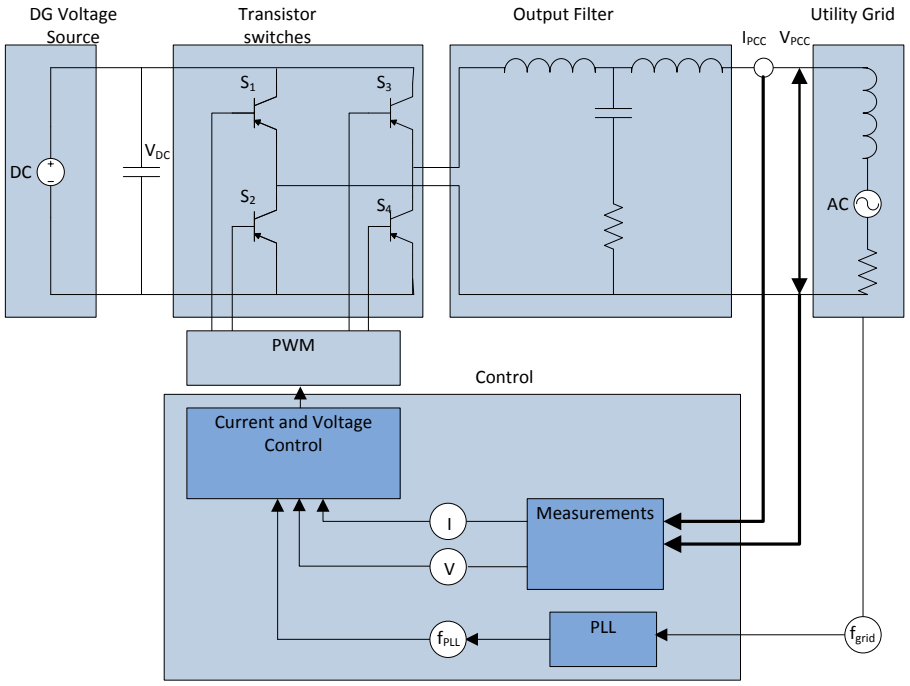

FIGURE 2.7: Inverter Architecture

The energy produced is modeled as a DC source, as it is the case for a photovoltaic energy source. The capacitance in parallel with the source keeps the voltage stable. The voltage is switched by the transistors, which create pulses that produce

a signal that on average resembles as closely as possible to a sine wave. The transistors technology used for power inverters is commonly Insulated Gate Bipolar Transistors (IGBT).

The control of the transistor switching is steered by the PWM. Based on the settings of the current controller and the frequency acquired by the Phase Locked Loop (PLL) from V_{PCC}, it adjusts its parameters in order to create pulses that mimic a fundamental with the frequency and amplitude dictated by the PLL and voltage control. In order to adjust the power factor, a phase delay can be incorporated in the design of the reference signal. The maximal frequency at which the PWM operates is called its switching frequency. Measurements of the Voltage, current and frequency at the PCC are obtained and fed to the controller, which adjusts the inverter settings based and the variable grid conditions. The pulses generated are shaped by the output filter of the inverter, which is essentially a low-pass filter, either consisting of an LC or LCL filter [49]. Its purpose is to eliminate the switching frequencies. There are other components in the inverter, such as relays that protect it from malfunctions in the grid.

Figure 2.7 shows the inverter architecture for a one phase device, while the design for a 3-phase system differs slightly, its mode of operation and control are similar.

2.5.1 Pulse Width Modulator

Even though DG power sources such as Photovoltaics generate DC power, long distance electrical transmission is done with AC. In fact, AC power distribution has a lot of flexibility and voltages can easily be modified with transformers. The purpose of the inverter is to take DC voltage and convert it to AC voltage. The Pulse Width Modulator generates the pulses that drive the transistor switches. A conversion from DC to AC involves switching the voltage. Grid-tie generators produce a pure sine wave, in order to meet the grid code requirements. While there are many inverter designs, for a sine wave generation, the most common configuration is to connect the DC voltage source to an H-Bridge, and switch appropriately. The voltage can be increased through a transformer after AC stage, or before by a DC-DC boost converter [50], whereas new topologies can perform voltage increase and AC conversion in a single stage.

The signal generated by the inverter is a sequence of pulses which encodes a sine wave. The duty cycle of the pulse is modified each cycle so that the averaged power transmitted over time is that of a sine. The most popular technique for creating a sine is PWM. It creates a digital wave, whose duty cycle is modulated so that it corresponds to a sine wave if averaged. Pure sine wave generators create a 50 Hz that is as clean as possible. Harmonics injected have a negative impact on the power system, since they contribute to heating and damaging components. For the simple two-level PWM, a triangular control signal, called the carrier, is compared to a low power reference signal, as depicted in Figure 2.8.

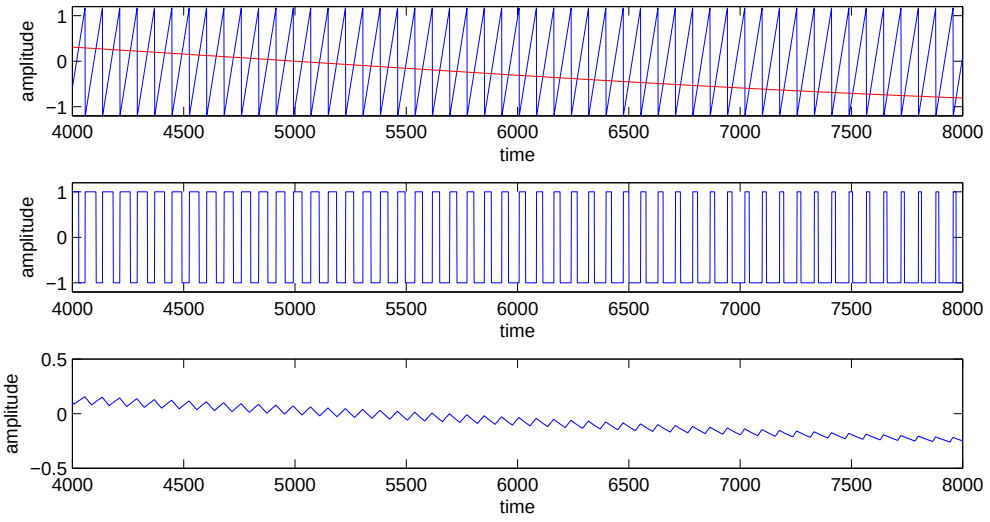

FIGURE 2.8: Pulse Width Modulator Functionality

The PWM triggers and produces a pulse when the reference signal has higher amplitude than the carrier. The output signal is a two level PWM signal, which triggers either positive or negative voltage at the transistors. When the generated signal is filtered by the output filter of the inverter, which in DGs is typically an LC filter or an LCL filter, the output voltage is the bottom plot on Figure 2.8 and approximates a sine wave.

Figure 2.9 shows the magnitude of the Fourier transform of the PWM pulses on the top plot, and of the filtered signal at the inverter output at the bottom. The harmonics present in the filtered signal are relatively low amplitude. The switching frequency is the high frequency signal to be filtered, set to 3200 Hz in the Figure 2.9. Thus the output filter is typically designed to attenuate the switching

frequency as much as possible, without affecting the fundamental. Figure 2.9 shows the frequency magnitudes of the PWM output before and after the filter.

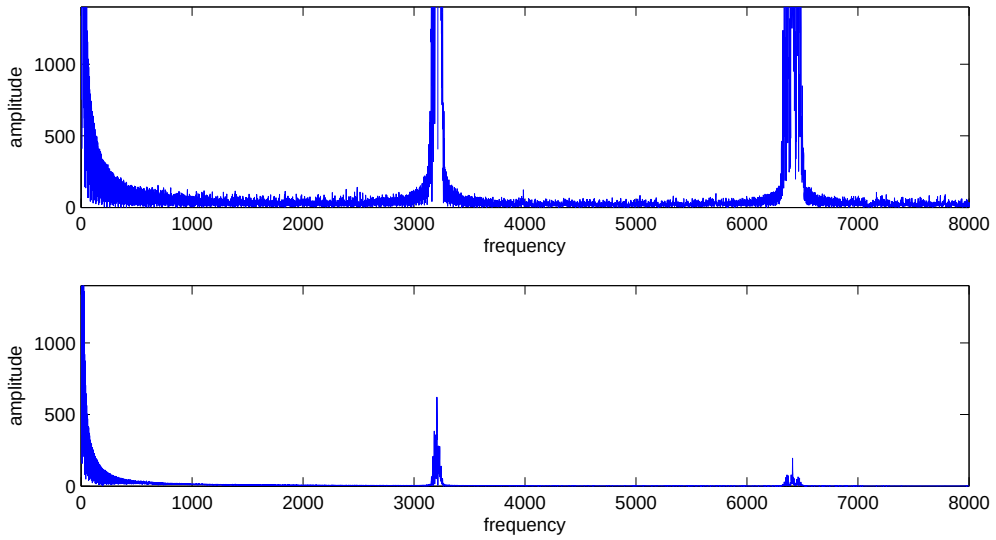

FIGURE 2.9: Inverter output spectrum, before and after the output filter

In order to reduce the harmonic injection even further, a three level PWM can be used. In this architecture, the applied voltages can be V_+, V_- or 0. The three level PWM used in conjunction with an H-Bridge is the most commonly used inverter PWM architecture in distributed generators such as solar generators nowadays. Its architecture implemented for a 3-phase system is shown in Figure 2.10.

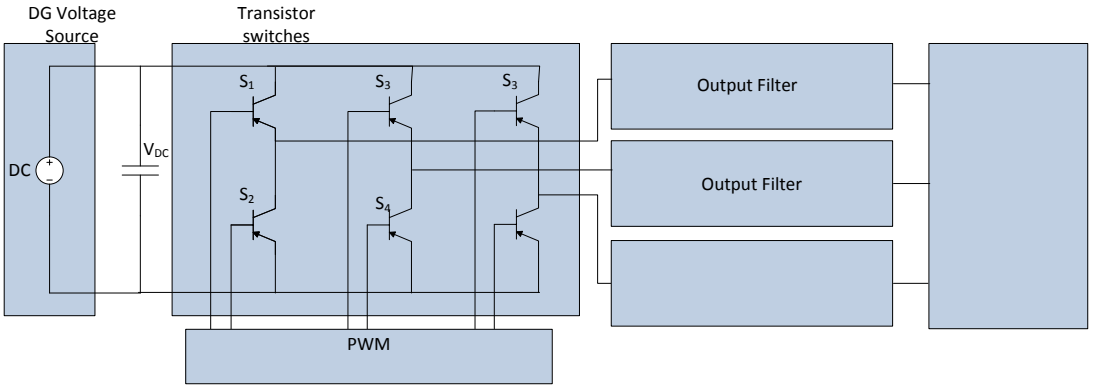

FIGURE 2.10: Three Phase H-Bridge PWM

As in a two level PWM, a triangle wave is used, but only half the amplitude of the reference is used to compare to the triangular signal. The resulting PWM controls half H-Bridge, which drives the DC voltage to the load. The other half is controlled to set the polarity, it could be steered by a rectangular signal. The functionality of the three level PWM is shown in Figure 2.11.

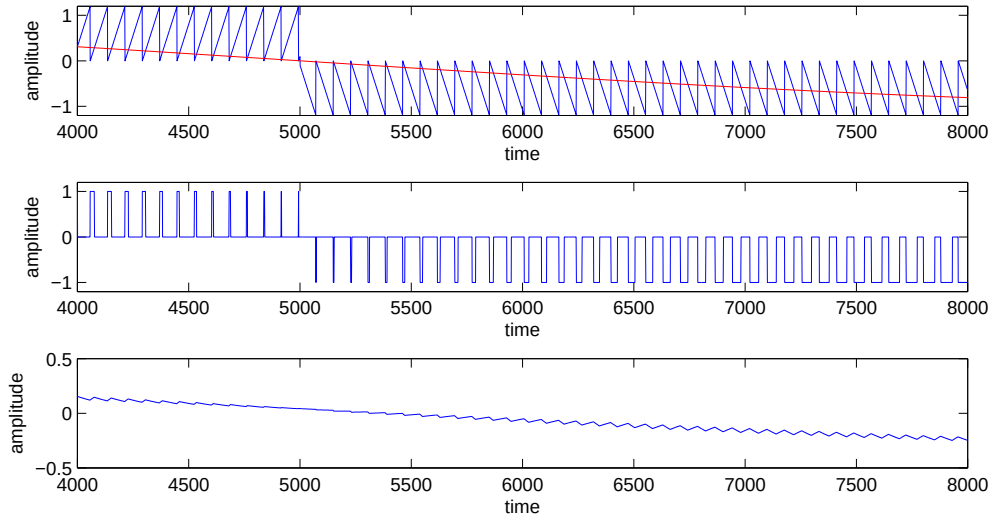

FIGURE 2.11: Half Bridge Inverter Output

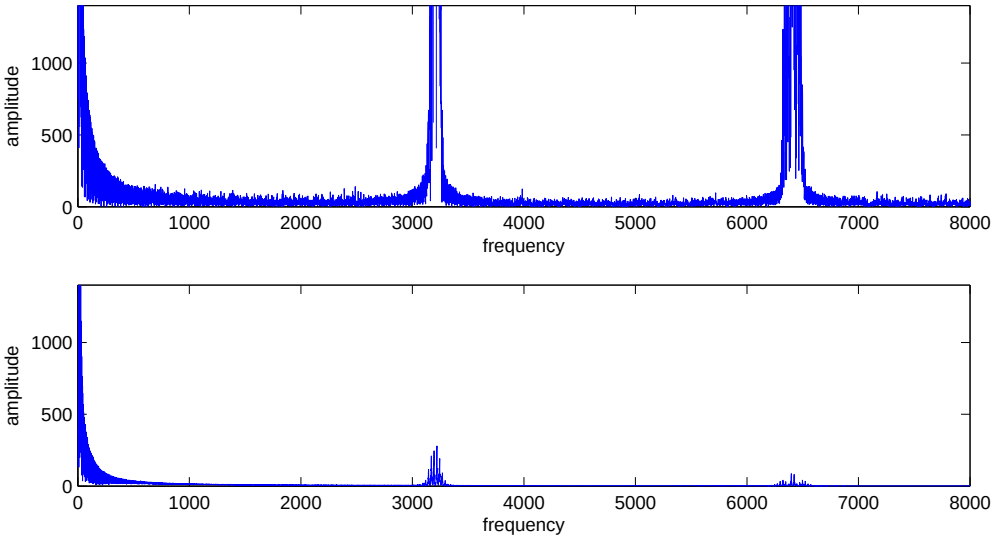

FIGURE 2.12: Half Bridge Inverter Spectrum

Figure 2.12 shows that the harmonics are clearly reduced for this architecture. This effect can also be seen on the time domain plot around the zero crossings of the where the three level PWM does a much better approximation of the sine.

Better performance can be obtained with more elaborate architectures. For instance 5-level architectures are developed as well. But as of now, the extra costs involved are not worth the performance improvements gained. In typical DG implementations, the three level PWM represents the best compromise between cost and efficiency.

The quality of the created output signal also depends also on the switching frequency. Ideally, higher frequencies should produce better results, since the output filter provides a higher attenuation on high frequencies. But the transistor technology limits the maximum threshold. The switching frequency usually varies between 10 kHz and 100 kHz depending on the applications and the technologies used. For lower frequencies, the transistors toggle less often and cause less switching loss at the inverter. But lower switching frequencies induce worse power quality [51] and cause higher harmonic losses. In addition, low frequency switching inverters are perceptibly louder, since frequencies up to 15 kHz are perceptible by the human ear. Higher frequencies produce a cleaner sine wave, are less noisy, but are less efficient since they render higher switching losses in the transistors. In the next section, an overview of the two most common transistor technologies is given.

2.5.2 Transistors

The switching of the DC power in order to generate AC occurs at the transistors on the H-Bridge in Figure 2.7. Two main technologies exist for the inverter transistors: the power MOSFET (Metal Oxide Semiconductor Field Effect), and the Insulated Gate Bipolar Transistor (IBGT). Each technology has its advantages, and there is an overlap between the domain of application on their specifications. Depending on the system and the parameters selected in each case, one is chosen [52].

IGBT is used in high voltage applications, and above 2 kV it is always the selected technology. Below 2 kV and above 600 V, it is preferred to MOSFET transistors. IGBTs can handle high currents, they can output large powers, and have a good

thermal operating stability. Even in temperatures above 100° Celsius they operate with a good efficiency. Their main disadvantage, is the current tail produced when the transistor switches off. In fact, the current in the transistor gate doesn't dissipate immediately, but decreases slowly, causing a loss. Thus, due to this slowly dissipating current, IGBTs cannot be switched at high frequencies, since time needs to be given for the current to clear. The switching frequency for IGBTs is typically limited to maximum 20 kHz.

Compared to the IGBTs, power MOSFETs have lower switching losses, and can be switched at much higher rates. Switching frequencies above 200 kHz are common. On the other hand, they have higher conduction losses, which is the reason that they operate at lower current and voltage and power, typically below 250 V and 500 W. They don't produce a current tail at switching as they switch more efficiently.

In DG inverters connected to the grid, IGBT occupy most of the market. The powers produced and the voltages are high so that the MOSFET transistors are not efficient enough, although emerging MOSFET based technologies are being developed for high power applications [53]. In the current state of the art, MOSFET is only utilized in some specific cases on the low voltage network.

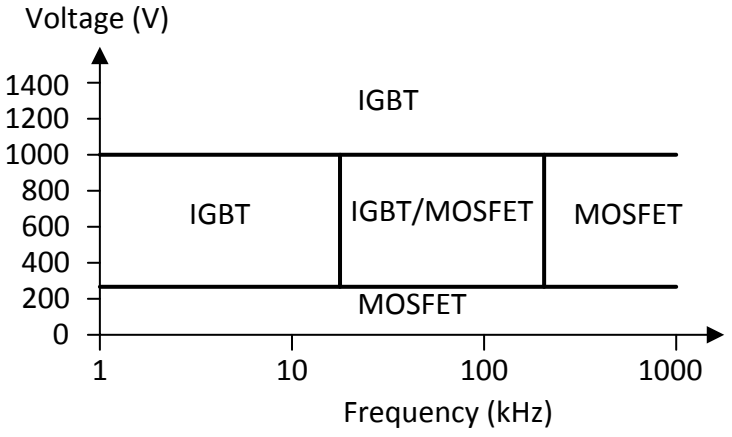

FIGURE 2.13: IGBT and MOSFET Applications

2.5.3 Amplitude Modulation and Control

In order to optimize and control the power delivery of the DG, the voltage amplitude and frequency are controlled and adapted continuously. For amplitude

modulation, two very important parameters are M_a and M_f. M_f is the ratio between the triangle wave and signal wave. It is typically an odd integer, and it determines the frequency of the generated harmonics in the output signal, which will be at M_f*f_c, where f_c is the reference signal frequency.

M_a is the ratio of the amplitudes of reference signal and carrier. It is always between zero and one. When it is above one, clipping occurs, causing a non linear relationship between carrier and signals and distortions. Between zero and one, the amplitude is linearly related to M_a. If M_a decreases, the amplitude decreases, but the amplitude of harmonics increases. Thus the output filter has to be dimensioned accordingly in order to attenuate the harmonics appropriately. Ideally, the designer aims at keeping M_a as close to one as possible. The phase of the output signals is adjusted by delaying the reference signal.

2.5.4 Inverter Output Filter

As seen in previous sections, the voltage pattern produced by the PWM consists of a sequence of pulses, that on average produce a sine wave. The voltage needs to be smoothened, i.e. the high frequency components of the generated signal need to be attenuated, so that a 50 Hz component that is as clean as possible remains. In most grid tie inverters, passive filters are used, consisting either of LC filters, or LCL filters. The state of the art contains literature on active damping of harmonics through modification of the inverter control [54]. These target specific frequencies and as of now, the passive filter is an essential component of the inverter. We will give a brief overview of the two most common configurations, the LC filter and the LCL filter.

2.5.4.1 LC filter

The LC filter is a second order filter, and has a quadratic dampening effect with increasing frequency. It provides 20 dB per decade attenuation after its cut-off frequency. While its performance is improved over a simple L filter, it presents a resonance frequency, and it has to be dimensioned with care. As shown in its Bode plot in Figure 2.15, below the resonance frequency, it shows insignificant gain. Its transfer function can be written as

$$H_{LC}(s) = \frac{1 + R_C \cdot C \cdot s}{L \cdot R_C \cdot C \cdot s^2 + L \cdot s} \tag{2.23}$$

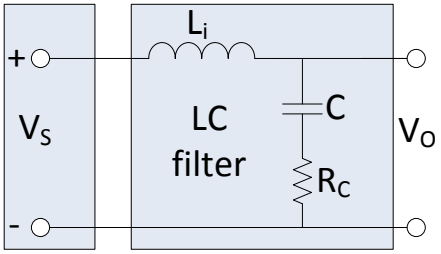

FIGURE 2.14: LC Filter Diagram

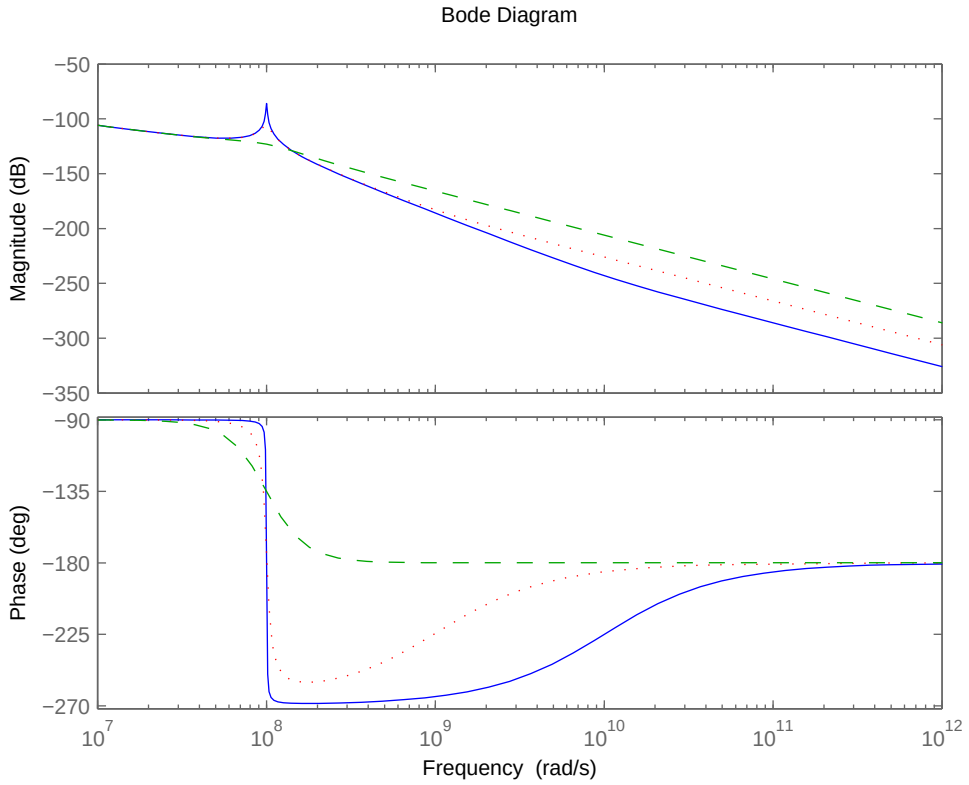

FIGURE 2.15: LC Filter Bode Plot, Blue: 0.001 Ω Damping, Red: 0.01 Ω damping, Green: 0.1 Ω damping

The PWM switches normally in the 10 kHz - 20 kHz range. In the design of the LC filter, care has to be put on the location of the resonance frequency. If its too high, it might not dampen the switching frequencies of the PWM efficiently. If

it is too low, it might amplify prominent harmonics such as the 13^{th} or the 11^{th}. Thus in common designs, the resonance frequency is placed in the 1000-2000 Hz range. The resonance frequency of the LC filter is given by:

$$f_{res} = \frac{1}{2\pi\sqrt{LC}} \tag{2.24}$$

2.5.4.2 LCL filter

The LCL filter has similar characteristics. For frequencies below the resonance frequency, the attenuation between the LCL filter and LC filter is similar, the second inductance only playing a minor role in that case [55]. For frequencies above the resonance frequency, due to the double inductances, the attenuation is 60 dB per decade. Its transfer function based on Figure 2.16 is shown on equation 2.25:

$$H_{LCL}(s) = \frac{1 + (R_C C) \cdot s}{(L_g + L_i) \cdot s + (L_g + L_i)(R_C C) \cdot s^2 + L_g L_i C \cdot s^3} \tag{2.25}$$

It also provides better decoupling between filter and grid impedance and lower current ripple across grid inductor. The analytical value of the resonance frequency of the LCL filter is:

$$f_{res} = \frac{1}{\sqrt{2\pi}}\sqrt{\frac{L_i + L_g}{L_i \cdot L_g \cdot C}} \tag{2.26}$$

In Figure 2.16, the performance of an LC and LCL filter is shown for the same total inductance. The LC filter is shown in red and the LCL in blue. For equivalent performance, the LCL filter can be dimensioned smaller than the LC filter.

Thus it is a preferred filter for grid tie inverters, but it has its drawbacks. The LCL filter is more vulnerable to oscillations, and magnifies frequencies greatly around its resonance, since its a third degree filter [56]. Figure 2.16 shows that the resonance peak is higher for equivalent filter component specifications. The common solution is to add a damping resistor, which is placed in series with the filter capacitor. The effect of the resistor is to attenuate the resonance peak, but it will also degrade the performance above the resonance frequency if its too large. For optimal performance, the value of the resistor is set to:

$$R_C = \frac{1}{\omega_{res} C} \tag{2.27}$$

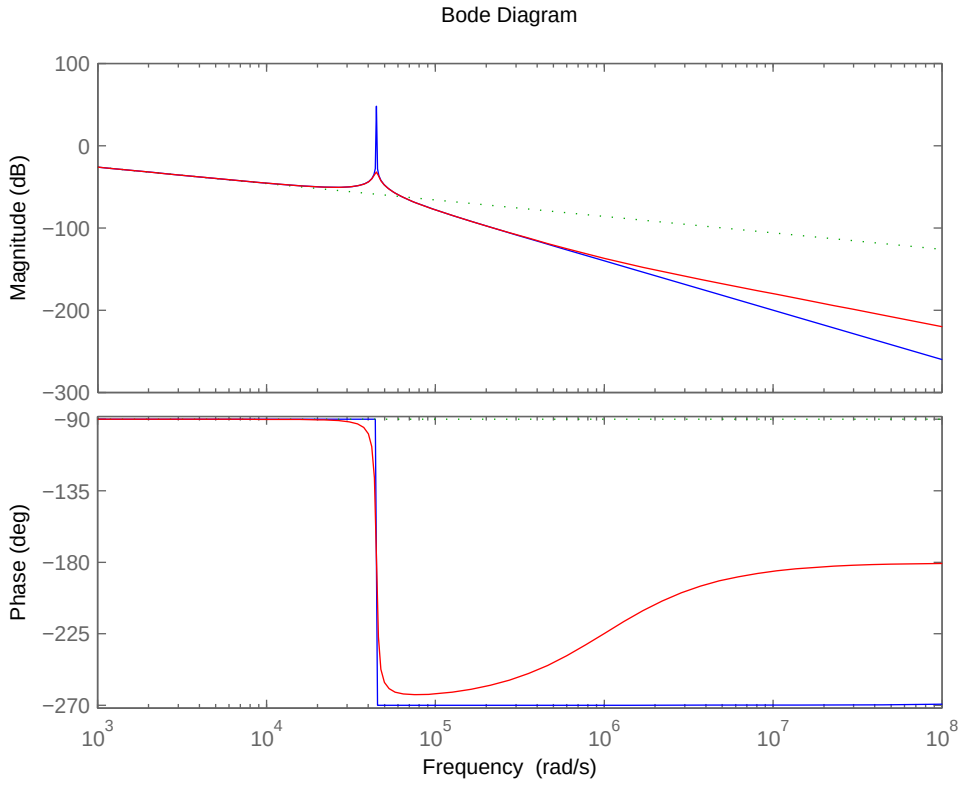

FIGURE 2.16: LCL Filter Bode Plot, Blue: 0.001 Ω Damping, Red: 0.01 Ω damping, Green: 0.1 Ω damping

The resonance frequency is commonly set to at most half the switching frequency of the inverter to provide adequate attenuation. It also has to be far enough from the grid frequency, so that the filter doesn't impact power delivery of the inverter.

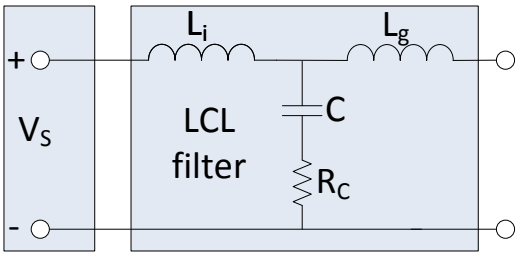

FIGURE 2.17: LCL Filter Diagram

It can also be seen that the optimal filter parameters have to be elaborated with grid impedance in mind, since the resonant frequencies and resonant peak are

impacted by the grid impedance. Nevertheless, for a properly designed system, a damped LCL filter exhibits the best performance.

The following recommendations are usual guidelines considered for the design of an LCL filter [57].

- The value of the capacitance is limited by the decrease of the power factor, which cannot be more than 5% at the rated power.
- The resonance frequency of the filter should be higher than 10 times the grid frequency and less than half of the switching frequency.
- The filter has to be designed such that the power quality grid codes are respected, that is the harmonics voltages and current injected in the power network are below the specified thresholds.

The main components of the distribution network have been described in this Section, and an emphasis has been put on the DGs inverter architecture. In the next Section, we will discuss methods for modifying the PWM's behavior and overlap coded signals on top of the 50 Hz generated. In further sections, these signals will be used for power system operations in order to improve protection mechanisms and monitoring functionality to the power system.

Chapter 3

Pseudo-Random Binary Sequence Injection on Inverter

The Pseudo-Random Binary Sequences (PRBS) are bit streams of '1's and '0's occurring randomly, but in a predefined manner. Thus the PRBS is not truly random, as its name implies [58]. If the PRBS consists of a long sequence, it can exhibit properties that mimic random signals and is adapted for testing and characterization purposes. PRBS sequences are easy to generate, and knowing their polynomial and seed, it is possible to reproduce the signal exactly and predict the sequence. This is a very useful property for channel identification, as the receiver will know in advance the expected incoming sequence. Pseudo-Random Binary Sequences are commonly used for transmission line and hardware characterization in communication systems [59], since component and channel testing typically involve the transmission of a predefined signal and its reception.

3.1 Generation

PRBS sequences are generated by bit shifts through a number of cascaded shift registers. One or a few of the shift register's outputs are tapped and XOR-ed before being fed back to the input of the first shift register. The total number of shift registers defines the degree of the PRBS sequence and establishes the run length of the sequence before it repeats itself. In fact, the length of the sequence is determined by the total number of possible combinations the states of the shift registers can assume. These properties are defined by the tap selections. For

each number of shift registers N, there is a finite number of tap combinations that provide a Maximum Length Sequence (MLS), for which the sequence length will be defined as:

$$Seq_{Length} = 2^N - 1 \tag{3.1}$$

Thus for a given seed, a system of degree N will allow the generation of a deterministic pseudo-random binary sequence of '1's and '0's of $2^N - 1$ elements. The architecture of the PRBS generator is called a Linear Feedback Shift Register (LFSR). The arrangement of feedback taps of the LFSR are expressed arithmetically as a polynomial modulo 2. This expression is called the feedback polynomial or characteristic polynomial. An LFSR with taps on the 3^{rd} and the 4^{th}, such as the system in Figure 3.1 can be described by the polynomial:

$$1 + x^3 + x^4 \tag{3.2}$$

where x^3 and x^4 refer to the tap set used.

The '1' in the polynomial does not correspond to a tap, it corresponds to the input to the first bit. In the polynomial representation, the powers represent bits that are tapped. The first and last bits are always connected as an input and output tap respectively. A polynomial that generates a sequence of 2^{N-1} is called an MLS. A necessary condition for an LFSR to generate an MLS are the following conditions:

- The number of taps are even.
- The tap positions are prime relative to each other, i.e. they don't have a common divisor.

In this case the feedback polynomial is called primitive. The MLS sequences are a subset of primitive sequences, and a list of MLSs for each sequence length is given in [60].

An example of an LFSR generating a PRBS of length 15 can be seen in Figure 3.1. The state diagram for the LFSR in Figure 3.2 consists of 15 different states of 4 bits. Each new state is obtained by shifting the previous state one bit to the right, and then replacing the left most bit by the result of a modulo 2 addition corresponding to the tap set used. The states of the registers cover all possible combination except '0000'. The bottom bit in each state, marked in bold shows

the output of the LFSR on that state corresponding to the sequence shown in Figure 3.1.

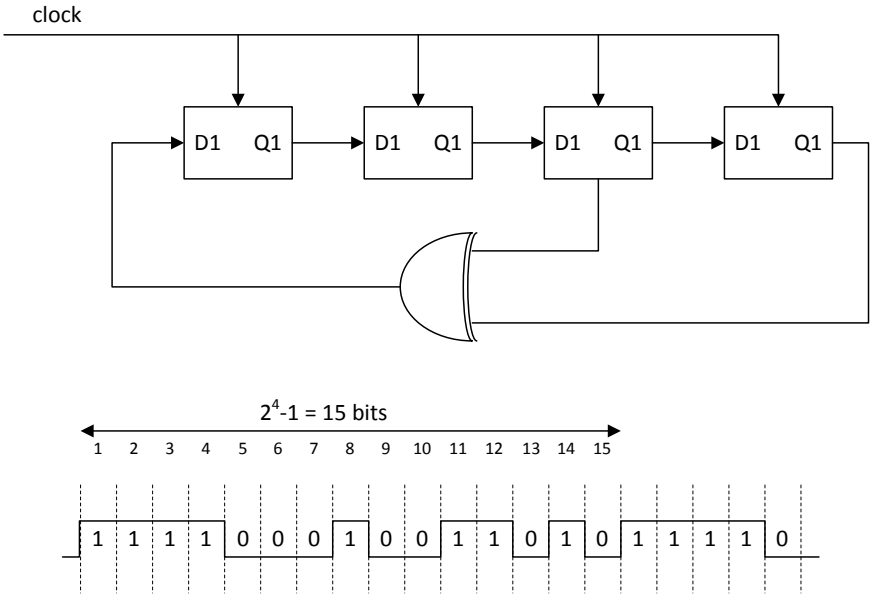

FIGURE 3.1: A Pseudo Random Generator with polynomial $1+x^3+x^4$, generating a repeated random sequence of 15 bits

Mathematically, at each cycle, the output of the LFSR can be written as:

$$X_T = a_1 X_{T-1} \oplus a_2 X_{T-2} \oplus a_3 X_{T-3} \oplus ... \oplus a_N X_{T-N} \tag{3.3}$$

where the coefficients $a1..an$ are set to '1' if that shift register is selected as a tap. X_{T-1} to X_{T-N} are the output of the shift registers, and X_T is the output of the LFSR. The output of any tap would produce a PRBS of the same characteristics, but with a different seed. During one period of the MLS, each state appears only once. The representation by a binary number of each register input defines the current seed of the LFSR.

3.2 Subsequence Properties

A peculiar characteristic of PRBS is that alternate bits in the sequence form the same sequence at half the bit rate. The same principle can be applied to further degrees, e.g. every fourth bit in the sequence forms a sequence that operates at the

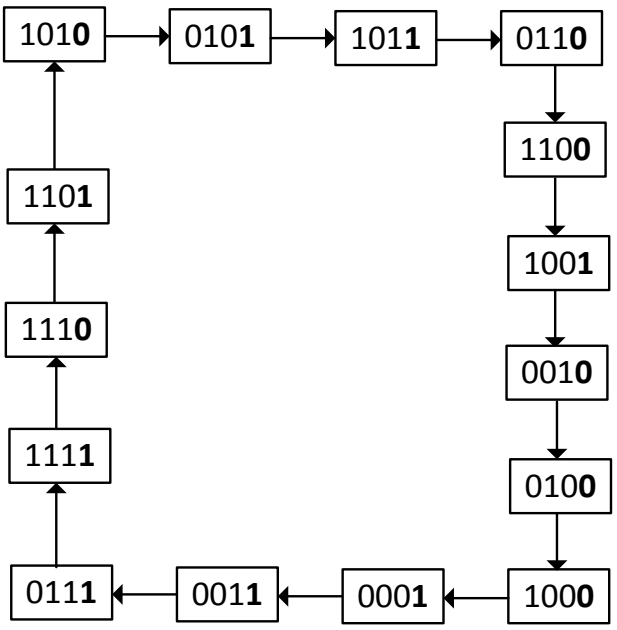

FIGURE 3.2: 4-bit LFSR with its state diagram, the output of the LFSR at each state is marked in bold.

quarter of the bit rate. The same way, if the generation of a sequence of frequency f is required, two identical sequences at frequency $f/2$ can be delayed by half a cycle and multiplexed. In this way, as shown in Figure 3.3, even a very low speed controller can generate sequences at higher speeds [19].

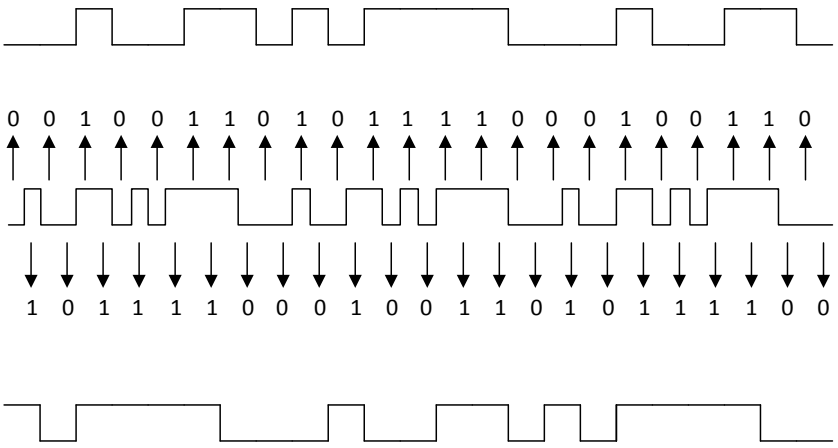

FIGURE 3.3: Multiplexing of two PRBS sequences of frequency f/2 to form one of frequency f

3.3 Correlation

Correlation provides a way to calculate the degree of similarity between two sequences. The correlation between two identical PRBSs is called its auto-correlation [19]. For Gaussian white noise, it assumes one of two possible values, describing whether the two sequences are in phase or not. Thus, it can be used for receiver synchronization of data, since a correlation of two identical sequences produces a spike when they are in phase. In fact, long PRBS sequences can be used as white noise for system identification. Figure 3.4 shows the auto-correlation and cross correlation between two MLS sequences.

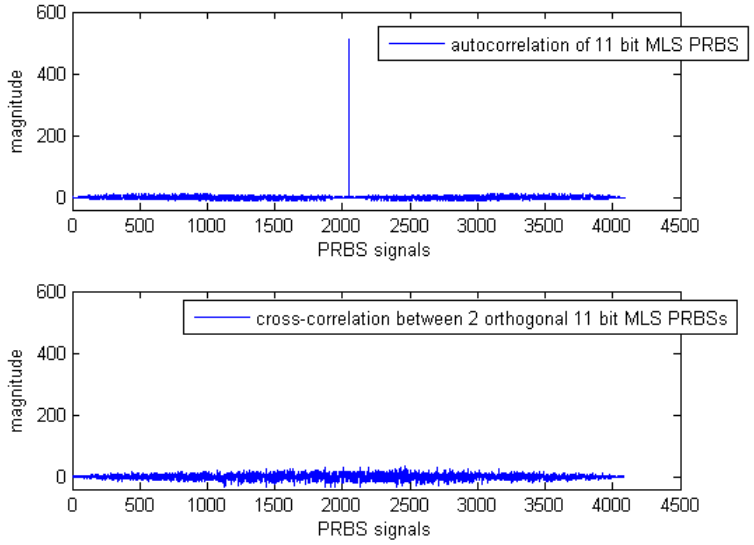

FIGURE 3.4: Autocorrelation of an 11 bit MLS PRBS, and cross correlation between 2 orthogonal MLS PRBSs

3.4 System Identification

It can be assumed that the system to be identified is represented as in Figure 3.5, and assuming that it can be regarded as a steady-state linear time-invariant system, the system output stimulated by the PRBS can be represented by the following equation [61]:

$$y(n) = \sum_{k=1}^{\infty} h(k)\, u(n-k) + v(n) \tag{3.4}$$

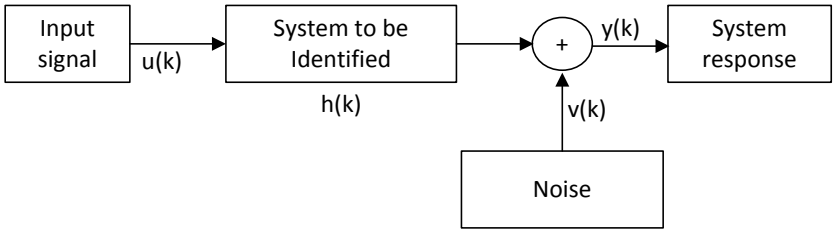

FIGURE 3.5: System to be identified

Where the $y(n)$ is the output signal of the system, $h(k)$ the impulse response of the system to be identified, $u(k)$ the input signal, which is the PRBS pattern in our case. The disturbances, modeled by white noise are represented by $v(k)$. The cross correlation of the input signal with the output signal is given by:

$$R_{uy}(m) = \sum_{n=1}^{\infty} u(n)\ y(n+m) \tag{3.5}$$

$$= \sum_{n=1}^{\infty} h(n) R_{ii}(m-n) + R_{iw}(m) \tag{3.6}$$

$R_{ii}(m)$ represents the autocorrelation of the input signal, and $R_{iw}(m)$ its correlation with an unrelated white noise perturbation. When the PRBS pattern is long enough, it starts to exhibit white noise properties. Thus $R_{ii}(m)$ becomes a Kronecker $\delta(m)$, while $R_{iw}(m)$ becomes zero.

$$\begin{cases} R_{ii}(m) = \delta(m) \\ R_{iw}(m) = 0 \end{cases} \tag{3.7}$$

When equations 3.6 and 3.7 are combined, the expression of the cross correlation is simplified significantly, and one obtains:

$$R_{uy}(m) = h(m) \tag{3.8}$$

This property enables the detection of the PRBS signal submerged in noise magnitudes larger than the stimulation.

3.5 Applications and Implementation

Pseudo-Random Binary Sequences can be utilized in a wide range of applications [62]. They are employed during design and testing of electrical equipment such as position encoders, measurement transducers or AD converters . The sequences are also frequently used in the field of communication, and also in system identification, i.e. in order to measure the frequency response of the systems under test. In addition, another wide field of application lies in scrambling, cryptographic applications and data checkers [63]. Finally, applications are found in surface characterization and 3D scene modeling, and in audio applications to test and characterize loudspeakers.

There are several methods to implement a Pseudo-Random Binary Sequence generator. It can be directly implemented in hardware, with a discrete shift register and flip-flops, using a microprocessor, or using a FPGA-based implementation. In addition, due to the low cost of memory, storing the complete sequence in a FIFO memory element has become a viable alternative as well. During acquisition, the receiver consists of the same LFSR that is used at the transmitter. The receiver needs to be synchronized initially. This is done through correlation, since the incoming PRBS codes on the receiver are known beforehand. Once synchronization is done, the received sequence is shifted through the LFSR bit by bit.

3.6 Power Spectrum

The power spectrum of a N-stage sequence has a $sin(x)/x$ envelope, as shown in Figure 3.6 [64]. The nulls in the spectrum occur at $f = n/T$, where T is the bit duration and n is an integer depending on the ratio between bit duty-cycle and sampling frequency. From 0 to $1/T$ the spectrum covers all the frequencies with a spacing of $1/(N-1)T$ Hz. The frequency spacing can be reduced by choosing a longer sequence. Due to the nearly uniform spectral density within the $2/T$ Hz band, the PRBS sequence is an ideal deterministic test signal, and is widely used in data communications to simulate the white noise type signals. An equivalent noise source with white Gaussian characteristics can be built with a long PRBS sequence generator [21].

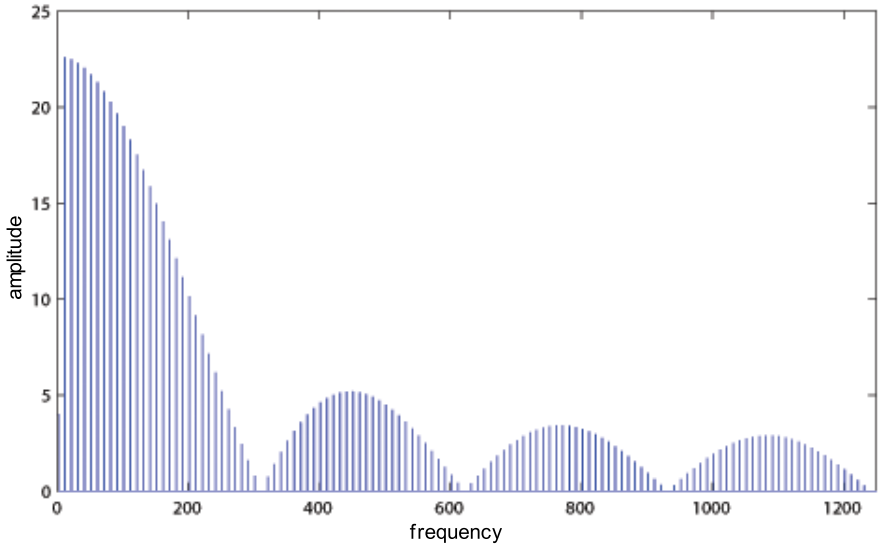

FIGURE 3.6: Spectral envelope of PRBS

From the description above, there are three degrees of freedom to shape the spectrum of the PRBS. namely the code length ,the bit duration and the positive duty-cycle of the bit. The longer the bit duration, the more dominant low frequency components will be. Choosing longer bits adds more zeros to the spectral envelope and amplifies the lower part of the spectrum. Figure 3.7 highlights several variations in PRBS bit-length and their impact on the spectral envelope.

All other parameters kept identical, reducing the duty-cycle of the bits increases the high frequency component, rendering a more flat spectrum. These two parameters are commonly changed in order to shape the spectral envelope to reduce the amplitude on problematic frequencies and to amplify the frequencies that are to be stimulated.

In addition, the spectrum can also be shaped through the sequence length. In fact, the code length has an impact on the spikes of the spectrum. Alternatives for the PRBS code injection are to either run a long PRBS code, or replicate a shorter one several times. The longer sequence will cover the spectrum more evenly, the spikes are less spaced. The shorter sequences have long distance between spikes, but the amplitude of the spikes are higher, thus focusing the energy on a limited number of frequencies, as it can be seen in 3.8. This allows to avoid frequencies that are not to tampered with, such as ripple control frequencies, in power system identification [65].

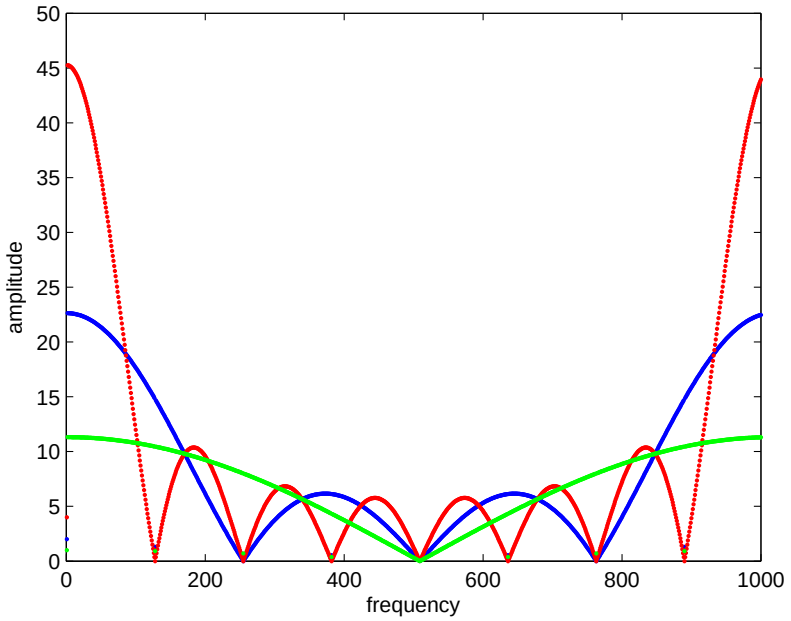

FIGURE 3.7: Impact of bit duration and bit-duty cycle on PRBS spectrum, Green: bit duration at half the sampling frequency, Blue: bit duration a quarter of the sampling frequency, Red: bit duration an eighth of the sampling frequency

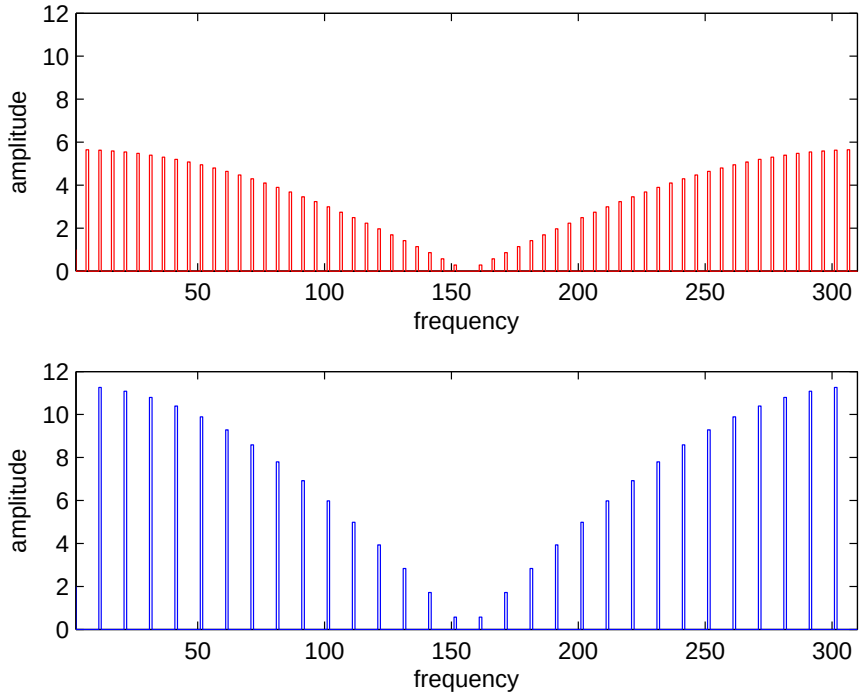

FIGURE 3.8: A Pseudo Random Generator with polynomial $1+x^3+x^4$, generating a repeated random sequence of 15 bits

3.7 Pseudo-Noise Sequence Variants

3.7.1 Maximum Length Sequences (MLS)

The MLS sequences are a subset of PRBS sequences, and have been presented in detail earlier, consisting of an important subset of PRBS sequences [66]. They exhibit ideal characteristics for auto-correlation and cross-correlation with other sequences. Thus they are well adapted for system identification. Their main drawback is that their number for each sequence length is limited. Only a small subset of tap settings for each length produces an MLS, and the exhaustive list can be found in [60]. For example, for a 6 bit PRBS, there exist only 6 MLS sequences which are listed below.

$$1 + x + x^5 \tag{3.9}$$

$$1 + x + x^3 + x^4 + x^6 \tag{3.10}$$

$$1 + x^5 + x^6 \tag{3.11}$$

$$1 + x + x^2 + x^5 + x^6 \tag{3.12}$$

$$1 + x + x^3 + x^5 + x^6 \tag{3.13}$$

$$1 + x + x^4 + x^5 + x^6 \tag{3.14}$$

For longer sequences the number of MLS's increases exponentially, e.g. a 30-bit LFSR can generate 17820000 orthogonal MLS sequences. Thus if only a small number or sequences are needed or if the LFSRs utilized are large, MLS is preferred. For cases, where a large number of shorter codes is needed (e.g. CDMA transmissions), alternative sequences might be better options.

3.7.2 Gold Codes

The auto-correlation properties of MLS are ideal. But, their main problem is the availability of enough codes in a system with a larger number of users. Gold codes allow the creation of a large number of codes with the same run length but inferior correlation properties [67]. As shown in Figure 3.9, they are generated through XOR-ing of two same length MLS sequences, and the sequences are shifted cycle by cycle synchronously. Since the two MLS sequences are of the same length, the generators remain in sync throughout the sequence. The auto-correlation of

Gold codes are non-maximal, thus worse than MLS sequences. Every position change in phase between the two base codes generates a new Gold sequence. The number of possible gold codes with similar correlation properties is very large. That represents their primarily attraction. In fact, any two MLS sequences of length L can generate $2^L - 1$ Gold sequences.

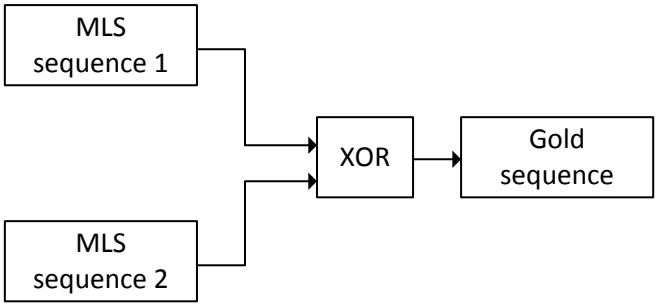

FIGURE 3.9: Gold code generation by combining two MLS sequences

Given that the number of codes is large, typically a subset is chosen so that the autocorrelation and cross correlation between the codes remains within a boundary.

3.7.3 Kasami Codes

Kasami sequences have good cross correlation properties. Like the Gold sequence, the Kasami sequence is derived from the MLS sequence. A secondary sequence is created from the MLS sequence by down-sampling by a factor T where $T = 2^{N/2}+1$ [68]. Kazami sequences are then formed by XOR-ing the original MLS and a cyclically time shifted versions of the secondary sequence.

3.8 Applications for Power System Characterization

PRBS sequences have unique properties that make them very suitable for excitation signals in characterization and parameter identification in power systems:

- **Spectrum:** Depending on the relationship between the code-length, sampling frequency and code frequency, the PRBS exhibits a white noise like spectrum for a certain frequency range, with zeros occurring at multiples of the PRBS clock sampling frequency. For impedance determination, a high amplitude is necessary in the desired frequency range in order to achieve optimal energy distribution and accuracy. This has to be mitigated with the injected Total Harmonic Distortion (THD) to find the adequate compromise between Signal-to-Noise Ratio (SNR) and harmonic pollution. The code length and its sampling frequency limit the resolution of the impedance spectrum that will be excited. The objective is to enable an injection method that will cover the desired range, with the hardware constraints of an inverter.

- **White Noise Behavior:** The PRBS exhibits white noise-like properties, and thus correlation techniques, eliminating measurement noise can be utilized for identification purposes.

- **Ease of Generation and Implementation:** The digital logic required for PRBS implementation consists of shift registers and XOR gates and can be implemented on a very modest digital controller. The inverter software or firmware could therefore be reprogrammed to generate PRBS sequences.

- **Low Crest Factor:** Injected in a network, its operational crest factor is very low and the instantaneous THD is significantly less than other identification methods [69] [70]. This is accomplished without compromising accuracy, since the low amplitude pulses, which are aggregated over the complete sequence, provide sufficient energy for identification. Since the grid codes mandate a low THD [71], the PRBS is more adapted than other proposed injection signals (i.e. spikes) to create a broad spectrum.

- **Correlation:** The power system is a complex entity with many different sources interacting with each other. Harmonics and interharmonics emitted from converters, non-linear loads, switching capacitors and switching inverters, create an environment with multiple interferences, rendering system characterization difficult. The correlation properties of the PRBS sequence allows the signal to effectively filter out all uncorrelated noises and to produce effective results even in very low SNR conditions.

3.9 PRBS implementation on a Single Phase Inverter

The system topology considered is depicted in Figure 3.10. It comprises a DC Voltage source, with a Pulse-Width Modulator based Voltage Source Inverter connected to the grid through an output low pass filter.

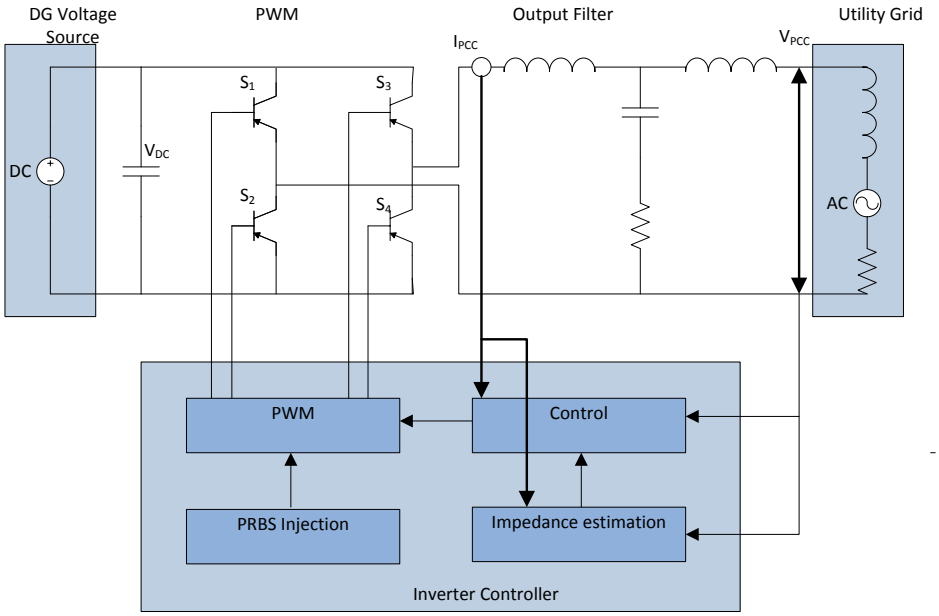

FIGURE 3.10: Grid-connected inverter with LCL filter and time-variant and frequency-dependent power grid

Typical modern grid tie inverters operate with LCL filters, due to their superior filtering capabilities at higher frequencies [54]. The main drawback of the LCL filter is its high resonance spike induced by the capacitance in parallel between the inductors. In order to reduce the gain of the resonance, a damping resistor is connected in series with the capacitor. This setup limits the currents passing through the capacitor and attenuates the voltage gain at PCC for the resonant frequency. An analytical model of a common inverter architecture has been established in Chapter 2, and the resonance frequency of the output filter is given in Equation 3.15.

$$f_{res} = \frac{1}{\sqrt{2\pi}} \sqrt{\frac{L_i + L_g}{L_i \cdot L_g \cdot C}} \tag{3.15}$$

From 3.15 it can be seen that f_{res} is dependent on the grid impedance and an increase in the grid's inductance causes a decrease of the resonant frequency. Thus, ideally the filter should be designed with an estimate of the power system's inductance in mind, so that the resonant frequency falls in the range:

$$f_g \ll f_{res} < f_{PWM} \tag{3.16}$$

In fact, it should be sufficiently larger than the fundamental frequency and distinct from prominent grid harmonics. This constraint minimizes its interference with the fundamental and the PWM's switching frequency.

The PWM control signal is used to steer an H-Bridge inverter. Details about the structure and functionality of a three level PWM have been given in Chapter 2. In this Section, several methods will be considered for overlapping PRBS sequences on the inverter output signal. The factors considered for an ideal implementation are the following:

- **No Hardware Addition:** The proposed solution should have minimal cost impact and involve software/firmware modification of the inverter's PWM controller. Solutions involving additional generators and transistors were not considered.
- **Minimal Impact on Inverter Control:** Solutions modifying the fundamental frequency and the reference signal attributes are more prone to have an impact on the voltage/frequency control of the inverter.
- **Minimal Transistor Switching:** Methods increasing transistor switching will render additional losses. Also, they will most likely increase switching frequency and go beyond the operational limit of the transistors. Thus methods with low switching will be preferred.
- **PRBS Correlation:** For identification purposes, it is important that the correlation with the PRBS is maximal. Some methods modulate on the fundamental a signal that is closely correlated to the PRBS signal, some produce one that is less correlated.

- **Low THD:** Methods with smaller THD are preferred. For the same strength of PRBS, some methods add more parasitic noise, others less.

Five of the considered methods are listed below. Their characteristics are plotted, and a quick assessment of their properties are given.

3.9.1 Fundamental Generation without Stimulation

As a baseline Figure 3.11 shows the parameter of the inverter's output signal without injection. The carrier frequency is set to 20 kHz, and the reference signal is a pure sine. In the PWM output spectrum, a spike is seen at the fundamental frequency as well as the switching frequency and its multiples. The cross-correlation with the PRBS shows a completely uncorrelated signal, and the purpose of the proposed methods is to create a correlation plot that is a close as possible to a delta function.

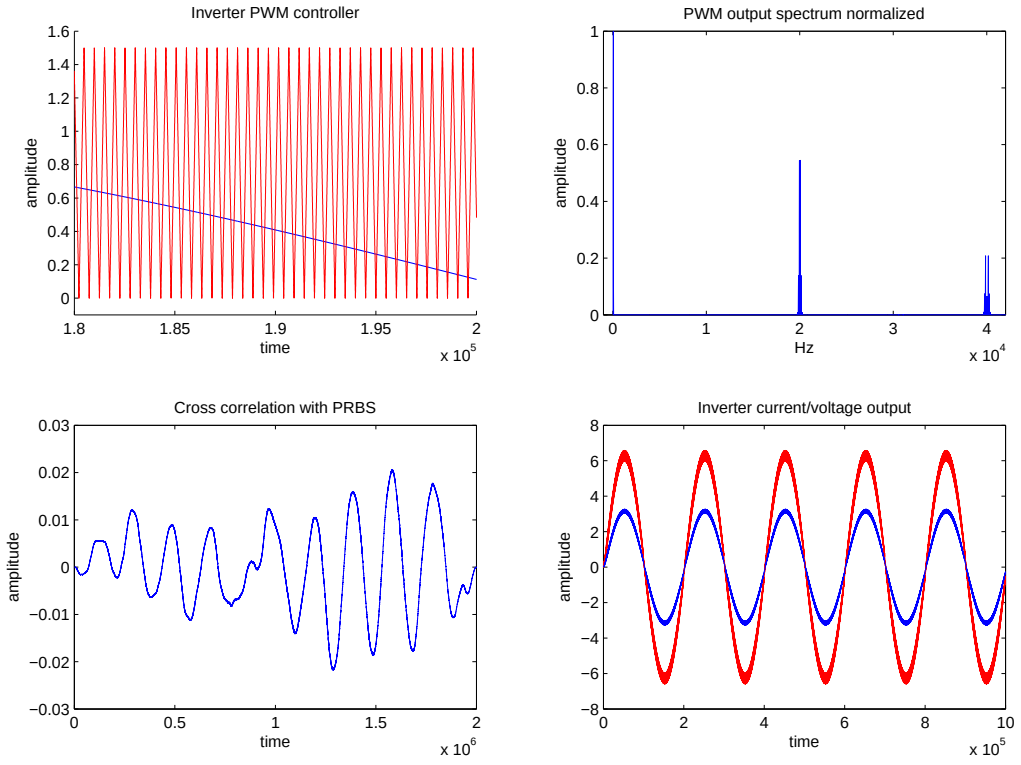

FIGURE 3.11: Baseline Inverter Output Signal

The current (in blue) and voltage at the PCC (in red), show clean signals, with minor noise due to the switching frequency.

3.9.2 Carrier Clock Modulation with PRBS

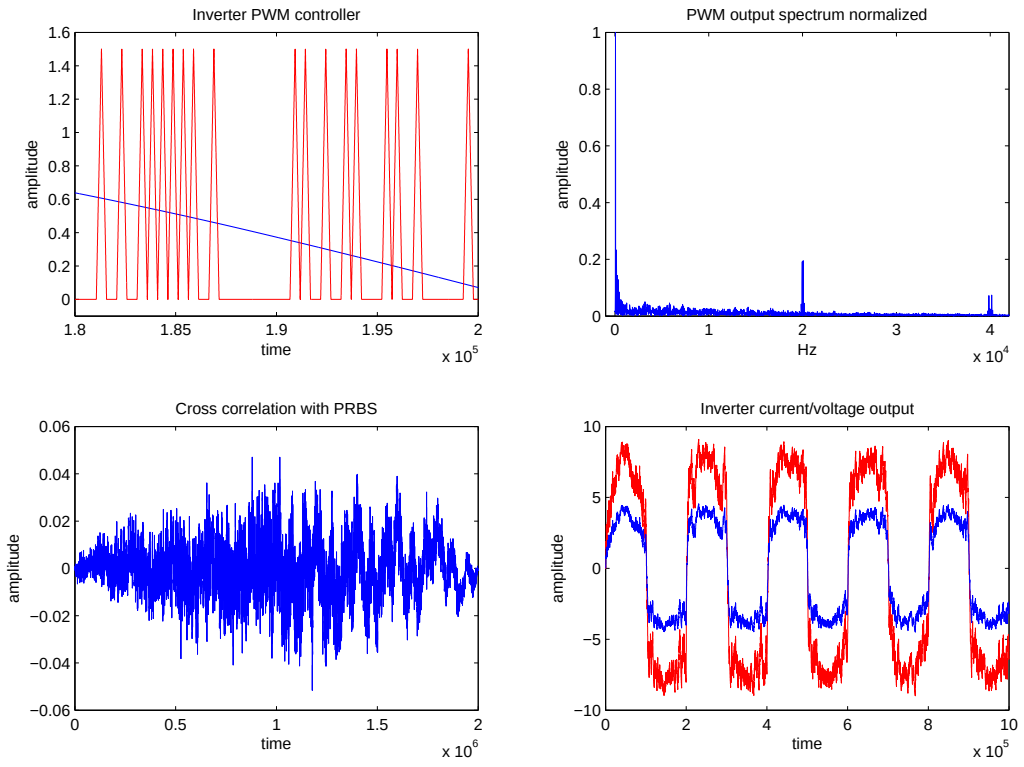

FIGURE 3.12: Carrier Clock Modulation

In this method, shown in Figure 3.12, one PRBS code is allocated to each carrier cycle. When the code is '0', no carrier signal is produced, thus no switching is generated. This effectively halves the switching frequency, by only toggling on cycles on which the PRBS code is '1'. The consequence of this manipulation is the modulation of the fundamental with variations correlated to the PRBS. The spectrum shows that the switching frequency peak is much lower, and that a broad range of frequencies are stimulated. On the other hand the correlation with the PRBS is very weak. Thus, this is an effective technique for broadband noise injection, but the obtained result is not satisfactory as far as code-correlation is concerned. Also, there is no possibility for fine-tuning the amount of noise injected, and as shown in the voltage and current time plots, the THD of the output parameters are unsatisfactory.

3.9.3 8-bit Parallel PRBS as a 'White Noise Generator' for the Carrier

This solution proposes to replace the carrier with a 8-bit noise generator comprised of 8 orthogonal PRBS sequences. A randomized carrier signal has the advantage of a broad switching frequency spectrum, as can bee seen in Figure 3.13. As expected, no switching frequency peak is apparent. Unfortunately, in this case the maximal switching frequency of the PWM had to be put twice as high as it was the case for the regular case. The number of switchings is withing the acceptable range, although the switching frequency threshold of the transistors might potentially be exceeded. The produced output wave is reasonable, but the correlation with the codes is very weak. Therefore, this solution is adequate for minimizing switching frequency peak for acoustic/resonance issues, but it doesn't produce satisfactory results for PRBS injection.

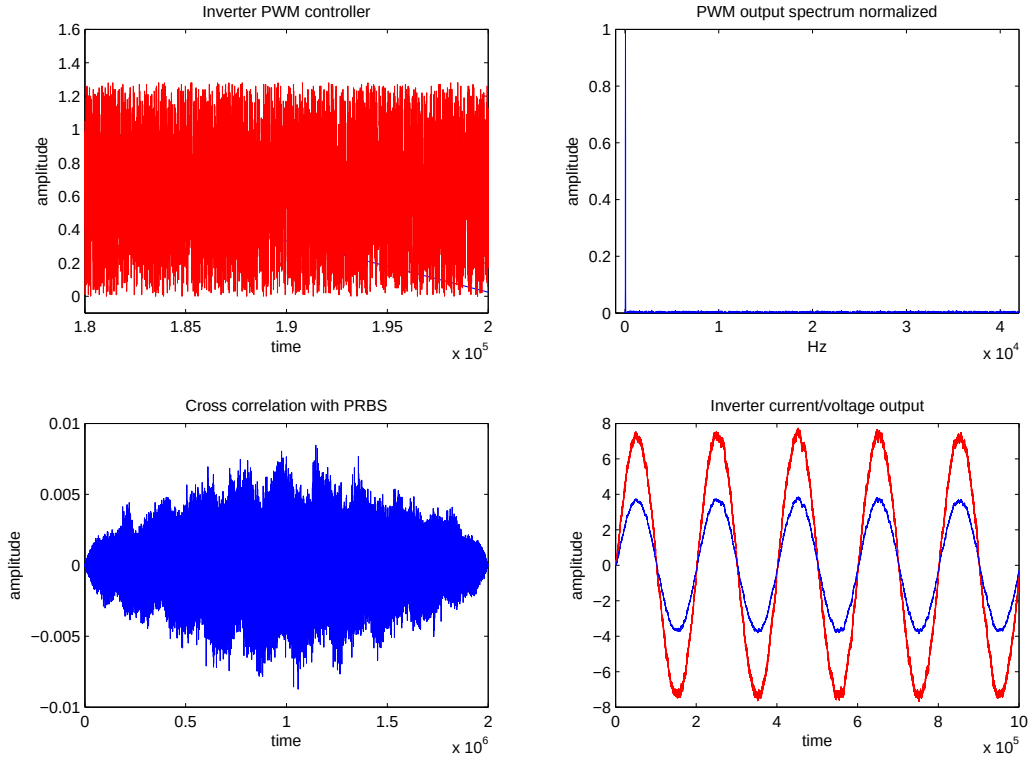

FIGURE 3.13: Carrier 8-bit Noise

3.9.4 Reference Signal Modulation with PRBS

The proposed technique modifies the reference signal to add the PRBS signal as a modulation, and assigns one PRBS code to the equivalent time period of each carrier cycle. This solution produces optimal results if the modulation is in sync with the carrier signal. This assumption is valid in ideal settings. In reality, the reference signal is provided by the PLL and various control related changes can alter the reference signal. These constraints make it difficult to guarantee that the modulation of the reference signal remains in phase with the carrier switching and thus difficult to obtain a clean signal at all times. On Figure 3.14, it can

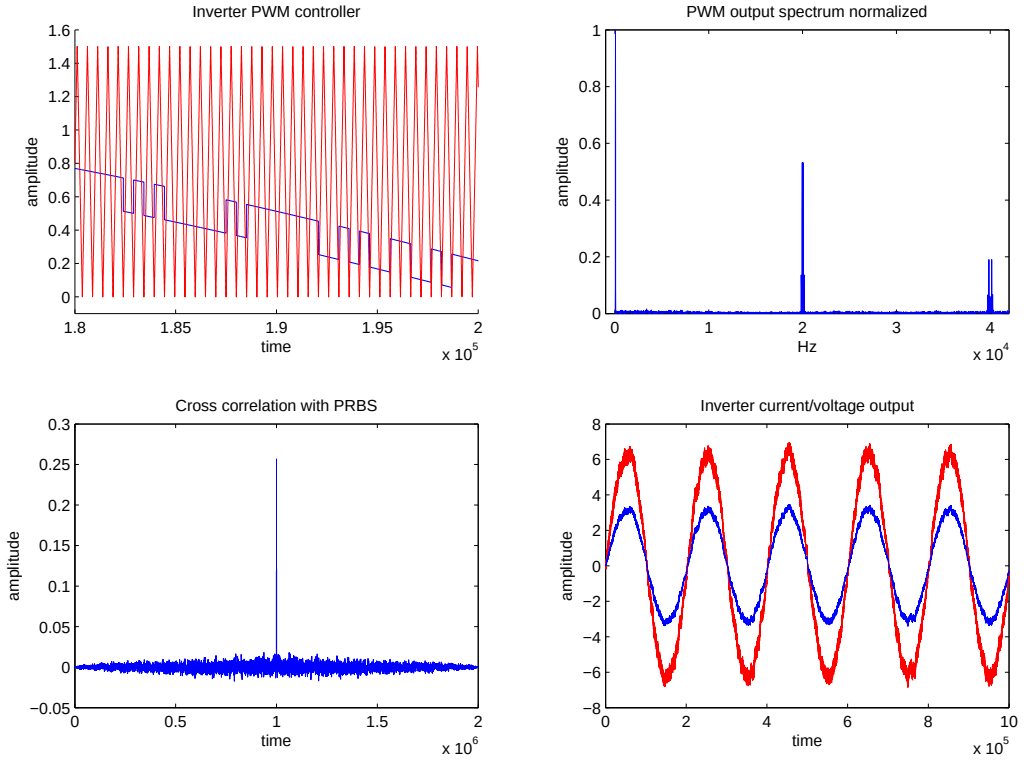

FIGURE 3.14: Reference Signal Modulation with PRBS

be seen that the correlation is excellent, the transistor switchings haven't been altered and that the spectrum contains the fundamental, switching frequency, and a broad range of low amplitude frequency components stimulated by the PRBS. The drawback of this method is the difficulty to synchronize effectively the reference signal stimulations with the carrier reference.

3.9.5 Carrier Modulation with PRBS

While the solution in the previous subsection did provide an acceptable method for signal injection, it is preferred to work with carrier modifications, since these modifications are well decoupled and have a limited impact on inverter and PWM control. Therefore, the solution proposed in this section raises/lowers the carrier triangle peak based on the injected code. This should in theory add a jitter to the created pulses, making '1' pulses a little wider and '0' pulses narrower. This solution is highlighted in 3.15;

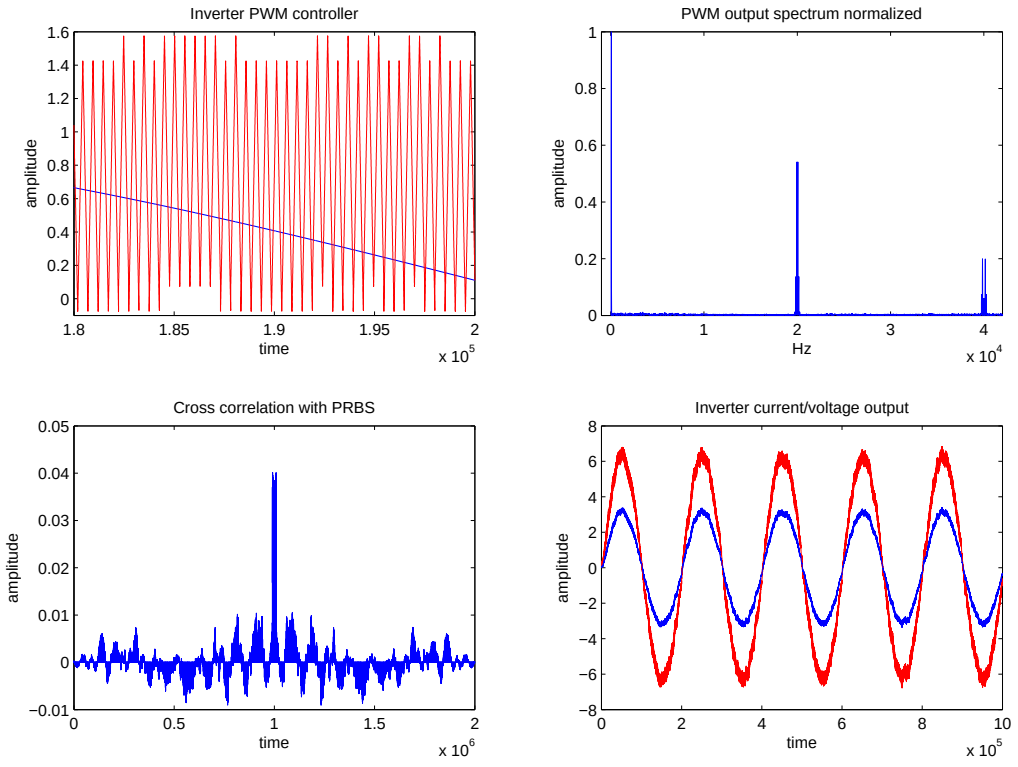

FIGURE 3.15: Carrier Modulation with PRBS

While it does work well for time intervals when the sine wave has a high amplitude, the zones with low amplitudes cause problems and frequent miss-switching is observed. Reducing the magnitude of the peak shrinks the problematic zones, but the problem remains and on fundamental frequency variations, the carrier and the reference might misalign and create erroneous stimulation signals for a certain time interval.

3.9.6 PRBS Duty Cycle in Carrier Signal

The previous experiments finally led to the solution adopted in this thesis. No modifications of the reference signal are required in this method, and the switching frequency of the carrier is not modified from the original shape. In each carrier cycle, a duty-cycle is reserved for PRBS generation. As seen in later Chapters of the thesis, good identification results can be obtained with a duty cycle of 0.5-5%. During this duty-cycle, the PWM if forced on a '1' PRBS cycle, and forced off on a '0' cycle. On the rest of the carrier cycle, the generated pulses produce the fundamental from the reference signal. The details of the operation mode can be seen in Figure 3.16.

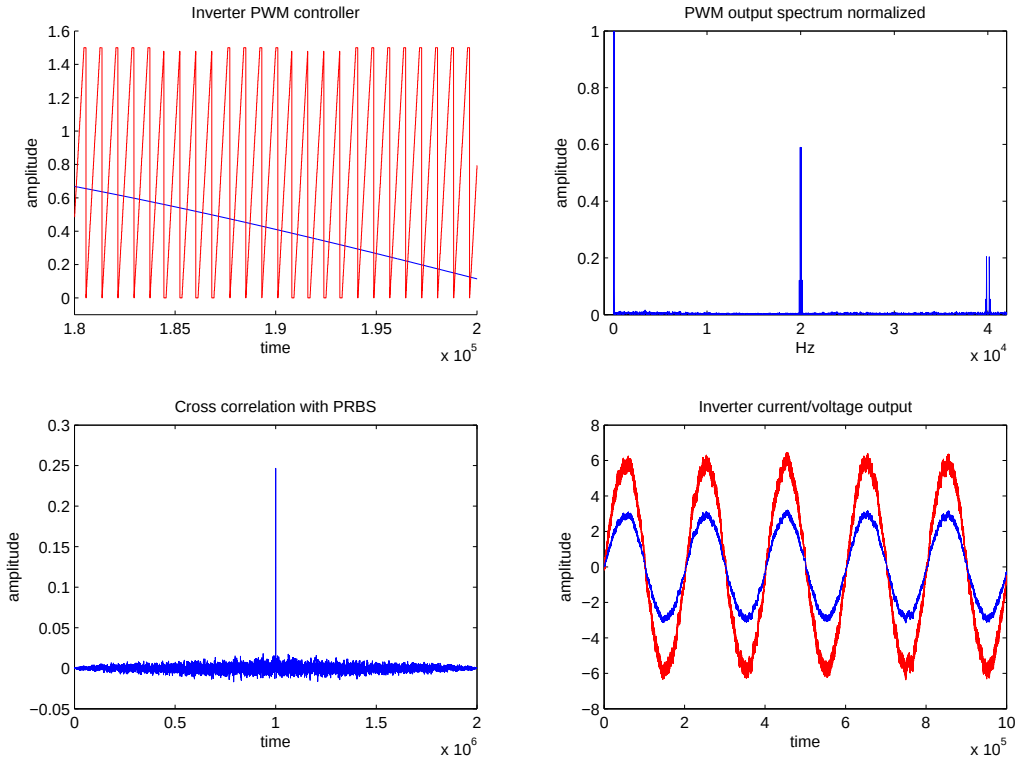

FIGURE 3.16: PRBS Duty Cycle in Carrier Signal

This solution combines all the advantages of the previous solutions, namely a broad and adjustable spectrum stimulation, good correlation properties with the injected code, and no transistor switching increase from the baseline. Effectively, the pulses produced by the standard method are added a jitter, based on the PRBS code.

3.9.7 Conclusions

In this Chapter, PRBS signals were investigated and their properties and attractiveness for system identification were highlighted. PRBS sequences are orthogonal to each other, stimulate a broad spectrum and are easy to generate. Methods have been proposed for having a PWM based inverters inject those codes in the power network while feeding in power. Several schemes requiring minor PWM reprogramming were presented. The final solution proposed meets all the desired criteria, since it is minimally intrusive in the inverter's operation, generates the stimulation signal without requiring additional hardware, and exhibits satisfactory spectral and correlation properties.

In the next Chapters, the proposed injection method will be used for characterizing various parameters of the power system. Chapter 4 treats the topic of islanding detection i.e. the standalone detection of the inverter about its connection status to the mains. The necessity and difficulty for this detection is highlighted, and alternative solutions of the state of the art are listed. Finally the solution based on PRBS injection is presented, tested and evaluated.

Chapter 4

Islanding Detection

4.1 Purpose of Islanding Detection

The IEEE definition of an island grid is a portion of an energized power system containing at least one power source and load that is disconnected for a specific time period from the rest of the network.

Power system islanding can be intentional or non intentional. Intentional islanding is the purposeful disconnection of a power system's sub-system, which is initiated knowingly, for example during disturbances in the system [72]. The created islands are then operated in a way that a continuous supply of power is available when the main power system is non-operational. The distributed generators feed the loads of the island until reconnection with the main utility system occurs. Intentional islanding is performed in a controlled manner, typically with no load flow between the island and the grid, and with frequency and voltage regulators monitoring and adjusting the parameters in the process. Although intentional islanding could theoretically improve customer reliability in outages, having DGs operate in islanding mode is currently very chlen gelallenging and requires studies of the impact on voltage profiles, protection mechanisms and load profiles. As of now, the costs involved in adding these capabilities for small DGs outweigh the advantages of having them operate in islands. But this paradigm is changing and research in island driven DGs has advanced the state of the art considerably [73].

On the other hand, unintended islanding typically happens during heavy load flow, and has a negative impact on the system, causing power imbalance leading

to voltage and frequency stability issues [74]. Thus, for typical systems, the current standard is to disconnect all DG sources from the island as soon as islanding has been detected.

In fact, if more energy is available in synchronous generators in the island than can be consumed by the loads, the high inertia of the rotating masses will cause the fundamental frequency to rise [75]. If there is a lack of power available, the opposite will happen and frequency drops. When excessive reactive power is available during islanding, the voltage increases; if there is a shortage, the island voltage decreases. Overvoltages and frequency variations can potentially damage components in the island and cause hazardous situations [76]. Typically, large power imbalances cause the island grid to collapse rapidly. But if generation and load stay more or less balanced, the island can stay operational for some time even without regulators.

DGs are commonly equipped with protective relays, in order to shield them from abnormalities in the system. Over and under frequency and voltage relays cause it to trip when the voltage or frequency go beyond its operational limits. DGs need to be able to detect islanding and initiate steps to protect them from unintended islanding [13]. In fact, power systems are comprised of very complex structures that can spread over continents and it is not always possible to fully comprehend their behavior with the limited visibility available. In addition, a large part of their operation is automated. For instance, many temporary faults are cleared without human intervention. Examples of temporary faults are the insulation breakdown by the interaction between components and external factors such as lightning strikes, wind or transient tree contacts during a short period of time [77]. Permanent faults require the damaged component to be repaired or replaced. The purpose of the recloser is to clear temporary faults in a simple manner, given that over two thirds of faults happening on the power system are temporary and are cleared by reclosers. In a system where a substantial amount of energy is produced by distributed generators, the situation becomes challenging. When the recloser is disconnected, the DG generators downstream in the temporary island might go out of phase with the mains. Upon reclosure, even a slight frequency discrepancy between the two systems can cause tremendous powershifts which can cause substantial damage to the electrical equipment and infrastructure [71]. Thus, in order to prevent these scenarios, either the DG needs to automatically disconnect to prevent these issues, or the operator needs to have other means of

TABLE 4.1: Outreclose Times in Germany

Voltage of Power System	Max Autoreclose open time
130 kV	1 second
50 kV	3 seconds
20 kV	20 seconds

avoiding this situation. Common reclose times in are set in Table 4.1. Automatic reclosing against an energized feeder also causes capacitive transition switching and high overvoltages. A DG is typically a weak energy supply with little inertia that doesn't have the capability to handle system transients. In addition, unintentional islanding can be a safety issue for the grid operator. If the maintenance personal disconnects a sub-grid for servicing, a DG in the sub-grid which still feeds in power can be very dangerous. References [78] [79] provide a comprehensive list of issues and solution for islanding in networks with DGs.

For DG islanding detection, the implemented checker needs to be reliable, and have minimal non-detection zones. Every bad tripping involves production loss and reliability loss. On the other hand every missed detection can have catastrophic effects. The method needs to be fast, and for instance react within the reclosers automatic response time shown in Table 4.1. An ideal islanding detection mechanism would operate in all conditions with high reliability and security. Unfortunately, designing a method with minimal non-detection zone for all situations and load profiles with minimal power quality impact is very difficult. Each proposed method in the literature varies by its sensitivity, quality and rapidity, and many methods fail in the critical condition where the island is nearly balanced with minimal powerflow at the fault.

4.2 State of the Art of Islanding Detection

There are numerous proposed method for islanding detection in the scientific literature, each of them having their own benefits and drawbacks. They can be typically categorized in three categories, passive methods, active methods, and impedance monitoring methods. In the following section, the main ideas proposed in the literature will be detailed.

4.2.1 Passive Methods

Passive methods use locally available data and measurements (e.g. frequency, voltage, current) in order to infer islanding status. The advantage of passive methods is that they don't interact with the system. There is no pilot or test signal injected, and there is no modification of the powerflows induced. Thus these methods don't have an impact on power quality or power stability. While some methods, do require communication with a central station, it is preferred that no communication is needed and a stand alone system is desired, since traditionally communication is deemed unreliable and expensive. On the other hand, recent strides in ICT technology have generated an increase in methods based on communication tools. Research in [80] for instance proposes to gather data from several PMUs to infer islanding status on DGs in a distribution network.

4.2.1.1 Voltage and Rate of Change of Voltage

The simplest and most common islanding detection method is based on voltage measurement. The voltage magnitude is measured at the DGs PCC, and the DG is equipped with a protection relay that reacts to over and under voltages. When a loss of mains occurs, the voltage fluctuates due to the imbalance between production and consumption. The protection relays are programmed to react to those over and under voltages, but in a way that Fault Right Through (FRT) grid codes respected, thus delaying the tripping appropriately in order to ensure that short circuit power is provided in case of a fault [81]. While this is the most common islanding detection mechanism in currently installed DGs, this method has a few drawbacks. In fact, over and under voltages can be caused by numerous events on in the power system, and the stand-alone relay cannot differentiate between islanding, sudden loss of load, generator tripping or line fault. In addition, there is always the possibility that islanding happens without major power imbalance, thus causing minimal voltage fluctuations and going undetected for some time period. In order to improve detection, methods based not on the voltage amplitude but on the rate of change of voltage have also been applied as an islanding detection mechanism [82]. This follows the principle that in distribution systems connected to a strong grid, voltage variations are slow, but that in case of an islanded system, the rate of change of voltage variations seen will be much higher.

4.2.1.2 Frequency and Rate of Change of Frequency

Frequency based passive islanding detection methods are commonly performed as an additional and complementary test to voltage checks. They are usually targeted for synchronous generators and take into advantage the fact that inherently, the frequency of rotating masses are related to the loads they are powering. When islanding happens and the local load of the subgrid exceeds their production, the generator slows down and since the generator cannot keep up and its rotation, frequency drops. In this situation, the island can be detected through an under-frequency relay. On the other hand, if there is a production surplus in the island, over-frequency is detected [83]. Frequency variations can also happen without islanding, causing false islanding alerts or sudden changes and transients from real load and production discrepancies. To improve the islanding detection reliability, the derivative of the frequency can be taken into account and Rate Of Change Of Frequency (ROCOF) is considered for islanding detection. This method doesn't rely on the change in frequency, but on df/dt. Thus, a DG disconnects when the frequency change rate exceeds a predefined threshold [84]. This function is disabled during startup and in order to prevent false tripping. The application of ROCOF is assuming that frequency changes occurring to normal grid operations are slow and will not exhibit as drastic and quick variations as during islanding.

4.2.1.3 Voltage and Current Harmonics Variation

Voltage and current harmonics are present in systems with high inverter penetration. Harmonic monitoring methods rely on non-fundamental noise present in the grid, e.g. transient noise and converter noise [85]. Islanding detection can be performed by taking into account the THD seen at the inverter output. Once islanding happens, the THD exceeds the threshold set by the detector and trips the generator. Assuming that the grid connection is stiff, a system connected to the mains will have considerably lower voltage THD than one operating in an island. Harmonics in the networks are produced by loads and generators, such as motor drives, inverters or non-linear loads.

For example, the method in [86] uses the switching frequency of the inverters Active Shunt Filter (ASF) to act as a naturally occurring harmonic, and estimates the impedance based on its magnitude variation. This class of identification methods has the disadvantage of relying on harmonics and inter-harmonics distortions

existing at all times. As their occurrence and amplitude cannot be guaranteed, it is not an dependable solution in critical situations. Thus, the main drawback of these proposed methods are that harmonics present are not predictable and that this method cannot always be applied as a high confidence tool for islanding detection.

4.2.1.4 Islanding Detection through Voltage Unbalance

Voltage unbalance is an additional method researched in recent years. Given that loads in the distribution networks are typically single phased, the system is most of the time operating in slight imbalance. This imbalance is amplified in islanded systems. The difference in powerflow in each phase will be the parameter used for islanding detector. With this method, the threshold setting will greatly vary depending on the connected rotating machines and unbalanced loads. The solution proposed in [87] relies on the ratio between negative sequence and positive sequence. By assuming that the impedance between an islanded system and non-islanded system are considerably different, a change of state will trigger substantial voltage fluctuations.

4.2.1.5 Vector Shift

Typically in a subgrid, the powering of the load is shared by local distributed generators and the main grid power. The voltage drop at the DG is determined by the power it delivers, thus by the current drawn form it. When an island situation occurs, power from the mains is lost, and the distributed generators in the island provides all power to the load. This will increase the current drawn and the voltage drop is increased as shown in Figure 4.1. The consequence will be an increased load angle. Islanding detection based on vector shift compares measurement samples in the time domain, and if sudden jumps are detected, a load angle change is assumed and the generator is tripped [88].

Unfortunately, as with most other passive techniques, other events on the grid can cause sudden load variation as well, such as line faults, or generators tripping/starting up. This is a common problem in passive methods, since the events that are monitored could be triggered by multiple causes and there is no completely reliable method to prevent non-detection and false-detection. Thus, active methods

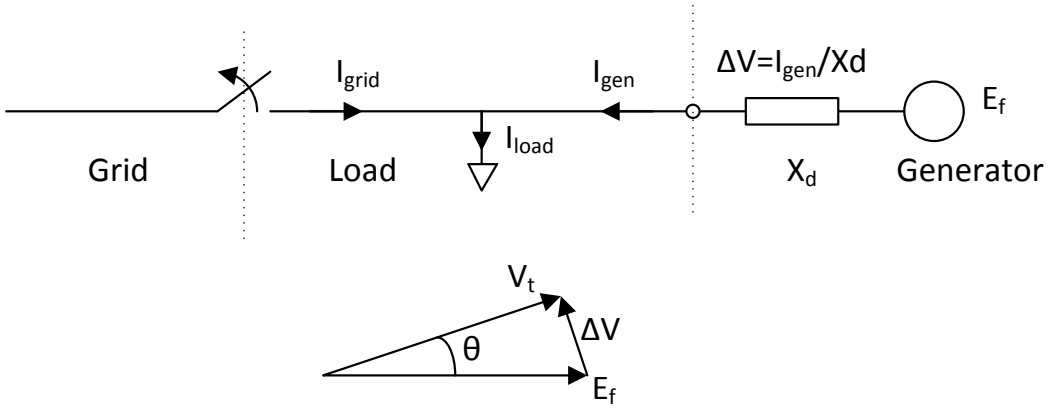

FIGURE 4.1: Voltage Phase Shift at Inverter PCC on Islanding

have been developed to increase the reliability of islanding detection, at the cost of reducing power quality and affecting the operations on the grid through slight modification of powerflows or injection of stimuli.

4.2.2 Active Methods

Active methods distort the voltage and current by modifying inverter behavior or by injecting signals, measure the grid's response, and obtain relevant information through signal analysis. Numerous active methods have been proposed in recent years, some focusing on effects of transients, others measuring the grid response to steady-state signals. Below are listed some of the most common islanding detection methods using a DG stimulation to improve detection accuracy. Some proposed techniques rely on modification of the inverters control mechanism and signal processing capabilities, while others require additional hardware infrastructure.

4.2.2.1 Inverter Induced Frequency Shifting

This method, also called Slip Mode Frequency Shift (SMFS), is an islanding detection technique for inverter based DGs [89]. It modifies the output frequency by drifting it away from the fundamental. The algorithm is implemented through small modifications of the inverter's PLL. In normal working conditions, the PLL tracks the phase of the fundamental. For the purpose of islanding detection, it is

modified so that it is always slightly out of phase with the fundamental. When the DG is connected to a stiff grid, the frequency remains stable and doesn't drift. On the other hand in an island, when the frequency is increased in the inverter control, the frequency measured at the PLL will drift and a negative phase error will be seen, causing the frequency to fall out of acceptable limits and tripping the DG. Thus, the DG tries to move grid frequency from measured value from PLL. If it succeeds, the grid is assumed to be weak and the DG is probably feeding in an island.

The implementation of this method is relativity straightforward, and non-detection situations are relatively moderate. Issues with this methods are mostly due to the impact of loads that have a high quality factor and resonance frequencies close to the line frequency. Also, systems with large amount of DG may see power quality issues and transients, due to the induced frequency variations caused by the inverters.

4.2.2.2 Inverter Induced Reactive Power Variations

This method can be applied on inverters that have the ability to control their reactive power output. If the reactive power output can be modulated, the controller can generate small fluctuations from the voltage regulator output. On a weak grid, these fluctuations will have a significant repercussion on power system and frequency fluctuation can be observed. On a strong network, the stiffness of the grid will dampen the fluctuations and no changes are observed. Thus, if frequency fluctuations can be detected following the inverter's reactive power variations, they can be interpreted as a sign of islanding. This method is proposed in [90], and in its implementation, if the observed frequency variations go beyond a certain threshold, islanding is assumed and the generator trips.

4.2.3 Impedance Monitoring

Impedance measuring for islanding detection has been the technique that has attracted the most research interest in recent years, mostly due to its theoretically very high reliability and dependability [70] [91]. The purpose is to characterize the Thevenin impedance seen from the point of common coupling of the inverter [92]. The main assumption being that the impedance difference between an islanded

system and a system connected to the mains are substantial. In typical distribution grid, this assumption is reasonable, therefore assuming that the Thevenin impedance can be measured precisely, the risk of non-detection and false alerts are minimal. As shown in Figure 4.2, the Thevenin impedance seen from the DG is $Z_{DG} + Z_{load}$ when the DG is islanded, that means when the breaker CB_3 is open. When the system is connected to the mains, the Thevenin impedance seen is $Z_{DG} + Z_{load}//Z_{grid}$. Given that the impedance of the mains is typically much lower than the loads in the distribution network, its variations seen on islanding are substantial. Like all other methods, sensitivity and threshold setting will be different for various system configurations.

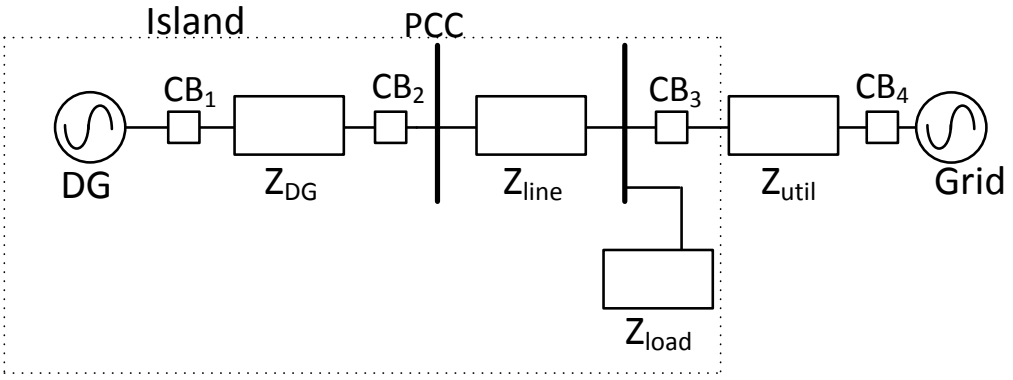

FIGURE 4.2: Impedance Variations due to Islanding

Numerous techniques can be used for impedance measurement, and these typically require dedicated hardware, consisting of a signal injector, voltage and current measurement device followed by signal processing performed on a digital controller.

In this thesis, an impedance measurement technique based on PRBS injection will be investigated. Before presenting the method elaborated in this thesis, some common techniques proposed in the state of the art for islanding detection will be shown.

4.2.3.1 Pulse Injection

One method for determining islanding is to monitor the transfer function $H(e^{iw})$ for variation in the perceived impedance. The transfer function corresponds to

the system's response to all frequencies, and signal processing techniques using pulse type disturbances have been used for impedance characterization [69]. One major advantage of these methods is that a short duration signal can stimulate a large bandwidth of frequencies, thereby providing information on system behavior on other frequencies but the fundamental e.g. strong amplitude harmonics and potential resonance frequencies.

Several techniques and variations have been presented in the literature [92]. The methods proposed typically make use of switching capacitors and/or power electronics in order to create transients. The drawback of this group of methods are the costs to integrate systems in high voltage networks, and the power quality loss they cause.

4.2.3.2 Continuous Harmonic Injection

These methods continuously inject signals at the inverter, addressing the problem of intermittence of impulses [93] [94] [95]. They can be single frequency or multi-frequency. Thus frequencies near dominant harmonics can be selected in order to avoid interference with system harmonics and fundamental and harmonics's impedance can be estimated through extrapolation.

In [18], a stimulus is selected for complex impedance spectrum measurement. This stimulus consists of a sum of sinusoids of the first 40 harmonics of the fundamental, shifted by a 5 Hz frequency shift, in order to avoid interference with major harmonics present on the grid. The complete spectrum is then obtained through interpolation between the measured frequencies. The impedance for each frequency is obtained by measuring the voltage amplitude for that frequency, in relation to the current injected. The current and voltage Digital Fourier Transform (DFT) is then produced after windowing through a Haning window. Finally the impedance for each frequency is obtained by dividing voltage by current.

The advantage of this method is the accurate broadband value of the impedance obtained. Also each harmonic injection can be curtained and adapted individually so that it doesn't violate the grid codes on power quality such as IEC 61000-3-2 [30]. Through periodic injection, the evolution of the impedance at the fundamental can be obtained, and big jumps are interpreted as a sign of islanding. By measuring the harmonics on frequencies not used for power delivery, the effect of

the generators is diminished and only the passive impedance is considered. Thus, variations in impedance most probably indicate structural changes i.e. an islanding situation. A computation with multiple frequencies increases the reliability of the measurement. By indicating broadband characteristics of the grid impedance it allow the detection of other crucial parameters such as detrimental resonance frequencies.

This category of methods has proven to be effective, if the inverter based injectors can inject the desired frequency spectrum. Problems to be solved reside in the amount of energy consumed by this technique and integration of multi signal generators in high voltage networks.

The method in this project presents an innovation that alleviates some major drawbacks of the harmonic injection methods: interference of multiple inverters and costs of injector installation. It proposes to assign a unique PRBS signal to each inverter that will interfere minimally with other inverter's signal. In addition, it intends to inject PRBS by the inverter by modifying its carrier shape, without affecting the control logic and hardware components of the inverter. In the next Section, the proposed method based on PRBS injection will be evaluated on a single phase inverter. Finally, a laboratory implementation of a custom inverter with PRBS injector is described and basic measurement results are provided.

4.3 Proposed Islanding Detection Method based on PRBS Injection

In this thesis, the developed islanding detection mechanism is an active method based on impedance measurement. The impedance of the sub-grid, as seen from the inverter's PCC is evaluated through injected stimulation signals. While these do increase the harmonic pollution in the power system, the signal amplitudes are very low, and the injection happens in short bursts. The proposed method is based on injection of Pseudo-Random Binary Sequences. These patterns have thoroughly been used in various engineering fields e.g. telecommunications and information theory, and their inherent properties suit well for system identification. The purpose of the proposed impedance identification technique is to improve upon existing methods on several aspects. Firstly, the method requires no hardware addition to currently operating grid-tie inverters. Secondly, in order to avoid grid

code violations, high amplitude transients are not injected. Thirdly, a wide enough impedance spectrum is estimated, so that the characterization can be employed other power system applications. Fourthly, the latency is low enough for time critical applications e.g. inverter power control or islanding detection. Finally, the losses due to impedance detection are minimal, in order to avoid the deterioration of system components.

The injection mechanism is depicted in Figure 4.3. In order to superimpose the PRBS on the 50 Hz fundamental, the carrier shape is altered so that the PWM naturally overlaps the PRBS with the reference signal to be generated. As shown in Figure 4.3, a '1' PRBS code corresponds to a slightly elevated triangle peak for one pulse, and a '0' PRBS code corresponds to a lowered peak. The original PWM response is depicted in blue in Figure 4.3, the altered one in red. The effect on the pulse train is that '1' pulses are slightly widened compared to the original PWM, '0' pulses slightly narrowed. Using these constraints, the PRBS code frequency will be limited to the inverters switching frequency.

Its spectrum, shown in Figure 4.4, is typically wider than the frequency range needed for identification purposes. Figure 4.4-A presents the normalized spectrum at the PWM. The peaks extending beyond the plot are due to the fundamental and the switching frequency of the PWM. On the blue plot, corresponding to the PRBS injected pattern, it can be seen that the complete spectral range has been elevated, which is the desired property for a broad impedance detection. The strength of the spectrum can be adjusted with the PRBS duty cycle. That the spectrum generated by the PRBS is relatively flat up to 2-4 kHz, which is ideal for system identification.

The moderate noise in the spectrum is principally due to the uneven ratio between the data sampling and PRBS code frequency. The minimal decrease of the switching frequency peak can be interpreted as the energy from the switching frequency being redirected to the intermediate frequencies. Figure 4.4-B shows the spectrum of V_{PCC}, at the output filter. The high frequency harmonics are dampened extensively, and beyond 3 ω_{res} , the generated excitation is not sufficient for adequate impedance detection. The amplitude of the PRBS spectrum depends on the magnitude of the carrier peak alterations. Simulation results show that even minimal alterations provide excellent results, since slight pulse modifications of the PRBS are aggregated over many carrier pulses. Thus longer PRBS periods can be used

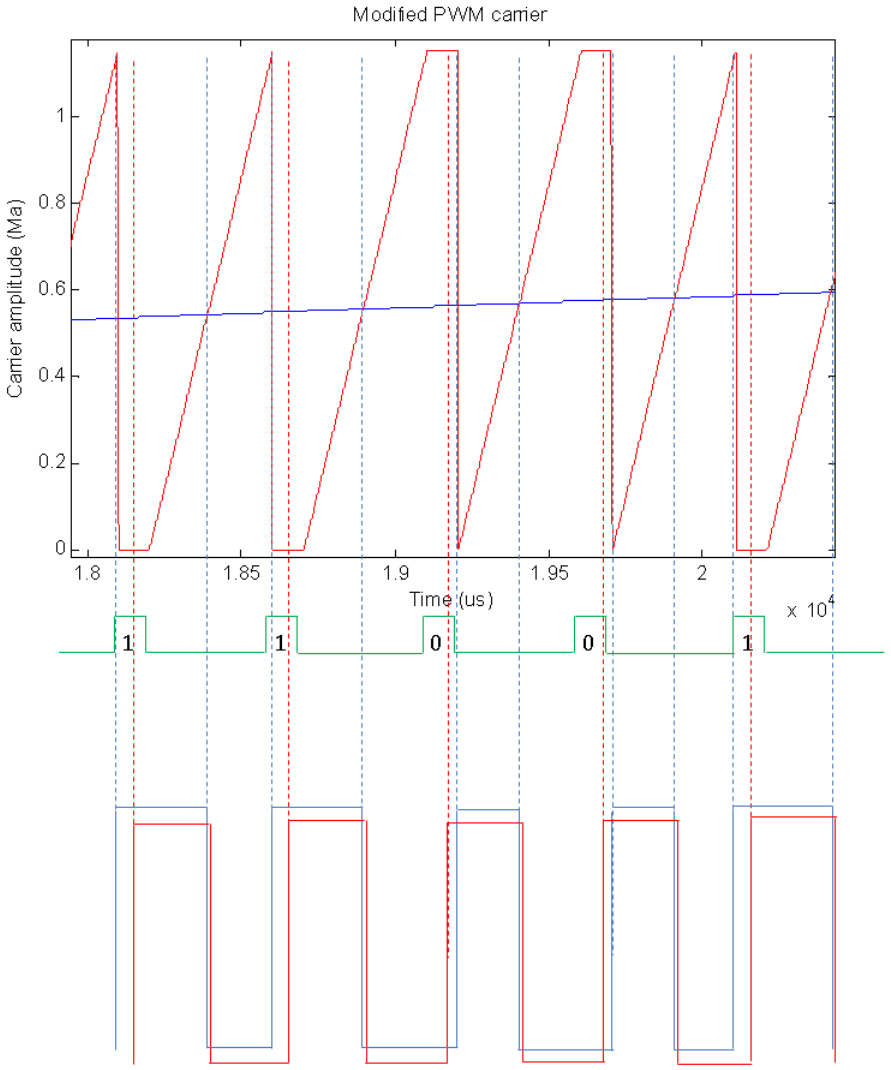

FIGURE 4.3: Grid-connected inverter with LCL filter and time-variant and frequency-dependent power grid B. PRBS implementation on PWM

to increase SNR and improve estimation accuracy, but they will in turn increase harmonic pollution, which is an undesirable side-effect.

Figure 4.5 shows the resulting output voltage time domain signal at the PCC. The Y axis amplitude is zoomed in around the sine peak in order to highlight the alterations. The see-saw type spikes represent the remainings of the switching and are operating at the switching frequency. The effect of the PRBS can be seen in a more low frequency type ondulation added around the original sine wave. In can also be seen that on average the changes produced to the sine wave are null, thus the PRBS added has are null DC component.

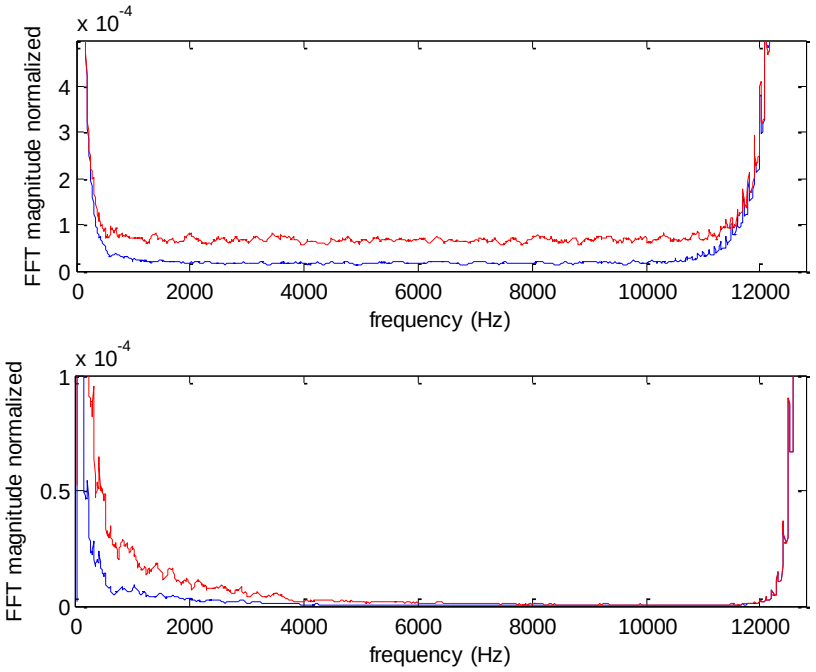

FIGURE 4.4: Spectrum at Inverter Output
A: Voltage spectrum at the PWM, red: original, blue with PRBS
B: Voltage spectrum at PCC, red: original, blue with PRBS

4.3.1 Grid Impedance Determination

The model setup for the impedance determination is described in Figure 3.10. The power grid is modeled by an impedance, consisting of a resistive component and an inductive component. While more complex grid models exist, for the purpose of islanding detection at the DG's PCC, a basic series inductive-resistive impedance, combined with an ideal source supply, is sufficient. In fact, the objective of islanding detection is to sense sudden changes of impedance, through the injected harmonics.

Under normal operation, the DG inverter, operating at 12.8 kHz, provides active and reactive power to the grid, and its spectrum, shown in Figure 3.6, contains the fundamental 50 Hz and harmonics consisting mainly of the inverter switching. Periodically, during four fundamental cycles, a 1023-bit PRBS burst is injected, modulated on top of the 50 Hz sinusoid, according to the method detailed in the previous section. During the burst, the PRBS is modulated over the fundamental. Using the V_{PCC} and I_{PCC} measured at the point of common coupling of the inverters power control loop, the complex impedance is calculated by the voltage

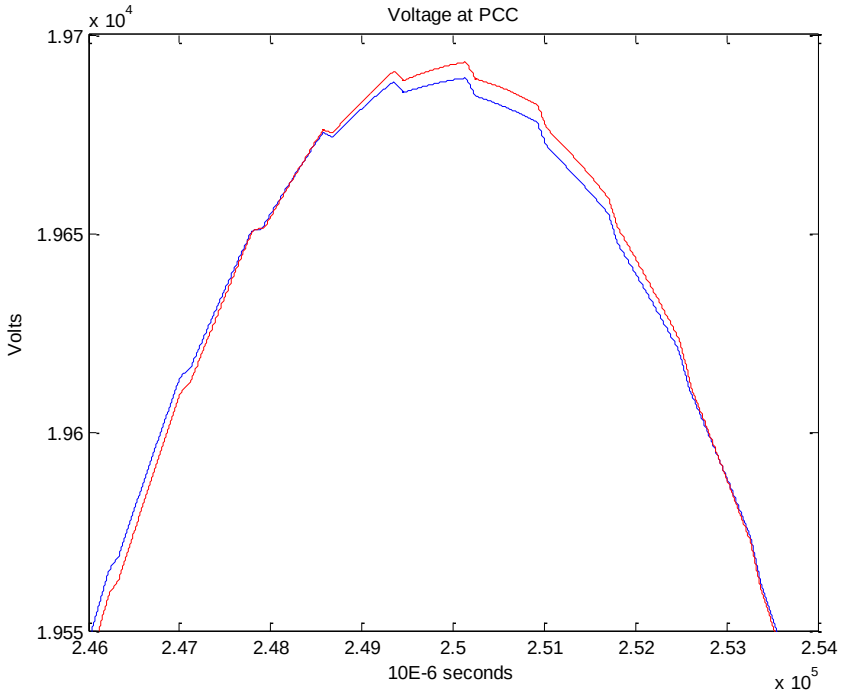

FIGURE 4.5: Time domain plot of V_{PCC}, blue: the original voltage, red: timplot with PRBS injection

to current ratio:

$$\underline{Z_g}(h) = \frac{\underline{V_{PCC}}(h)}{\underline{I_{PCC}}(h)} \tag{4.1}$$

$$\underline{Z_g}(h) = \frac{V_{PCC}(h) \cdot e^{j\varphi v(h)}}{I_{PCC}(h) \cdot e^{j\varphi I(h)}} \tag{4.2}$$

In the equations above, V_{PCC} and I_{PCC} represent the complex line voltage and current at a given frequency. The ratio of their magnitude and the difference of their phase represents the complex grid impedance at a given frequency, its amplitude is and its phase using a Discrete Fourier Transform. In fact, any periodic time function $f(t)$ can be represented by the sum of harmonically multiple complex phasors.

$$f(t) = \sum_{n=-\infty}^{\infty} c_n e^{j\omega nt} \tag{4.3}$$

The coefficient c_n can be calculated numerically and one obtains:

$$c_n = \frac{1}{T} \int_{-T/2}^{T/2} f(t) e^{-j\omega wnt} dt \tag{4.4}$$

Thus each phasor can be calculated by solving Equation 4.4 in order to obtain the complex coefficient c_n.

The objective is to obtain the grid impedance at PCC for all harmonics and inter-harmonics in order to get the complete spectrum:

$$Z(f) = \frac{DFT_{(V(t))}}{DFT_{(I(t))}} = R_{grid} + j \cdot X_{grid} \tag{4.5}$$

where DFT denotes the Discrete Fourier transform of the time domain measurement of the voltage and current at the PCC.

The PRBS codes are aligned and synchronized with the fundamental, so that the DFT over four full fundamental cycles generated minimal spectral leakage. Furthermore, the presented technique has a latency of 80ms, and is fast enough for power grid related applications, which have time constants that are usually larger by at least one order of magnitude. In the next Section, analytical data on SNR, THD and impedance accuracy will be discussed using Matlab simulations.

4.3.2 Simulations

Simulations were carried out using Matlab with Simulink. A detailed discrete-time model of a single phase grid-connected inverter has been considered for the performance of the proposed estimation method. The system structure is depicted Figure 3.10 and its operating parameters are listed in Table 4.2.

TABLE 4.2: Parameter Values Used in Simulations

Paramter and Designation	
Filter inductance Lf1	17.7 mH
Filter inductance Lf2	05.7 mH
Filter capacitance Cf	3.45 mμF
Filter damping resistance Rd	11.2 Ω
PWM switching frequency fPWM	12.8 kHz
Vg grid voltage	20,0 kV
Sampling frequency	10e5 Hz
Grid resistance	0.08 Ω
Grid inductance	0.4 mH
PRBS code length	1023
PRBS carrier amplitude modification	0.5-3%

The LCL filter parameters are selected according to [54]. A 1023 PRBS code is injected, with the code frequency set to the carrier frequency: 12.8 KHz. The 1023 codes are injected in 80ms and Figure 4.5 shows a magnified snapshot of the grid voltage's evolution at PCC for the nominal case and with PRBS injection. The PRBS induced variation are comparatively small, the main harmonics are the switching harmonics and a jitter induced distortion.

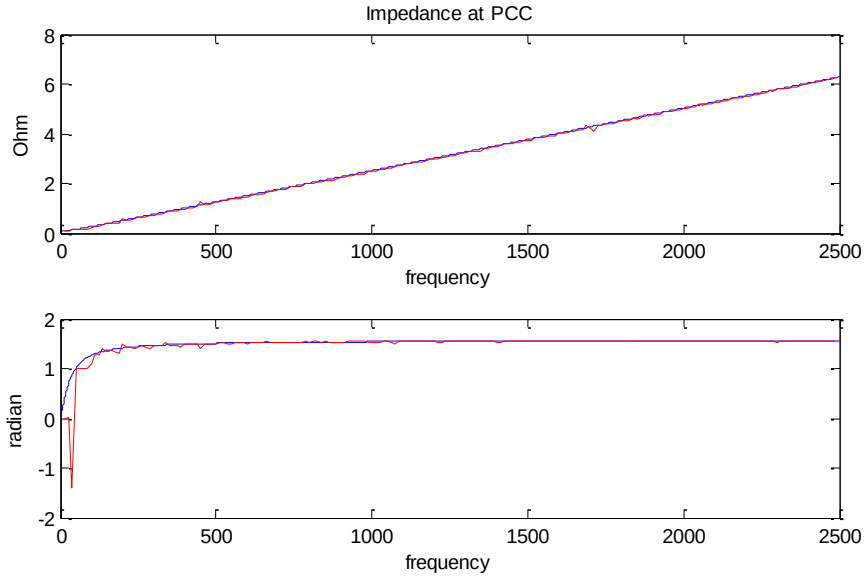

FIGURE 4.6: Impedance estimation at PCC, blue: Theoretical impedance to be detected, red: result of impedance estimation through PRBS injection

The calculated impedances from online transfer function identification are depicted in Figure 4.6 and 4.7. Figure 4.6 shows the impedance at PCC. The expected RC spectrum is shown in blue, and the red plot is the result of the real-time identification technique. No smoothing or averaging process has been applied, in order to highlight the performance of the proposed method. The results are quite accurate, and due to the correlation properties of the PRBS, very resilient to noise. Thus, good results can be obtained in high interference conditions, where the amplitude of the injection is much lower than the environmental noise. Table 4.3 shows the harmonic pollution injected by the proposed measurement technique for different injection strengths values.

Excellent results can be obtained with very little distortion, and with higher injection amplitude, the rate of return declines. Finally, the remaining impedance estimation error is mainly due to quantization error and spectrum leakage and

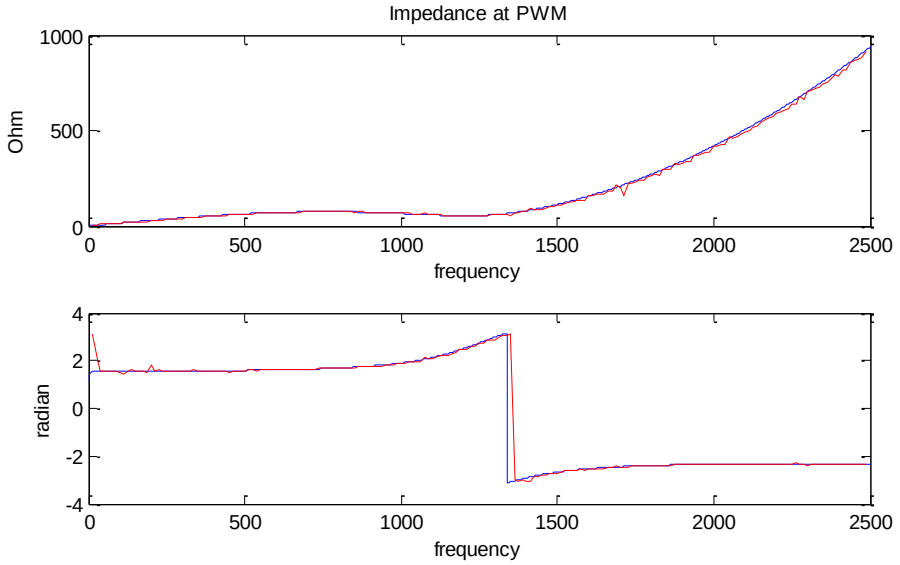

FIGURE 4.7: Impedance estimation at Inverter output, blue: theoretical impedance, red: impedance estimated through PRBS injection

TABLE 4.3: THD and Impedance Error for various injection magnitudes

	no prbs	prbs 0.5%	prbs 1%	prbs 3%
THD	1.51E-04	1.67E-04	1.86E-04	2.42E-04
Impedance Estimation Error	N.A.	10.44%	7.29%	6.08%

could be improved by lengthening the PRBS code sequence or applying windowing filters. This in turn would deteriorate the THD and execution latency. Therefore, a compromise has to be made in order to find the right balance. A 6% estimation error is very accurate, and the obtained islanding detection tool is very capable to operate reliably even in complex distribution grids.

4.4 Contributions and Outcome of Simulation Results

The number of distributed power electronic based generators connected to the grid is increasing and their influence on grid infrastructure, stability and reliability is growing. The real-time knowledge of the equivalent grid impedance at the

inverter's PCC is crucial for filter design, power quality evaluations and grid status determination. An advanced multi-purpose real-time estimation method for frequency dependent grid impedance determination method has been presented in this Section. The method is based on PRBS sequences, which have been extensively used in system identification, communications and information theory. An innovative technique injecting PRBS on the inverter's Pulse Width Modulators has been introduced and a detailed description has been provided and islanding detection in distorted grid conditions have been discussed.

The proposed method estimates the equivalent grid impedance over a significant frequency range with a high resolution. It provides a high degree of flexibility; longer injections provide higher frequency resolution and accuracy, shorter patterns reduce latency and THD. In the next Section, the proposed technique is implemented in a prototype converter at SnT's Netpower Laboratories in order to verify the performance in real settings and confirms the simulations research. A LabVIEW based inverter protocol is built for the purpose of this testing. Using FPGA based hardware control, the carrier shape of the Pulse Width Modulator is changed according to 4.3, and the impedance of a passive load is characterized using the method described above.

4.5 Laborarory Implementation

The description of the setup used for experimental validation of the PRBS injection technique is done in this Section. A custom built inverter is used for this purpose. The test setup uses NI Single-Board RIO General Purpose Inverter Control (GPIC), which is programmed using LabVIEW and periodically generates a PRBS. This section describes the hardware and software implementation done. Descriptions of elements used for the experimental setup are given below.

4.5.1 Hardware

The general overview of the system implemented is shown in Figure 4.8.

The overall hardware design of Inverter has following subsystems:

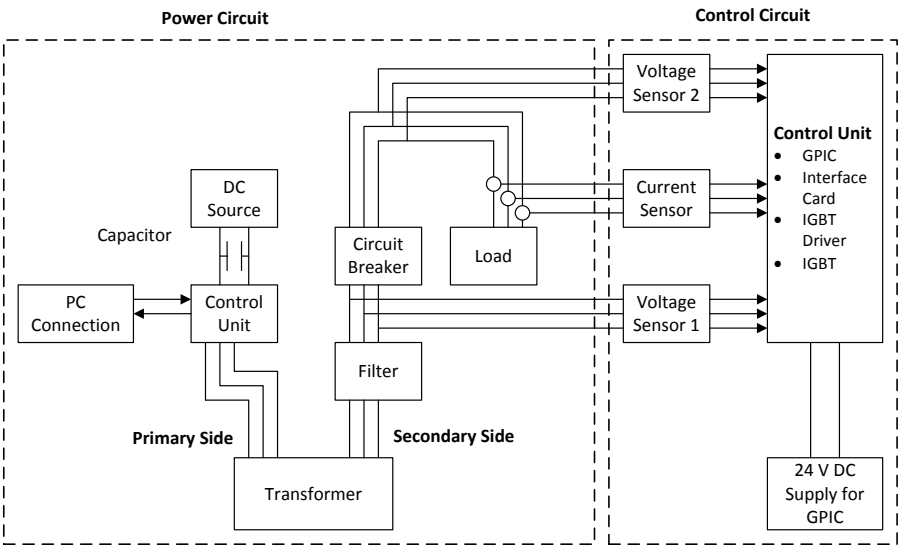

FIGURE 4.8: General overview of the System

- **DC Power Supply:** The DC power supply is variable power source which has been used for simulating Distributed Energy Resource connected to the inverter. It is a SM660-AR-11 with maximum output of 3300 W and voltage and current range 0-330 V and 0-11 A respectively [96].

- **Electrolyte Capacitor:** It is used as a DC link between the DC power supply and inverter to prevent large transients generated at the output side of the inverter from reaching back to the DC supply and to act as a buffer for smoothing out DC voltage variations. Electrolyte Capacitor with capacitance of 400 μF has been used as the DC link capacitor with maximum rated voltage and current, 1100 V (DC) and 40 A respectively.

- **Control Unit:** The control unit consists of GPIC from National Instruments (NI), Interface Card, IGBT Driver and IGBT. The general overview of the control unit is shown in Figure 4.9.

- **NI Single-Board RIO GPIC:** is a typical stack of NI sbRIO-9606 (Single-Board RIO) control and monitoring system, NI GPIC RIO mezzanine card and custom interface board which is configured as per the requirement of the user [97]. GPIC is programmed using a comprehensive NI LabVIEW graphical system design toolchain that includes simulation which make digital computing and compiling quite user friendly. The interface card takes the signal from the GPIC and appropriately delivers it to IGBT drivers for

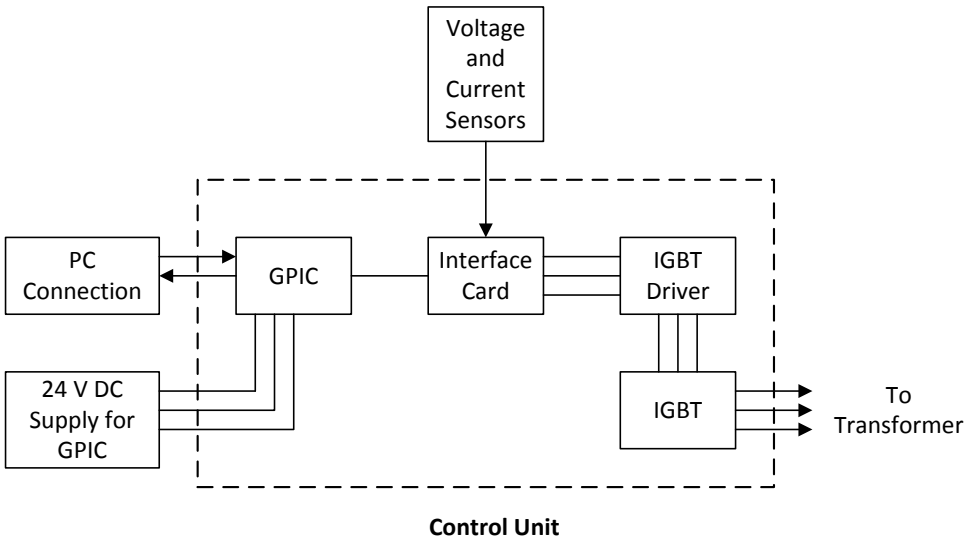

FIGURE 4.9: General overview of the control unit

switching of IGBTs. Thus, it allows control of IGBT drivers which control IGBTs for generating AC output voltage. It is connected to a base board with IGBT driver which contains all necessary components for optimal and safe driving of IGBT modules. The gate signals produced are used for switching the IGBTs which are connected to variable power DC supply described earlier. The 3 phase AC output at the IGBTs is then connected to the primary side of the Transformer.

- **Transformer:** The transformer used in this work is a 5 kVA, Dzn0 type, air core step up transformer and is used to provide isolation of the output neutral from the source, to step up the output voltage at IGBTs and to provide impedance that limits fault current or acts as a noise filter. The transformer is designed to work for with a PWM switching frequency upto 16 kHz.

- **Output Filter:** The LCL Filter used reduces the harmonics in the current generated by IGBTs switching and obtain low current distortions. It has a maximum rated operating voltage of 480 V with 56 A per phase for 50 Hz frequency.

- **Circuit breaker:** A 4-pole circuit breaker from is used to connect or disconnect the inverter from the load. The maximum voltage and current rating are 6000 V and 15 A.

- **Voltage and Current Sensors:** Two voltage sensors and one current sensor are connected in the inverter circuit to measure and to control the output voltage and current of the inverter. Voltage sensors are connected before and after the breaker and measured voltages are sent into the GPIC for PWM generation. Current is measured after the breaker. Figure 4.10 shows the inverter cabinet with all hardware components implemented.

FIGURE 4.10: Lab Inverter Setup

4.5.2 Software

All the simulations of the system and the control were developed using LabVIEW, which is the system design software created by National Instruments. The main program is called VI (Virtual Instrument) and it can have a number of Sub-VIs. The GPIC used in this paper for inverter control has three different programming levels:

- **Host Computer (highest level):** Provides user an interface for programming and monitoring of the system.
- **Real-Time (medium level):** Executes the control algorithm received from Host Computer and sends the data to the FPGA level for processing. The processed data is then received at Real-Time level and communicated to the Host Computer.

- **FPGA level (low level):** Does simple processing of the data, and sends out the control command. It is also the fastest, since processing is done in hardware rather than software.

  When the program is running, each level does its own job. The actual FPGA and Real Time programming done has been briefly described.

4.5.3 FPGA Programming

Inside the FPGA, the inverter control is implemented using 5 different control loops:

- **Analog input loop:** Analog input loop reads simultaneously the instantaneous values at the output of the inverter from the interface card with analog input pins.

- **PWM generation Loop:** Generates high speed PWM signals based on the outputs of the control loop. The sawtooth waveform and PRBS is generated with a Sub-VI and is started by a Restart PRBS function that injects on the sawtooth waveform for a limited cycles depending upon the Iteration Stop value set and initial seed value specified. The loop also has a Sub-VI which marks the starting of the PRBS injection. Thus, the PRBS generation takes place only when the voltage of Phase A is zero. An 11-bit LFSR is implemented with a PRBS sequence length of 2047 and has 4 taps so that it can be used for all LFSR up to 16 bit. The PRBS generator generates modified sawtooth with PRBS at 4 different magnitudes depending on the selection of the Binary Selector switches provided for the control and PRBS code generated i.e. '0' or '1'. Where Sequence 1 is the PRBS with lowest magnitude and Sequence 4 is the PRBS with highest magnitude.Sawtooth waveform for PWM and modified PWM is generated using LabVIEW FPGA DDS (Direct Digital Synthesis) generator. The FPGA DDS generator generates repetitive waveforms with high degree of frequency and phase control. The reference waveform to be generated is specified in the look up table in FPGA DDS generator which is a straight line when PRBS is not activated. Figure 4.11 shows table preview of the look up table for sawtooth waveform generation. Similarly the lookup table for the Sequence 1 to Sequence 4 has been implemented. When the PRBS is activated, the output waveform is

generated depending on the code value generated by the PRBS generator and binary selector switch configuration selected. Figure 4.11 shows a table preview of the lookup table implemented for PRBS code '0' and PRBS code '1' with PRBS sequence 2 selection.

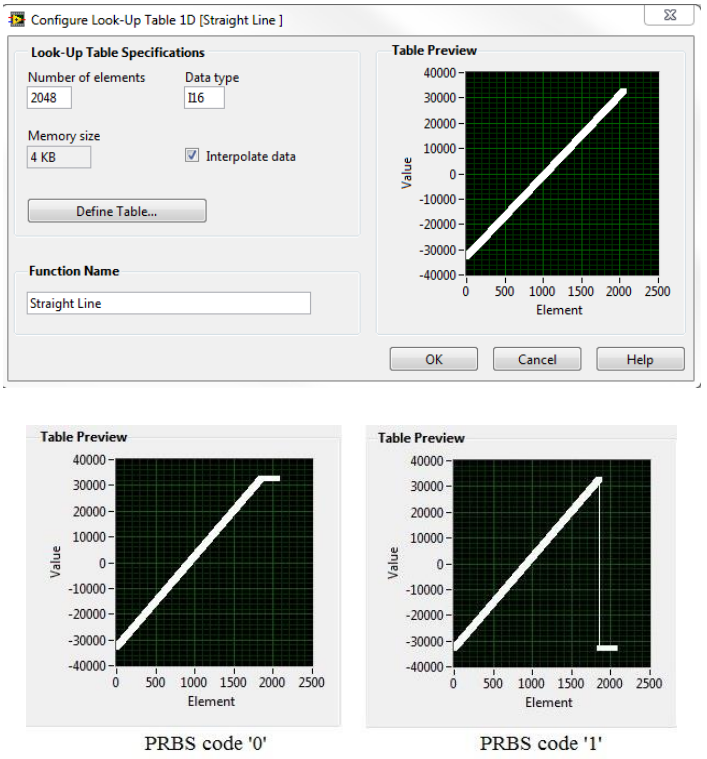

FIGURE 4.11: Configuring the sawtooth lookup table ; Table preview of the lookup table for PRBS code '0' and '1'

The waveform generation operates at 12.8 kHz. The sawtooth waveform generated is then compared with three phase sine voltage signal generated by the control loop for PWM generation. The PWM generated controls the switching of IGBTs.

- **Reference Sine:** The loop generates a reference three phase sine signal which is the signal that is desired at the output and used in analysis loop to synchronize the output voltage of the inverter with the desired signal.
- **Analysis Loop:** The analysis loop is synchronized with Analog Input Loop and computes the coordinate transformations, RMS value of voltage and active and reactive power of the inverter.

- **Control Loop:** Uses PID control algorithm in the d-q reference frames to control voltage.

4.5.4 Real-Time Programming

In the FPGA the memory is limited so each of the memories, logic blocks etc... should be carefully used. In order to reduce the stress on FPGA and to increase its reliability the major complex operations are implemented in Real-Time. The Real-Time VI implemented has a front and back panel. The front panel is used for user interaction and is used for display and control and in the back panel the actual programming has been done.

4.5.5 Results

A three phase inductive load of 80 mH is connected to the output of the inverter and with the grid impedance identification technique discussed the impedance spectrum for the inductor is identified.

For the impedance spectrum measurement, the inverter output is set to AC voltage of 10 V with DC power supply to 50 V. An 11-bit PRBS code on each phase is injected with the initial seed value '10100110000' and voltage and current values are measured only for Phase in our experiment. PRBS is injected for sequence length of 2047 which is approximately 160 ms with PRBS settings at width Sequence 2. The Voltage is measured across Phase A and neutral of the inductor and current is measured by measuring voltage across a shunt resistor of 1 Ω. The measurement data is collected through an oscilloscope and then Fourier transform of voltage and current is then performed in MATLAB.

With these system settings the voltage and current waveform seen on the oscilloscope at the output of the inverter is shown in Figure 4.12. The yellow plot corresponds to the voltage and pink to the current. The Scope plots shown are not filtered and data from these plots has been used for grid impedance spectrum identification. The harmonic content is partially due to the switching frequency, partially due to the PRBS code injected.

The results were obtained by PRBS injection using Sequence 2 for impedance spectrum identification of the inductive load. The voltage and current seen before

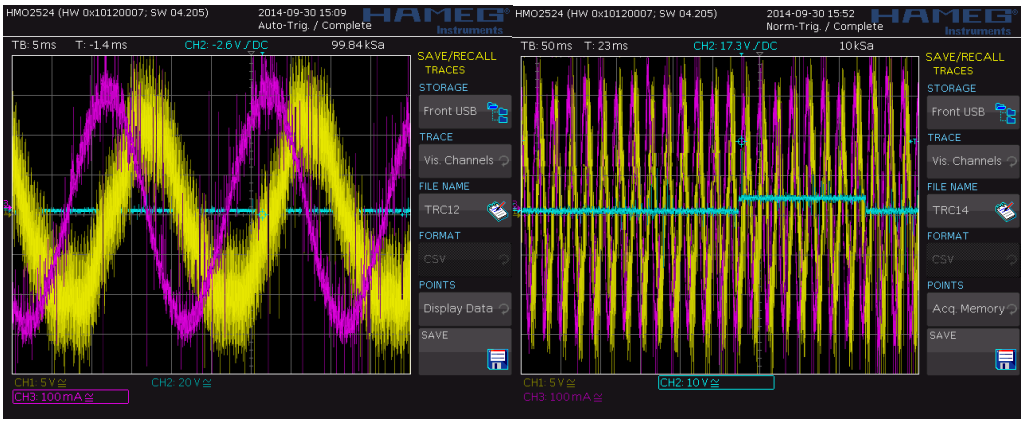

FIGURE 4.12: Inverter Output Voltage and Current ; Voltage and Current Waveform with and without PRBS injection using Sequence 2

and after the PRBS injected is shown in Figure 4.12. The yellow plot corresponds to the voltage, pink to the current and the blue line shows the period for which the PRBS is injected.

The data measured is then processed in MATLAB to plot the voltage and current spectrum when the PRBS is injected and to plot the impedance spectrum upto a frequency of 1000 Hz. The frequency of 1000 Hz has been chosen as cut-off because as per EN50160 [98] the harmonic orders up to 20 of fundamental frequency are considered as principally informative.

The impedance spectrum obtained from the voltage and current spectrum for the inductive load for PRBS sequence 2 is shown in Figure 4.13. The blue plot corresponds to the theoretical impedance spectrum and the red plot corresponds to the estimated impedance spectrum obtained by PRBS injection.

Voltage spectrum and current spectrum observed here exhibit the PRBS characteristics which mean that the proposed technique is implemented correctly on the inverter. Also the calculated impedance spectrum is close to the theoretical impedance spectrum of the inductive load. Also despite of the system noise while taking measurements through oscilloscope impedance measurement has not been affected which is attributed to correlation properties of the PRBS that makes it resilient to noise. In order to improve results, and alleviate the spectral instability of the PRBS, the data has been averaged over 20 Hz wide frequency bins. This has a smoothing effect on the obtained plot, and dampens the slight mismatches between voltage and current spectrum. The results obtained are very satisfying up

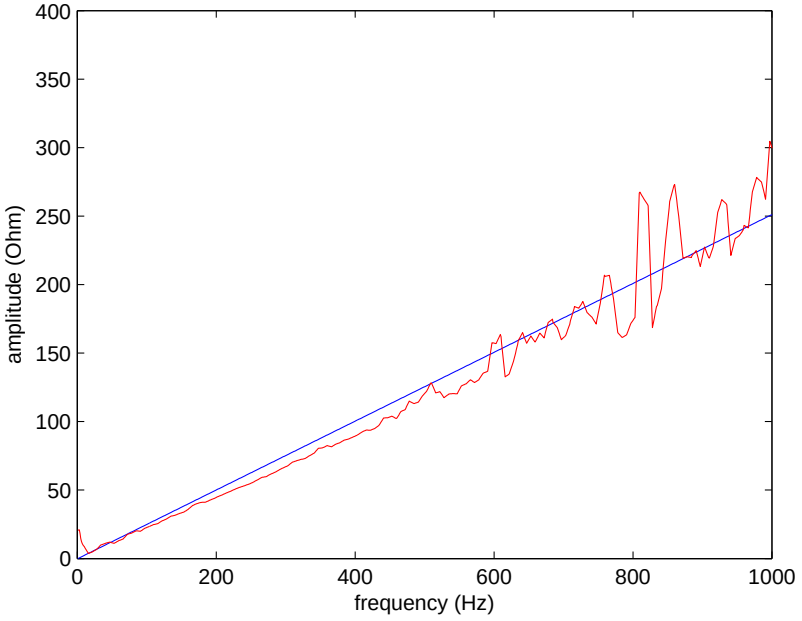

FIGURE 4.13: Impedance Spectrum Estimation for Inductive Load

to 500 Hz. On higher frequencies, the results are less accurate, mainly due to the low SNR of the PRBS injected harmonics. Nevertheless, the results are acceptable, but improvements can be obtained either by increasing the PRBS strength on higher frequencies, using a higher order LFSR, or by widening the frequency bins over higher frequencies.

4.5.6 Contributions

The results obtained confirm that the proposed technique estimates the equivalent grid impedance over a significant frequency range with high resolution on a real time basis. It also provides a high degree of flexibility and can be implemented with no additional hardware requirements. Several points for improvement are envisaged for further research. The modified PWM inverter hardware proposed in this research has output voltage limitations due to the DC power supply source used. A possible future work could be the implementation of a better DC power supply source to produce higher voltages at the output of the inverter. Though for the different power level, the control will be practically identical but with the increase of voltage there is possibility of decreasing the impedance estimation error. Finally, after verification of this novel method of online grid spectrum

identification technique the future research aims on implementing prototype of an island grid in the SnT Netpower laboratory by connecting two inverters and then using PRBS for determining the impedance parameters between them in order to verify that the proposed technique is robust to a realistic environment and would represent a promising grid monitoring and diagnostic tool.

Chapter 5

Power Line Parameter Identification

5.1 Purpose

The last decade has seen a big rise of harmonic pollution on the power network, due to the liberalization of power markets and the proliferation of high frequency switching power electronic inverters [99]. Thus, broad spectrum characterization of line impedances has been a coveted goal for the prediction of resonances, harmonic propagation and voltage distortions [70]. Historically, the power network impedances have been estimated by dividing the distribution system down to its functional elements and summing the impedance of each component. In general, power systems are relatively accurately modeled if all the parameters of the system are well characterized, but this is not always feasible.

Errors in the calculations can happen for many reasons. Varying operating conditions such as temperature and humidity along the line can affect its parameters, and [100] [101] have shown that numerous in service power lines might have values that poorly reflect the real measured impedance. This might have adverse effect on distance protection, relay settings and state estimation results [102]. In addition, a consequence of the open energy market is that higher constraints are put on the transmission lines, which are frequently pushed to their capacity and thermal limit [103].

Rather than fixing line capacity values based on conservative estimates, network operators could take the real-time transmission line status into account [104]. Accurate and online transmission capacity estimation could be beneficial for congestion management and energy pricing strategies [105]. The authors in [106] highlight the impact of the thermal limit of the powerlines and the curtailing done on DG in order to avoid overloading the lines. Also research in [107] has concluded that the thermal limits of the transmission lines have an impact on line usage efficiency and economic dispatch. A study on the influence of the thermal limits of transmission lines on dispatching is presented in [108], and it concludes that an hourly forecast of real-time transmission capacity would be beneficial on economic dispatch.

This Chapter describes a novel power line impedance estimation technique, implementing a method based on modifications of the Pulse Width Modulator's pattern on the inverters, as seen in previous Chapters. The next Section covers the main methods for transmission line characterization proposed in the research literature.

5.2 State of the Art

In this Section, an overview of methods employed for transmission line characterization are presented. They are divided in two categories. Classical approaches model the lines by taking into account its material properties, geometrical properties and environment properties. These also include methods where the line is taken off the grid and characterized through a set of predetermined stimulation tests.

One the other hand, online characterization has only been researched recently [109], partly due to the proliferation of inverter based distributed generation and energy market liberalization, which have brought added complexity to powerflows, voltage stability issues, and power quality deterioration. Depending on the application, they allow to have up to date information on the status of the powerline and improve powerflows, voltage stability and power quality.

5.2.1 Classical Approaches for Line Characterization

5.2.1.1 Characterization through Analytical Model and Weather Predictions

In traditional approaches, as described in [110] [111], an estimation of meteorological conditions is used to determine the parameters of the lines, taking into account factors such as the tower geometry and cable parameters. In addition the transmission model utilized has to be chosen carefully in order to reflect the needs of the applications. The understanding and limitation of the transmission line models used has to be comprehended clearly, since modeling assumptions have an impact on the accuracy of the obtained results. Typical line models are described in Chapter 2. The power lines models are classified as short, medium or long lines. This classification is a compromise between the required accuracy and the simplicity of the calculations. The Pi model, shown if Figure 5.1 is frequently used as a transmission line model.

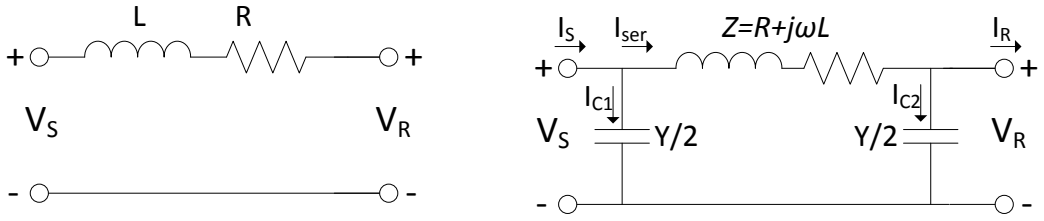

FIGURE 5.1: Short and Medium Length Transmission Line Model

Transmission line resistance, inductance and capacity have to be estimated accurately. Other factors, such as cable temperature and line sag (for overhead lines), play an important role as well and are determined based on calculations.

In Figure 5.1, the resistance is considered to be that of a uniform conductor, and it is proportional to its length and inversely proportional to its cross-sectional area. It is also dependent on the resistivity of the conductor. In addition, conductor resistance is also greatly affected by temperature. For example an ACSR conductor operating in cold conditions at 10°Celsius experiences a substantial resistance (about 40%) when going from an unloaded condition to a heavy load condition where conductor temperature can reach 100°C [111].

The self-inductance of a conductor is dependent among others on its geometry, its distance to earth and the ground resistance. The mutual impedance between conductors is directly related to the distance between them. Thus the geometric configuration of the transmission line has a strong impact on its inductance.

The calculation of the capacitance of a line is based on the relative position of the conductors, the height, and the presence of a ground wire. For short transmission lines (80 kilometers or less), the shunt admittances is neglected.

The obtained models are then employed for instance in EMS tools, State Estimation tools, and protection systems. But these models can sometimes yield erroneous results, especially for lines that have been in service for a long time. Thus experimental line characterization can be performed, as described in the next section.

5.2.1.2 Power Line Characterization on Disconnected Line

Research in [112] describes a method where conductors are disconnected from the network in order to assess their operational parameters. A signal generator injects a low voltage signal into an isolated line. The stimulation used can be white noise or sweep covering the 10Hz to 10kHz range. The applied voltage and the current measured are processed by a dynamic signal analyzer, which provides the broad spectral impedance function by dividing the voltage by the current. Several measurements are averaged to improve the accuracy of results. The setup utilized in [112] is depicted in Figure 5.2

5.2.2 Online Transmission Line Characterization

In order to alleviate dynamic uncertainties regarding line parameters, online measurement methods have been designed to characterize the line impedance in an experimental manner. While offline methods [112] allow the determination of the precise impedance value, these methods can only be operated infrequently, they only provide the status of the power line at a specific time, and cannot assess dynamic variations of the parameters and be used for online system monitoring.

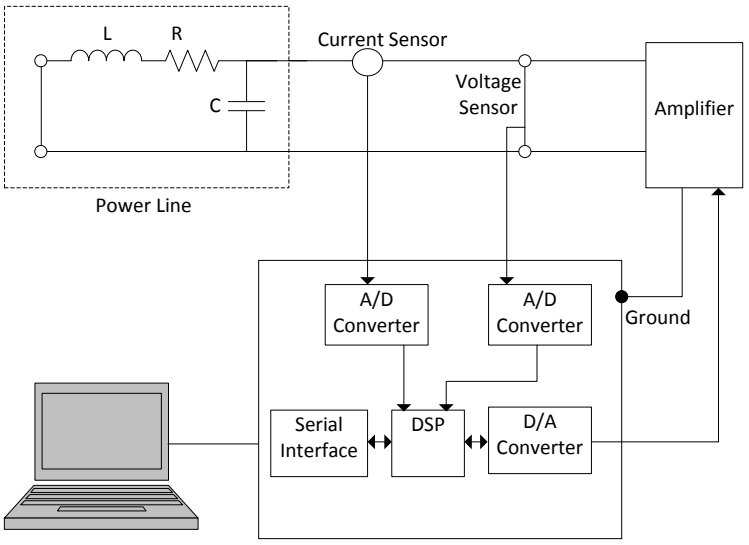

FIGURE 5.2: Instrumentation for Line Impedance Measurement

5.2.2.1 State Estimation Based Line Characterization

State Estimtion (SE) is used for powerflow computation and real-time voltage and current determination on the power network nodes, using a limited number of measurements [113]. The aggregation of measurements gathered at several locations is processed in an iterative least-square based algorithm in order to estimate the system states. As proposed in several publications, the algorithm can be tweaked to obtain power system parameters, e.g. by analyzing the residual of the SE algorithm [114]. In Chapter 6 global power system parameter identification based on decentralized independent measurements and state estimation is analyzed.

5.2.2.2 PMU Based Line Characterization

The research in [115] [116] [117] propose a transmission line parameter estimation method based on Phaser Measurement Units (PMU). The described method relies on synchronous measurements located at strategic positions on the power network. The exact and synchronous phasor components of the voltage and current at different location of the line provide an estimation of the line parameters, such as series resistance, series reactance and susceptance. Based on these measurements, an equivalent Pi-model is estimated, linking the phasors data with the unknown

variables. This information can then be relayed to various applications such as protective relaying and powerflow analysis.

5.2.2.3 System Characterization Based on Signal Injection

Similar to the methods proposed in subsection 5.2.1.2, these methods propose the parameter estimation of a transmission line, but while it is operational. They distort the voltage and current by injecting signals, measure the response, and obtain relevant information through signal processing. Some studies focus on analyzing harmonic rich transients, while others injected steady-state signals and measured their response. In [69], the impedance is calculated through the injection of a sum of sinusoids. The solution provided in [18] injects short triangular pulses with rich harmonic content to estimate the grid impedance's full spectrum.

Parameter identification based on stimulus injection through PWM has also been a coveted researched topic for induction machines [118]. The method proposed in [119] [120] utilizes a PWM inverter for machine identification at standstill. It operates in specific modes in order to identify the characteristics of the induction motor. For rotor resistance identification, a sinusoidal current with DC bias is injected. For rotor time constant identification a constant DC current is injected on the d-axis, while keeping the q-axis to 0. [121] operate in similar fashion, utilizing a sinusoidal stimulation from the PWM inverter in order to excite and estimate different characteristics of the induction machine.

In the next Section, a line characterization method based on PRBS injection at the inverter is proposed. It is expanding the research in the previous Section, and re-utilizes the stimuli generated for islanding detection. The signals generated at numerous locations in the distribution grid, are detected at the transformer sub-station. Through cross-correlation between the received distorted signal and the sequence, the parameters of the propagation channel are estimated. Simulations on a test grid verify that the proposed algorithm is robust to a realistic environmental noise and can be employed as a transmission line monitoring and diagnostic tool.

5.3 Proposed Method

The identification method utilized in this research relies on stimulations injected through a PWM; it creates a stimulation signal based on PRBS sequences. The research covered in this Chapter aims at extending the scope of active system identification methods for transmission lines. It considers requesting an ancillary service from the inverter based DG on the network for stimulation injection, while they are online. The generated signal is used for channel estimation by measuring its distortions at various locations in the network, where the stimulation propagates. The proposed line characterization method builds on the previous Chapter and the grid tie-inverter's signal injection technique is reapplied. Consequently, Pseudo-Random Binary Sequence based pilot signals are used for channel estimation.

The inverter injects the deterministic broadband voltage and current pattern on the network, generating voltage and current distortions that propagate along the powerline. These are measured at the substation of the distribution grid. The receiver knows the employed pattern beforehand, and it continuously monitors the line in order to detect it by correlating with the PRBS code. Once a correlation peak is detected, the distortions of the received signal are evaluated in order to model and reconstruct the impedance of the powerline. The interaction between sender and receiver happens implicitly, and this method doesn't necessitate external Information and Communications Technology (ICT) infrastructure. The senders are the grid-tie inverters present on the distribution grid. The operation principles are detailed on a single phase inverter topology, but considering a balanced three phase topology, the same algorithms can be reproduced on each phase.

In the next Section, an overview of channel estimation through correlation is given. In Section 5.3.2 a system topology is depicted on which the method is applied, and a detailed analysis of the algorithm flow is provided in Section 5.3.3. In Section 5.3.6 simulation results are analyzed, and the outcomes are evaluated in order to assess the efficiency of the proposed method.

Furthermore, algorithm improvements through Successive Interference Cancellation (SIC) are investigated, and their performance on a test network evaluated.

5.3.1 Background

As seen in previous Chapters, several properties of the PRBS sequence make it an ideal stimulation signal for grid identification. Depending on the relationship between the code-length, sampling frequency and code frequency, the PRBS exhibits a wide 'white noise-like' spectrum for a defined frequency range, with zeros occurring at multiples of the PRBS clock sampling frequency. The PRBS can be detected at various locations of the power network through correlation. In addition the correlation with the code can provide information regarding the transfer function of the transmission path.

Assuming that the system to be identified can be regarded as a steady-state linear time-invariant system, the system output stimulated by the PRBS can be represented by the following equation:

$$y(n) = \sum_{k=1}^{\infty} h(k)\, u(n-k) + v(n) \tag{5.1}$$

Where the $y(n)$ is the output signal of the system, $h(k)$ the impulse response of the system to be identified, $u(k)$ the input signal, which is the PRBS pattern in our case. The disturbances, modeled by white noise are represented by $v(k)$. The cross correlation of the input signal with the output signal is given equivalent to the impulse response of the system [21].

$$R_{uy}(m) = h(m) \tag{5.2}$$

The operations required for system identification are depicted in Figure 5.3, which summarizes the setup and operations to be performed for impulse response determination.

The relationship between impulse response and transfer function is shown in Figure 5.4. The transfer function of the target in frequency domain can then be derived by applying the Fourier transform to $R_{uy}(m)$.

The model of the grid-tie inverter used for this research is depicted in Chapter 2. It comprises a DC Voltage source, with a Pulse Width Modulation based Voltage Source Inverter (VSI) connected to the power network through a low pass LC-filter.

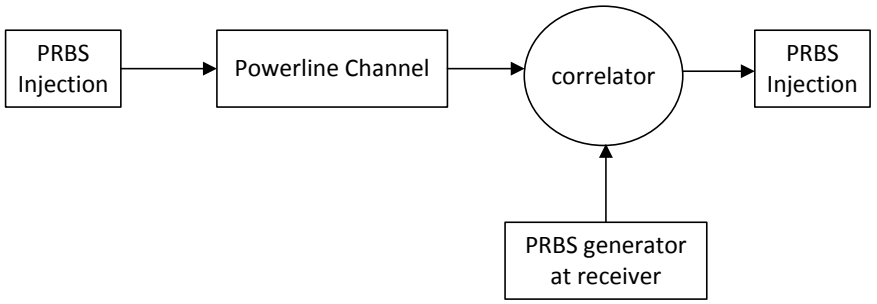

FIGURE 5.3: Impulse Response Determination

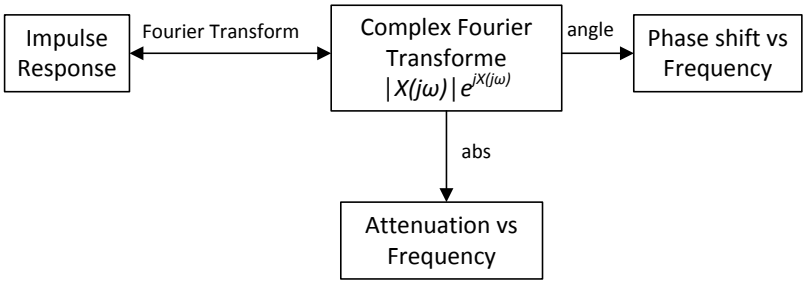

FIGURE 5.4: Mathematical Relation between Impulse Response, Transfer Function and Phase Shift

5.3.2 System Model

A basic sub-grid topology is considered for the application of the channel estimation methodology. The distribution grid depicted on Figure 5.5 represents the studied system. The parameters of the cables, transformers and loads are based on data from the power network in Luxembourg. The system configuration is limited to a substation with two feeders in order to illustrate the algorithm, and research on extended grid structures will be covered in the next Chapter. The system is characterized for one phase, and an equivalent procedure can be setup for each phase in order to identify each phase individually. The studied configuration consists of a power generator connected to a voltage transformer distributing power through two feeders. Connected to the feeder are residential loads, and inverter-based distributed generators are located at the end of each feeder.

The impedance of the transformer is chosen according to [122], to represent a

typical medium voltage transformer. The electrical parameters of all the components of the system are described in Table 5.1. The intended frequency identification range is up to 2000 Hz, since typically the first 40 harmonics are considered for power quality considerations in European grid codes [98]. [123] analyzed the impedance of the power transformers and shows that for the studied frequency ranges, a resistive-inductive model is adequate for the sub-station transformer. The loads on the line are chosen according to average consumption data based on the Luxembourgish medium voltage and low voltage network.

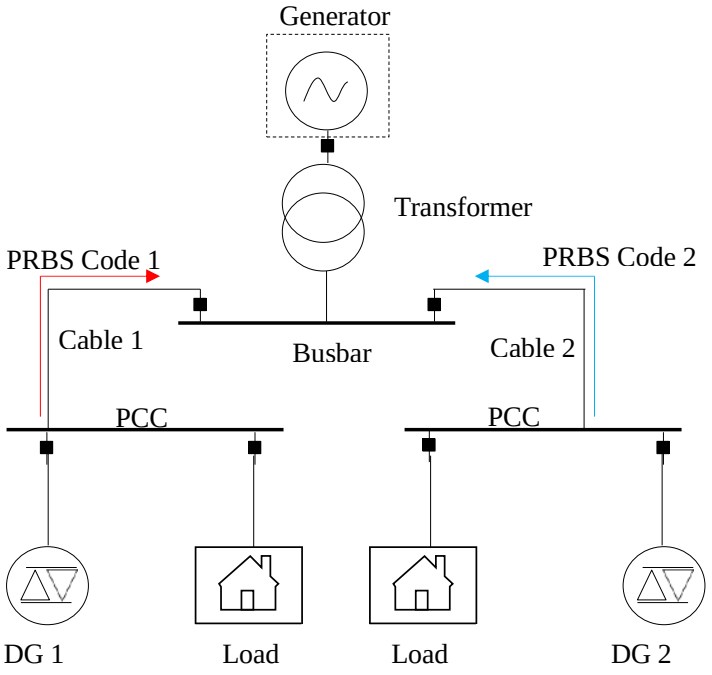

FIGURE 5.5: Distribution network model used for system identification

For the relevant frequency ranges and for the cable lengths that are considered, an inductive-resistive model represents the system relatively accurately. Nevertheless, this is not a limitation of the described non-parametric identification method, as no constraints are set as far as the model evaluation is concerned. Further research, taking into more complex cables models is possible, and it would merely affect the interpretation and modeling of the system identification procedure. The electrical model of the system is depicted in Figure 5.6. The modeled consumer loads are comparatively small with a high cos ϕ.

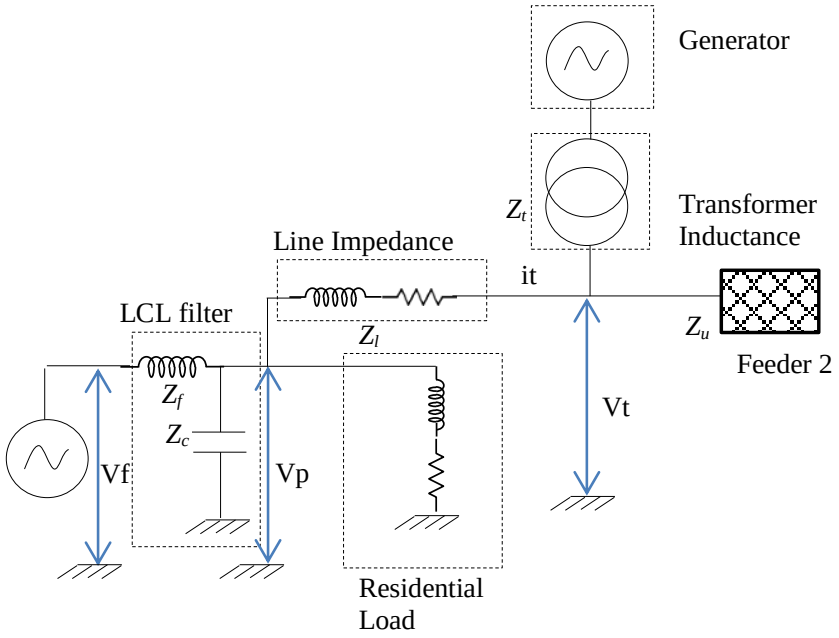

FIGURE 5.6: Electrical representation of distribution network model

5.3.3 Model Estimation

A correlator is able to extract weak data submerged in high amplitude uncorrelated signals. Therefore, a low amplitude PRBS signal generated at the inverter can be detected at the receiver through continuous correlation with its code. Assuming that the system under study is linear and stationary, according to the equation 5.2, by correlating the voltage at the inverter v_f (the PRBS code) with the current at the transformer i_t, the equivalent impulse response and transfer function can be obtained. The equations below show the results of this operation for the described model, $h(n)$ being the transfer function of the propagation path, and R_{vf} the autocorrelation of the stimulation:

$$v_f(t) * i_t(t) = \sum_{n=1}^{\infty} v_f(n)\, i_t(n+m) \tag{5.3}$$

$$= \sum_{n=1}^{\infty} h(n)\, R_{v_f}(m-n) \tag{5.4}$$

Transposed to the frequency domain the following equations are obtained:

$$\overline{V_f} * I_t(\omega) = H_i(\omega) |V_f(\omega)|^2 \tag{5.5}$$

$$H_i(\omega) = \frac{\overline{V_f} \cdot I_t(\omega)}{|V_f(\omega)|^2} \tag{5.6}$$

Equation 5.6 indicates the transfer function between the inverter voltage and transformer voltage, from which the transmission parameter line can be extracted.

At the substation, the PRBS code generated by each inverter is known in advance. The electrical diagram of the system, shown in Figure 5.6, is used to calculate the resulting impedance. The voltage and current swings generated will be detected through a correlator. The substation is equipped with measurement instruments that capture the current from each feeder and the voltage at the busbar with a high dynamic range up for up to several kHz. The generated PWM patterns at the inverter can be predicted if the PRBS pattern is known, and based on the attenuation of the patterns at the substation, the parameters of the line can be determined.

The objective of the channel identification is the spectral characterization of the impedance Z_l, knowing the voltage at the substation V_t, the current from the feeder at the substation i_t, and the PRBS pattern generated at the PWM of the given inverter. Residential loads connected in parallel can be neglected in the calculations, since typical loads on a residential network are too small to have a substantial impact. In order to obtain the analytical value of Z_l, the equations below can be derived from Figure 5.6.

$$\frac{V_t}{V_p} = \frac{(Z_t \parallel Z_u)}{(Z_t \parallel Z_u) + Z_l} \tag{5.7}$$

$$\frac{V_p}{V_f} = \frac{Z_c \parallel ((Z_t \parallel Z_u) + Z_l)}{(Z_t \parallel Z_u) + Z_c \parallel ((Z_t \parallel Z_u) + Z_l)} \tag{5.8}$$

Combining Equation 5.7 and 5.8 , the ratio between V_t and V_f can be obtained:

$$\frac{V_t}{V_f} = \frac{Z_{tu} \cdot Z_c}{Z_c Z_l + Z_c Z_{tu} + Z_f Z_c + Z_f Z_l + Z_f Z_{tu}} \tag{5.9}$$

Where Z_{tu} the upstream impedance is given by:

$$Z_{tu} = \frac{Z_t + Z_u}{Z_t \cdot Z_u} \tag{5.10}$$

Equation 5.9 represents the voltage transfer function between the inverter PCC and the substation. Assuming that measurement of voltages and currents at all feeders are available, for each feeder an equivalent equation can be established, combining Equation 5.6 and 5.9, in order to obtain the expression of the powerline impedance.

$$Z_l = \frac{\left(H_i \cdot \frac{V_t}{i_t}(Z_c)\right) - (Z_c \cdot Z_f)}{Z_c + Z_f} - \frac{V_t}{i_t} \tag{5.11}$$

The equation above is used for estimating the parameters of the line Z_l. The measurements are performed for the time interval of the PRBS sequence. That interval has to be precisely located at the receiver. In 5.11, the parameters of the inverter's filter Z_c and Z_f are known. The voltage V_t and current i_t are the synchronized current and voltage measurements at the transformer substation, and H_i consists of the transfer function of the system as obtained through Equation 5.6.

The continuous correlation of V_t with the PRBS sequence generates a peak when the stimulations effects are seen at the receiver. This allows an implicit synchronization between sender and receiver. As described in the next Section, voltage and current measurement for the PRBS time interval are stored, and transposed to frequency domain. These will render the complex values for $V_t(\omega)$and I_t (ω) in 5.11. The result of the cross-correlation produces the impulse response of the transmission path, which can be transcribed to complex frequency parameters, as shown in Figure 5.4. For this method produce appropriate results, the exact sequence of the generated codes must be known at the receiver and upon detection of the correlation peak, the exact duration of V_t and it containing the stimulation is determined and analyzed.

This operation can be performed for multiple feeders. The constraints being that:

- The parameters of the downstream DG's filter is known by the channel estimator.
- The receiver at the substation knows each DG's unique orthogonal PRBS code

5.3.4 Receiver Synchronization

In order to reduce the Total Harmonic Distortion (THD) on the line and optimize energy utilization, the emitter shouldn't continuously send the pilot sequence, but only at periodical intervals in order to capture transient anomalies such as islanding in the required timeframe. Grid parameters are typically stable enough such that an occasional identification procedure would suffice. Thus, an implicit algorithm needs to be established for the receiver to recognize the data frames on which the identification needs to be performed in order to cover a full PRBS sequence. The proposed solution does not require communication or synchronization via ICT between transformer and the DG. The receiver module at the transformer substation is permanently scanning for the patterns, by performing a continuous correlation with the PRBS code. The method doesn't rely on synchronization packets, but a constraint is put on the sender to initiate the PRBS at the positive edge of the fundamental. The fundamental is therefore used as a synchronizing token between the sender and the receiver. The receiver's correlator uses that information as a trigger to initiate its operations, as shown in Figure 5.8. The cross correlation with the PRBS code is used in order to localize the start of the sequence.

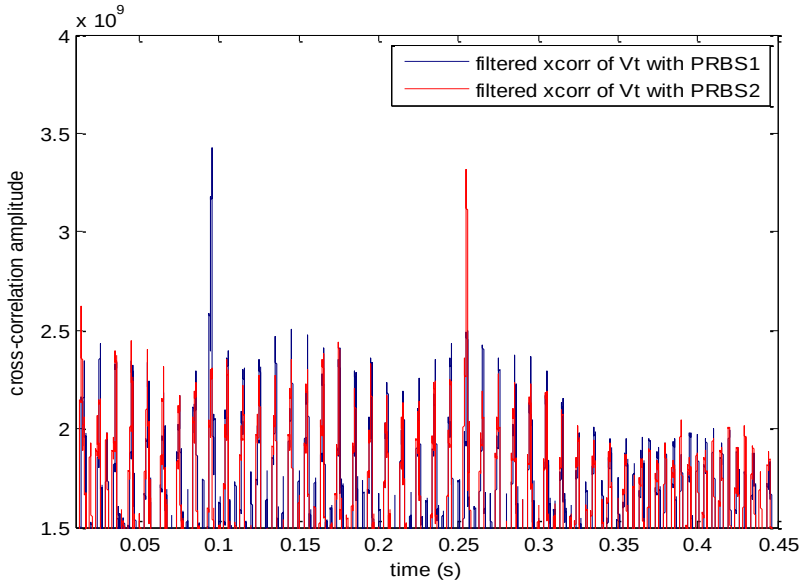

FIGURE 5.7: Correlation at receiver with PRBS codes from inverter: Code 1 detected at time 0.1s, Code 2 detected at time 0.25s

The time domain signal obtained shows a distinctive peak at the start of the pulse on Figure 5.7 for multiple incoming codes. Once a threshold is selected for detection of the start of the pulse, the identification procedure starts on the trigger of this detection procedure.

5.3.5 System Identification with Multiple Senders

Through correlation with the PRBS code, uncorrelated noise is filtered out during system identification. Therefore all transients, as well as white noise and orthogonal PRBS patterns are strongly attenuated. This is not the case for strong periodic signals such as the fundamental and harmonics, which cause localized peaks on the transfer function. The method described in this paper is a procedure elaborated in [124]. It is a simple technique, which exhibits good results for slow varying systems such as power systems. The proposed solution stores the last data frame as a default noise profile and subtracts it from the current frame in order to remove the fundamental and its harmonics.

The flowchart in Figure 5.8 describes the algorithm applied at the receiver. At the desired rate of operation, the sender generates a complete PRBS sequence. This causes voltage and currents swings to propagate on the power network. On the positive edge of the fundamental, the receiver collects data corresponding to several complete PRBS duration and stores it in a local First-In-First-Out (FIFO) buffer. The system is assumed to be time invariant for the duration of the channel estimation.

The presence of the PRBS pattern is detected by a peak on the cross correlation. This peak corresponds to the total contribution of all the PRBS pulses, thus a longer PRBS pattern and wider pulses will increase the reliability of the detection procedure. If no peak has been detected, the data is shifted up in the FIFO buffer of frames, and the process is initiated again at the next positive edge of the fundamental. If a peak has been detected the impedance is calculated according to the described procedure, and its value is stored in a time-stamped impedance buffer. For a configuration such as Figure 5.5, where multiple senders are present, the receiver performs both correlations at each step and locates each peak individually. If both PRBS sequences have been emitted at the same time, the same frame will be exploited for characterizing both powerlines.

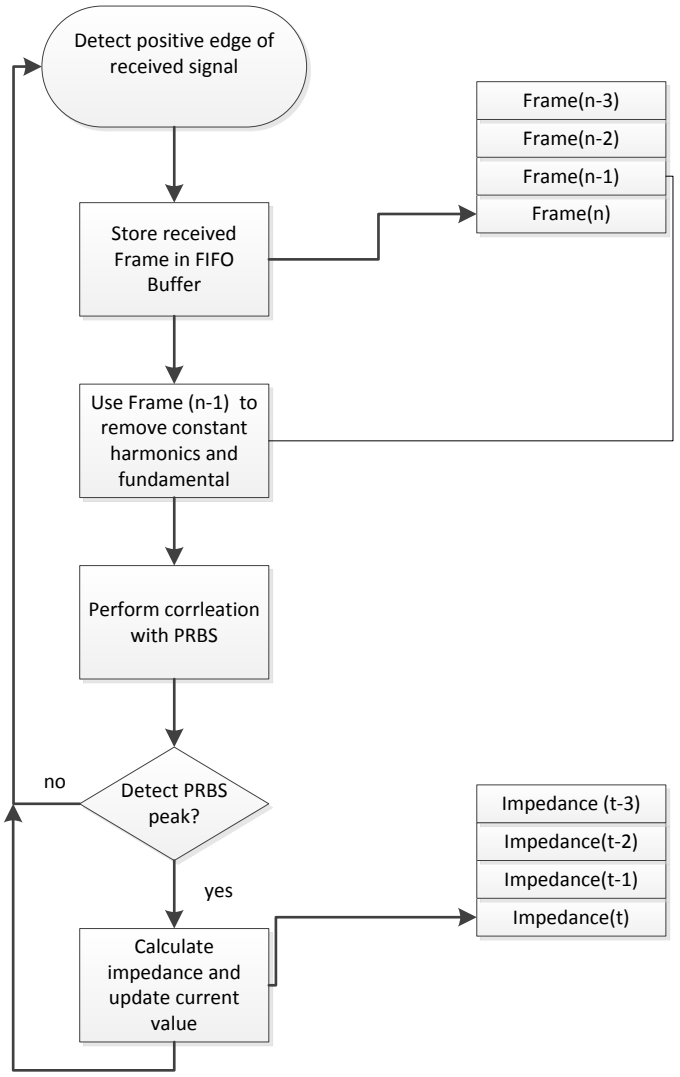

FIGURE 5.8: Flowchart of Receiver Algorithm for Channel Estimation

5.3.6 Simulation Results

Simulations have been performed using the setup described in previous Subsections. The parameters of the inverter and system are shown in Table 5.1.

The polynomial for DG1 is:

$$x^{11} + x^9 + 1 \tag{5.12}$$

The polynomial for DG2 is:

$$x^{11} + x^9 + x^6 + x^5 + 1 \tag{5.13}$$

TABLE 5.1: System Parameters

Stimulation Parameters	
PRBS code length	2047
Sampling Frequency	20 kHz
Carrier Frequency	12800 Hz
Codes per fundamental Cycle	256
PRBS Carrier Duty Cycle	1.5 %
Electrical Parameters	
Z_c	5Ω, 9.45e-1 μF
Z_f	10 mH
Z_t	0.12Ω, 20 mH
Z_l	0.2Ω, 3.2 mH
Z_{l2}	0.4Ω, 6.4 mH
Load power	P=0.001 MW, Q= 0.0001MW

On the second fundamental cycle, a 2047 bit PRBS pattern is injected in the system, using 1.5% of the carrier cycle at the inverter for pilot injection. In order to avoid spectral noise due to the limited time window, a Hanning window is used to process the data. Given the sharp low-pass characteristic of the LC filter beyond the resonance frequency, an additional lowpass filter for data processing is not necessary to avoid anti-aliasing. Current and voltage are measured at the transformer substation, and the voltage patterns at the inverter are reproduced, based on knowledge of the PRBS pattern and the operation of the PWM inverter. The PRBS excites the complete frequency range in interest. The detection process is performed as depicted in Figure 5.8, with the knowledge that the pattern always starts at the positive edge of the fundamental.

Figure 5.9 plots the impedance of the powerline based on equation 5.11, using the PWM pulses as V_f. This method can be applied if the inverter's PWM pattern is accurately known at any given time, which is not always possible if the frequency and the control of the inverter are varying over time. In addition, it can be seen that the contribution of the loads are minimal, since they have not been incorporated in the model calculation. For the loads to have an impact over identification, they would have to be increased by one or two orders of magnitude. In situations where this scenario could arise, the proposed research could also serve as a grid monitor for abnormal load variations.

Figure 5.10 shows the impedance estimated at the transformer, correlating with the PRBS pattern, rather than the PWM pulse signal. The results are exploitable,

but less accurate, especially when approaching the filters resonance frequency. The reason for this loss of accuracy is due to two reasons. This is due to the fact that a perfect alignment of the PRBS code with the voltage/current is difficult. Any slight time-shift causes changes in the spectrum that has large repercussions on individual frequencies. The harmonic noise present due to the fundamental generation, especially on low PRBS amplitudes, interference generated by harmonics for the generation of the fundamental corrupt the identification frequencies, leading to inaccuracies.The results are significantly improved by increasing the PRBS strength or by averaging the results over wider frequency bins.

In Figure 5.9 and 5.10 it can be seen that the interference between the two signals is well filtered out, due to the orthogonality of the used codes. This proves that the described technique is powerful enough for a system with multiple senders. To the receiver, the correlation of each code cancels out the contribution of the other code very efficiently code, and the effects of the interference are very limited. This method enables an online simultaneous wideband frequency identification of multiple paths, which would have been very hard to achieve with traditional methods.

5.3.7 Contributions

The method proposed in this Chapter estimates a broad spectrum impedance of the powerline using PRBS stimulations. Knowing the transfer function over a wide range allows the operator to have knowledge on potential power quality issues and address them promptly. Unlike other referenced methods such as PMU based identification, the infrastructure required for the proposed method relies on existing inverter based DGs present on the grid. In addition, explicit synchronization is not necessary for the described method, as the PRBS correlation will implicitly enable the syncing between sender and receiver. PMU based methods will require integration of these devices into the system, and have them communicate their measurements in real-time for online monitoring. For the proposed method, spectral resolution, SNR and accuracy can be improved with longer PRBS sequences. As far as other active injection methods are concerned, such as [69] and [18], concurrent measurement is problematic since the stimulations will interfere with each other and cause estimation errors. The orthogonality between PRBS code solves this problem in a very simple manner.

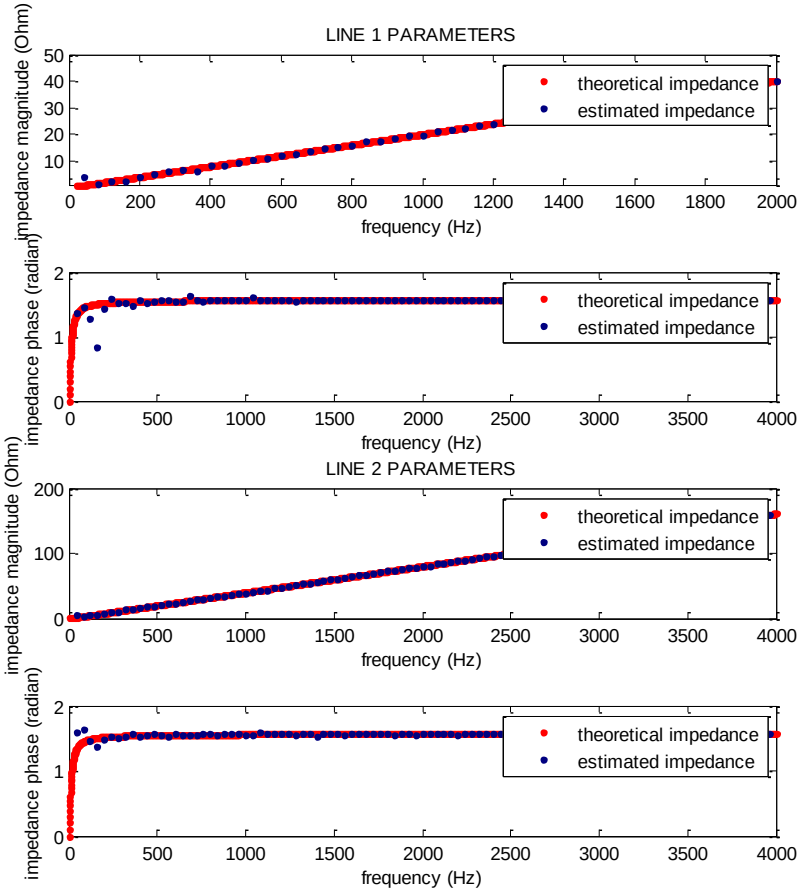

FIGURE 5.9: Impedance estimation two Inverter emitting simultaneously, correlating with the PWM signal

The results indicate that the proposed implementation can be used for identification of complex systems. It provides real added value to existing parameter identification methods, especially when broad spectrum online and concurrent measurement are required. The major benefit of using PRBS codes for identification are the wide spectrum range, the easy implementation on the inverters and their resilience to noise on the power line. Using orthogonal codes, the 'noise' injected by other inverters are filtered out as well.

Nevertheless, the lowpass nature of the powerlines attenuates the orthogonal properties of the signals at the receiver, and situations can arise when codes from other inverters corrupt the PRBS. This can be especially the case when the PRBS signals of two inverters are emitted at the same time, and one of them has a much larger

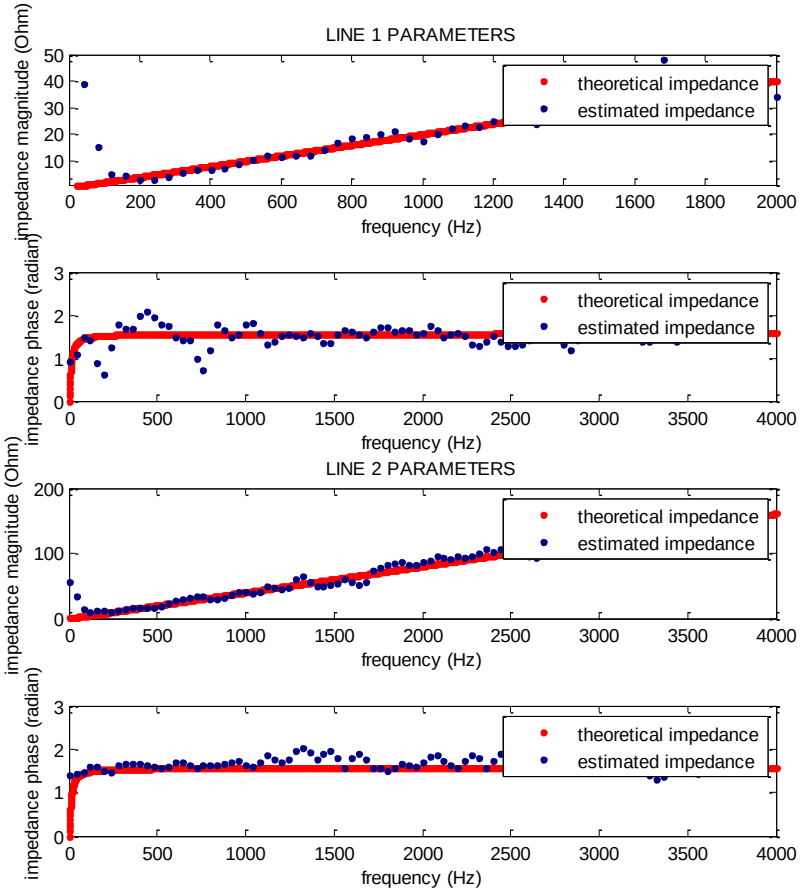

FIGURE 5.10: Impedance estimation two Inverter emitting simultanesouly, correlating with the PRBS code

magnitude at the substation that the other e.g. due to the lower impedance of its propagation path. For these specific situations, optimization techniques from communication technologies such as Successive Interference Calculation (SIC) [125] can be applied to improve results.

5.4 Performance Improvement Through Successive Interference Cancellation

5.4.1 Successive Interference Cancellation

Successive interference Cancellation has been successfully applied in telecommunications for many years [126]. The proposed innovation is the adaptation of this technique for grid parameter estimation, in order to cancel interference from concurrent pilot signals. Successive Interference Cancellation is a technique derived from CDMA research, where it is used as a tool for performance improvement and 'near/far effect' mitigation on multi user detection. When correlating with orthogonal codes, a parallel interference cancellation is performed; an alternative is to perform a Successive Interference Cancellation when additional information about the system is known beforehand [127]. The approach involves successively canceling the interference starting from the strongest users. Equation below transcribes the current signal at the receiver:

$$r(t) = \sum_{k=1}^{K} A_k \cdot a_k(t - \tau_k) \cdot \cos(\omega_c t) + n(t) \tag{5.14}$$

- r_t being the received signal,
- K the total number of simultaneous emitters
- A_k the amplitude of the k^{th} user's PRBS sequence
- n(t) additive uncorrelated noise
- cos(ωt), the fundamental over which the sequence is modulated on each emitter

The PRBS sequences injected by all emitters are known, but no knowledge of the energy of the individual emitters is needed. The strongest value is not known beforehand, but is detected from the strength of the correlation of each emitter's PRBS signal with the received signal. The correlation values are forwarded to a selector which determines the strongest correlation and selected the corresponding signal for system estimation and interference cancellation. The process is repeated

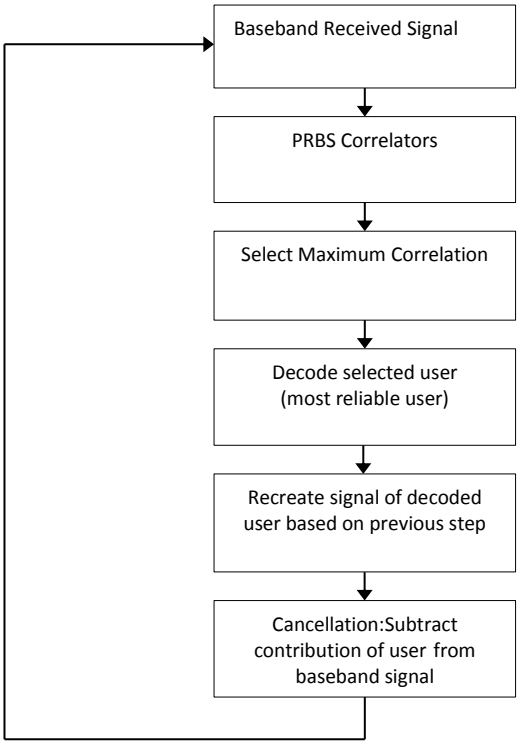

FIGURE 5.11: Successive Interference Cancellation Flowchart

until the weakest signal is decoded. The process flowchart is depicted on Figure 5.11.

The plus interference for the n^{th} user after cancellation is described by the equation below:

$$C_{j+1} = \sum_{k=j+2}^{K} A_k I_{j,j+1}\left(\tau_{k,j+1}\right) + n_{j+1} + \sum_{i=1}^{j} C_i I_{i,i+1}\left(\tau_{i,i+1}\right) \tag{5.15}$$

Where $I_{k,i}$ represents the cross correlation of the different codes:

$$I_{k,i}\left(\tau_{k,i}\right) = \frac{1}{T}\left[\int_0^T a_k\left(t-\tau_{k,i}\right)\cdot a_i\left(t\right)dt\right] \tag{5.16}$$

In Equation 5.15, the first term represents the inter-code interference due to imperfect orthogonality of all users that have not been canceled yet. The second term is due to noise in the system, the third term is due to imperfect cancellation.

In this research, an adapted version of the SIC algorithm will be applied. Performance improvement over traditional PRBS system identification will be measured and quantified for a predefined system model, which is described in the next subsection.

5.4.2 Application of SIC to model

The first step consists in continuously correlating the transformer current with all the PRBS codes of the system. When a correlation peak for any code is obtained, the steps shown on Figure 5.11 are performed. The strongest peak detected is selected for identification and the propagation path of that code is characterized through correlation with the PRBS code using Equations 5.6 and 5.11. This provides an estimation of the impedance of the propagation path from the inverter to the transformer. This information is used to recreate the current signal injected by the inverter at the transformer, taking into consideration the PRBS pattern generated at the inverter. The recreated current is subtracted from the transformer current, and the resulting current is used for identifying the second strongest. The powerline corresponding to the second strongest signal is then estimated using the resulting current I_{rec} from Figure 5.12. This operation is performed recursively until all simultaneous peaks are treated.

In traditional system estimation, every signal is decoded treating the other signals as interference. In contrast, the SIC receiver is a multiuser receiver: one of the users, say user 1, is decoded treating the others as interference, but user 2 is decoded with the benefit of the signal of user 1 already removed. Thus, it can immediately be concluded that the performance of the conventional receiver is suboptimal. The benefit of SIC over the traditional receivers is particularly significant when the received power of one user is much larger than that of the other: by decoding and subtracting the signal of the strong user first, the weaker user can get a much higher accuracy than when it has to contend with the interference of the strong user.

5.4.3 Model Setup

A similar sub-grid topology as the one in the previous Section is considered for channel estimation. The distribution grid depicted on Figure 5.13 represents the

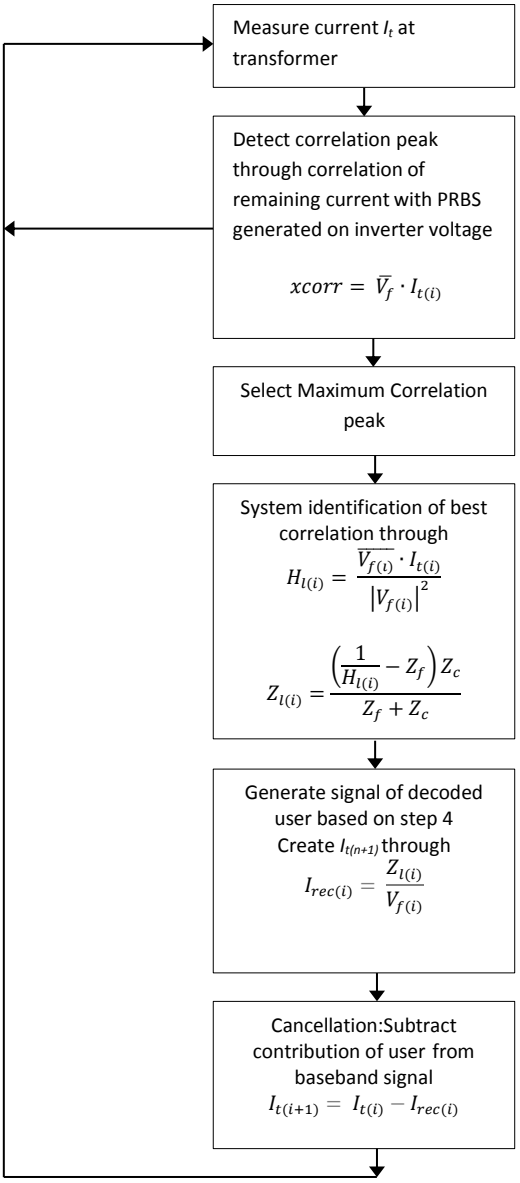

FIGURE 5.12: Flowchart of SIC algorithm for Grid Parameter Identification

studied system. The system configuration is limited to a substation with feeders in order to illustrate the algorithm. The studied system consists of a power generator connected to a voltage transformer distributing power through four feeders. Connected to the feeder are residential loads, and inverter-based distributed generators are located at the end of each feeder.

The electrical parameters of all the components of the system are described in Table 5.2, and are similar to those used in the previous section. The line impedances are selected to be very different from each other in order to illustrate the benefits of

SIC. The estimated impedance of the powerlines consists of the propagation path of the stimulation, which includes among other busbars, connectors, switchboard, fuses and the cable itself.

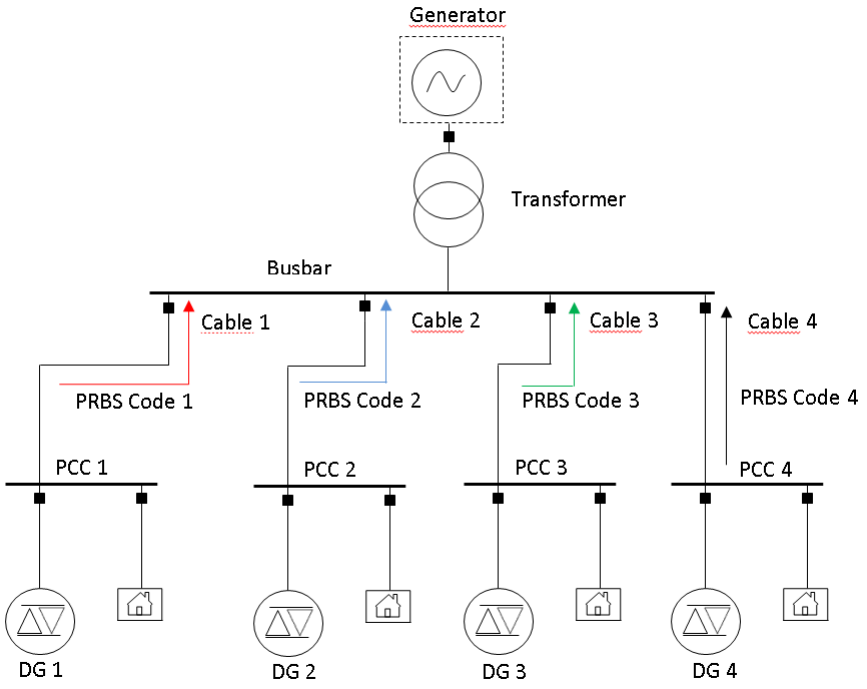

FIGURE 5.13: Distribution network model used for system identification

5.4.4 Estimation results with SIC

The simulation outcomes are shown in Figures 5.14 and 5.15. For the strongest signal, the results are identical, given that no interference cancellation has been performed on that one. But it can be seen that on the other signals, the relative improvement is considerable, apart from the low frequency end of the spectrum, where the SIC method constantly overestimates the impedance. This is also the case in the non-SIC method, but to a much lesser degree. This can be explained by the fact that the fundamental is present on all signals, and has not been considered for the identification procedure, since we only use the PRBS code to correlate with the current. Its effect is corrupting the surrounding frequencies, making the transfer function for these frequencies less responsive. This effect is magnified by SIC, due to the cumulative effect of the recursive algorithm. This issue can be resolved by:

TABLE 5.2: System Parameters

Stimulation Parameters	
PRBS code length	2047
Sampling Frequency	20 kHz
Carrier Frequency	12800 Hz
Codes per fundamental Cycle	256
PRBS Carrier Duty Cycle	1.5 %
Electrical Parameters	
Z_c	5Ω, 9.45e-1 μF
Z_f	10 mH
Z_t	0.12Ω, 20 mH
Z_{l1}	0.6Ω, 3.2 mH
Z_{l2}	1.2Ω, 6.4 mH
Z_{l3}	2.4Ω, 12. mH
Z_{l4}	4.8Ω, 25.6 mH
Load power	P=0.001 MW, Q= 0.0001MW

- Increasing the spectral resolution by lengthening the PRBS sequence
- Taking into account the fundamental which will make the algorithm more complex and dependent on inverter control
- Additional filtering and signal processing

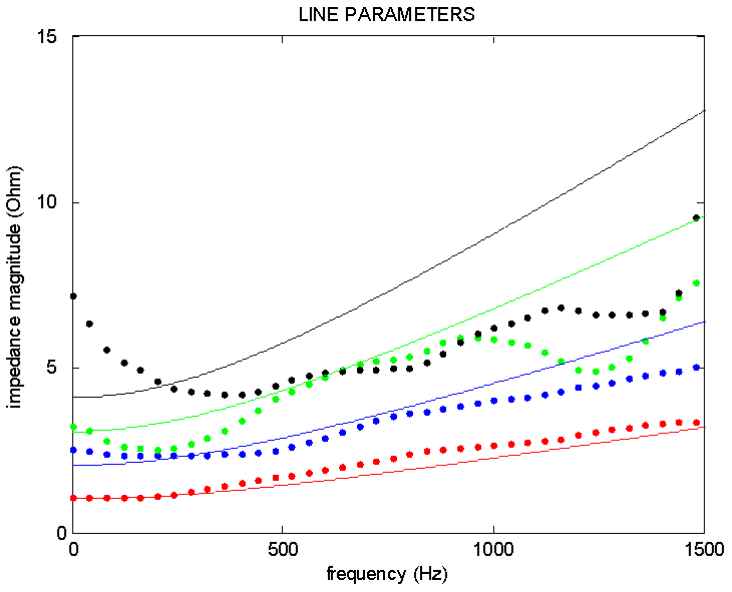

FIGURE 5.14: Line characterization of four power lines using 'parallel' identification

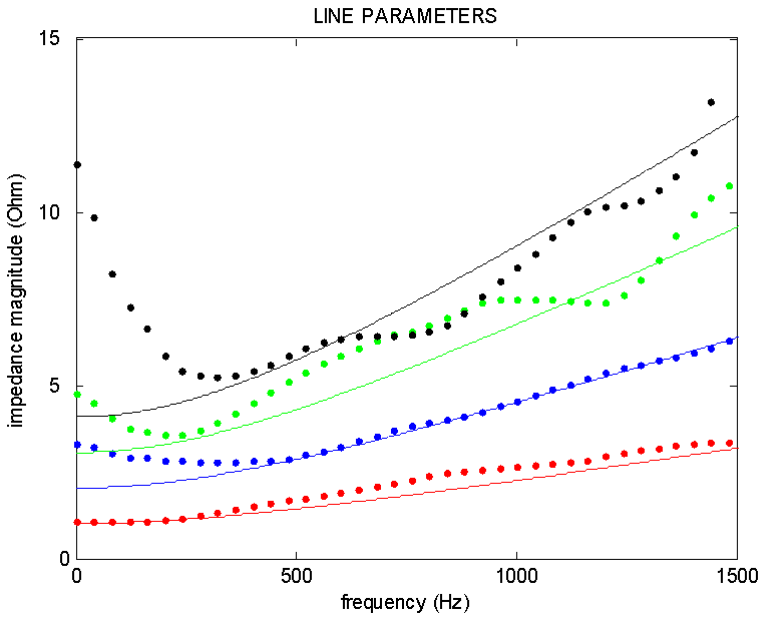

FIGURE 5.15: Line characterization of four power lines using SIC identification

The results confirm the proposed implementation can be used for multi-generator systems. It can be seen that SIC clearly improves results, especially for weak signals, and that adding that functionality to the proposed grid monitoring tool improves significantly results at no additional cost.

5.5 Contributions

A monitoring tool such as the one proposed in this paper will assist grid operators in supporting and accommodating modern and complex smart grid tools that are being developed. An advanced multi-purpose real-time estimation method for frequency dependent grid parameter determination has been presented. The method is based on PRBS sequences, which are injected as pilot signals from the inverter. PRBS sequences have been extensively used in system identification, as they exhibit great qualities such as wideband ease of implementation and orthogonality. The proposed method characterizes the propagation channel over a significant frequency range with a high resolution. It provides a high degree of flexibility; longer injections provide higher frequency resolution and accuracy, shorter patterns reduce latency and THD. Simulation results show that the proposed method

operates accurately in systems with multiple injectors, as long as each injector operates with codes orthogonal to the others.

In the next Section the objective is to identify additional parameters in a larger test-grid. In particular, we will focus on systems with multiple emitters and multiple receivers, where several measurements are combined using Weighted Least Squares methods in order to produce a global image of the network.

Chapter 6

Power System Parameter Identification

6.1 Introduction

This Chapter introduces a novel methodology for identifying parameters associated with the power system model. The proposed algorithm addresses the line parameter and topology identification task in the scope of state estimation. The goal is to reduce the a priori knowledge for state estimation, and to obtain online information on the power system network.

The mathematical model of the power system is utilized by Energy Management System (EMS) applications in the elaboration of their algorithms. Examples of such parameters are transmission line parameters, status of power switches and status of distributed generators [17]. The most important EMS tool is state estimation [128], but other state-of-the-art tools such as network topology reconfiguration [129], adaptive feeder protection in presence of DG [130] [81] use this model as well in order to optimize powerflows and guarantee proper behavior of the protective devices.

Traditional state estimation is performed under the assumption that all the network parameters are assessed correctly, and that state estimation inconsistencies are due to inaccurate measurements. But errors may also be due to topology or parameter errors, which can lead to correlated measurement divergence and deteriorate results [102] [101]. Many factors can influence the reliability and precision

of the network parameter models. Among others, meteorological conditions such as temperature and humidity along the line can have considerable impact [111].

The developed parameter estimation method relies on injected stimulations in the power system. Broadband stimulation signals are injected from distributed generators and their effects measured at various locations in the grid. To process and evaluate this data, a novel aggregation method based on weighed least-squares will be proposed. It combines and correlates various measurements in order to obtain an accurate snapshot of the power network parameters. In order to test its capabilities, the performance of this algorithm is evaluated on a small-scale test system.

6.2 State of the Art

Several parameter estimation methods have been researched and they are mostly based on modifications of existing state estimation algorithms [131] [132].

6.2.1 Parameter Estimation Based on State Estimation Residual

The first group of research analyses the residual of the state estimation procedure and looks for correlation patterns, linking measurement residuals to parameter errors [114] [133] [134] [135] [136]. This analysis is performed once state estimation is complete, and is added as an extra step to the algorithm.

In fact, if there are existing errors in the network model, the results obtained by state estimation are incorrect, and a link can be made between the model errors and state estimation residuals [137]. The status of this residual can be exploited in order to infer inaccuracies in system parameters.

This feature can be used for identifying errors in system topology, as well as electrical parameters of the lines. Parameter errors, like measurement errors, create a bias in the state estimation residual. But unlike measurement errors, parameter errors will show a consistency in a sequence of measurements which will reveal their mathematical model. That bias in the sequence of measurements allows the characterization of model errors.

Since the effect of parameter errors on residuals are coupled to the system state, a two state method is proposed in [114]. First, a bias vector is estimated that combines parameter errors with a current system state. Then, the parameter errors are extracted from a group of bias vectors based on successive state estimation runs.

6.2.2 Extended State Vector

The second group of methods uses an extended state vector and constraints on the system in order to identify the parameters to be discovered [138] [139] [116]. Additionally, research in [140] uses a Bayesian approach to identify relevant topological changes, through a second level processing of the state estimation algorithm. The method proposed in [136] adds additional soft constraints, modeled as pseudo-constraints for generalized state estimation in order to identify the correct network configuration.

The method in [139] is based on the Lagrange multipliers of the model constraints. A set of extra parameters corresponding to network parameter errors are added in the state estimation equations. Once the state estimation results are obtained, residuals of the measurements are used to calculate the Lagrange multipliers associated with the model errors. A threshold is being set, above which the errors are being considered significant and the equivalent parameter is considered to be erroneous.

6.2.3 Stimulation based method

The research in this paper considers a novel parameter estimation method based on active identification [20] [141] [142]. The method distorts the voltage at the DG by injecting a broadband stimulation, measures the current response to those signals, and obtains relevant information through correlation between the stimulation and its response. The broad spectrum currents generated are additionally measured at nearby locations in the power network in order to estimate the transfer function of their propagation paths. Several measurements are combined using a network parameter model based on the power system's admittance matrix and a Weighed Least Square (WLS) algorithm is applied in order to infer unknown system variables.

In this Chapter, the proposed active identification method based on PRBS patterns is described. The stimulation injection method applied on PWM based inverters is identical to the one used in the previous Chapters. A system parameter estimation method based on multiple concurrent measurements is proposed and a novel WLS-based algorithm, applied on the system's admittance matrix is elaborated. Finally, the method is applied on a distribution network and simulation results for practical system settings are obtained.

6.3 Proposed Method

6.3.1 Stimulation Signal

The proposed system identification method is based on stimulation injection. The inverter based stimulation generation method will be the one described in Chapter 3 and Chapter 4. In fact, the objective is to reuse the stimulation signals generated for islanding detection, and measure them at various locations in the grid.

The PRBS code used in this Chapter is a 12-bit PRBS consisting of 4095 codes. The code length corresponds to one carrier cycle, which is operating at 12800 Hz, thus each fundamental cycle contains 256 codes. The correlation operations, and transfer function determination will be performed as in Chapter 5.

6.3.2 Model Based System Parameter Estimation

The power network is a complex grid of networked components. Due to the slow dynamics and high inertia of power systems, the system can be considered invariant during the stimulation injection. Also, due to the orthogonality property of the PRBS signal, it will be assumed in the analytical model that interferences between stimulations and other signals are effectively filtered out. Thus, in the elaboration of mathematical model, it will be assumed that only one PRBS stimulation signal is present as an active injection signal during its time period.

The sources inject broadband stimulation patterns on the power network. There are N injecting emitters on the network, and the matrix V_s represents the Discrete Fourier transform of all voltage stimulations. At the M receivers, the resulting

broadband current is measured and correlated with the PRBS codes of the N senders according to Equation 5.3. A correlation peak is detected when the signal is present. The transfer function between the emitter and the receiver is established based on 5.3 - 5.6. As the PRBS stimulates a wide frequency band, this relation can be established up to several kHz, above which the spectral content of the PWM based PRBS wanes off and identification becomes challenging. Figure 6.1 illustrates the general configuration of the system and the problem to be solved.

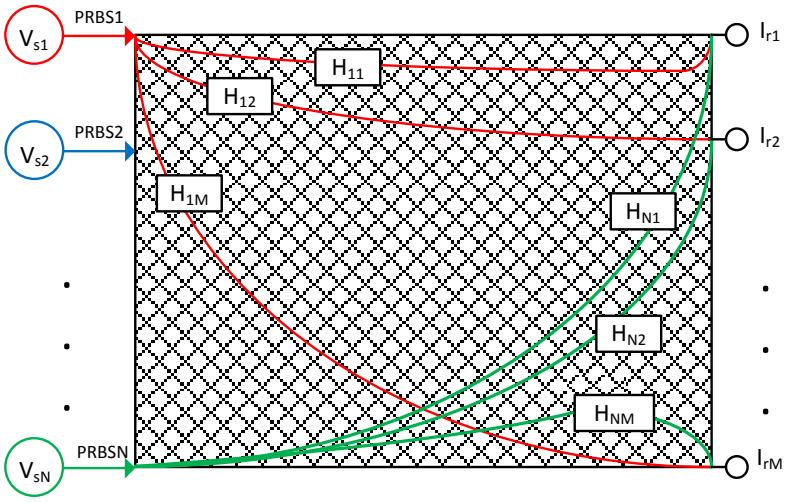

FIGURE 6.1: Power Network Identification through voltage stimulation and current measurements

For each source V_{sK}, the relationship between the source and the receivers is defined by the matrix of the injections in network :

$$\overline{V_{sk}} = \sum_{i=1}^{M} {H^{-1}}_{ik} \times I_{ki} \tag{6.1}$$

where

$$\overline{V_s} = \begin{bmatrix} \overline{V_{s1}} \\ \overline{V_{s2}} \\ \vdots \\ \overline{V_{sN}} \end{bmatrix} \tag{6.2}$$

$$H = \begin{bmatrix} H_{11} & H_{12} & \cdots & H_{1M} \\ H_{21} & H_{22} & \cdots & H_{2M} \\ \vdots & \vdots & & \vdots \\ H_{N1} & H_{N1} & \cdots & H_{NM} \end{bmatrix} \tag{6.3}$$

$$I_r = \begin{bmatrix} Ir_{11} & Ir_{12} & \cdots & Ir_{1N} \\ Ir_{21} & Ir_{22} & \cdots & Ir_{2N} \\ \vdots & \vdots & & \vdots \\ Ir_{M1} & Ir_{M2} & \cdots & Ir_{MN} \end{bmatrix} \tag{6.4}$$

Each of the N emitters creates a current stimulation at each of the M receivers. Thus an NxM matrix of transfer function is established in order to characterize the dynamic relationship between each sender and receiver. This matrix H, shown in Equation 6.4, characterizes the transfer functions of each path shown in Figure 6.1.

On the other hand, the electrical dynamics of the power network are described by its admittance matrix as well. In order for the H matrix to correspond to the admittance matrix, the following changes are performed, assuming that the power network under study has K nodes, where K<N and K<M. The V_S matrix is modified to a matrix of K elements, with zeros injection on nodes without PRBS stimulation.

The current measurement at the node of each emitter corresponds to the equivalent voltage stimulation and e.g. Ir_{31} represents the current measured at node 3, resulting from stimulation from node 1. The current resulting from the PRBS at the DG is measured and evaluated. The I_r matrix is expanded to a KxK matrix, with 0 values on power network nodes without measurement.

For topology identification, the objective is the evaluation of relay settings and DG connection status. An infinite impedance models a line with an open relay setting. For a closed relay setting, the impedance of the powerline itself is considered in the admittance matrix. Thus, each element of the admittance matrix will be composed of line admittances, loads, source admittances, with binary unknowns related to each of the relay settings to be discovered. These binary values depend on the connection status of the relays and DG status. The configuration of system under study will look as depicted in Figure 6.2 and the equations to be solved are rewritten for a given frequency ω in Equation 6.5.

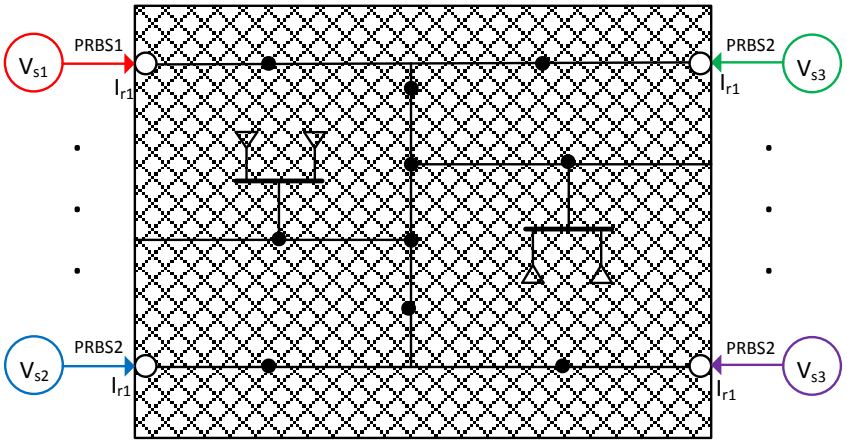

FIGURE 6.2: System identification in power network, using voltage sources as pilot injectors

The equations to be solved for each frequency ω are:

$$\overline{V_{sk}(\omega)} = \sum_{i=1}^{K} Ymatrix^{-1}{}_{ik} \cdot \omega_{(loads,sources,lines,relays)} \cdot Ir_{ki}(\omega) \tag{6.5}$$

In the next sub-section, a Weighed-Least-Squares method will be applied for the iterative estimation of the unknown parameters.

6.3.3 Overview of WLS algorithm

WLS is an optimization algorithm, whose objective the determination of the most likely state of the system based on the measured data. A common method to acquire this estimation is to perform Maximum Likelihood Estimation (MLE), a typical technique employed in statistical analysis. The errors on the measurements are assumed to have a known probability distribution, and the mathematical relations are established, representing the unknown parameters in terms of the probability functions of all measurements [143]. This function is called the likely hood function and it will attain its maximum when the estimated values of the unknown variables hit their real values. The optimization system to be solved is to maximize the likelihood function by estimating the real values of the unknown parameters to be characterized.

It will be assumed that measurements have a Gaussian error distribution, with a mean μ and variable σ^2. Thus the normal probability density function for a random variable is defined as:

$$f(z) = \frac{1}{\sqrt{2\pi}\sigma} e^{-\frac{1}{2}\left(\frac{z-\mu}{\sigma}\right)^2} \tag{6.6}$$

where z is a random variable, μ the mean of z, and σ the standard deviation of z. Doing the variable substation:

$$u = \frac{z-\mu}{\sigma} \tag{6.7}$$

one obtains:

$$E(u) = 0 \tag{6.8}$$

$$Var(u) = 1 \tag{6.9}$$

And the new function to be dealt with becomes

$$\Phi(u) = \frac{1}{\sqrt{2\pi}} e^{-\frac{u^2}{2}} \tag{6.10}$$

which is the standard Gaussian probability density function.

The joint probability density function of m independent measurements, all having the same Gaussian distribution, can be expressed as as:

$$f_m(z) = f(z_1)f(z_2)...f(z_m) \tag{6.11}$$

where z_i is the i^{th} measurement. $f_m(z)$ is the likely function of z, indicating the probability of observing a particular combination of measurements. The optimization objective is to maximize $f_m(z)$, by adjusting the parameters of the function μ and σ. In order to simplify the calculations, $f_m(z)$ is replaced by its logarithm and the modified likely function can be expressed as:

$$L = \log f_m(z) = \sum_{i=1}^{m} \log f(z_i) \tag{6.12}$$

$$= -\frac{1}{2}\sum_{i=1}^{m}\left(\frac{z_i-\mu_i}{\sigma_i}\right)^2 - \frac{m}{2}\log 2\pi - \sum_{i=1}^{m}\sigma_i \tag{6.13}$$

The goal of WLS is to maximize the likelihood function, and thus it can be obtained by either maximizing:

$$\log f_m(z) \tag{6.14}$$

or minimizing:

$$\sum_{i=1}^{m} \left(\frac{z_i - \mu_i}{\sigma_i} \right)^2 \tag{6.15}$$

Considering the residual r_i for each measurement, which is defined as:

$$r_i = z_i - \mu_i = z_i - E(z_i) \tag{6.16}$$

where μ_i and $E(z_i)$ for each measurement z_i can be expressed as a non-linear function $h_i(x)$to the system state vector x. The square of each measurement is compounded by a weight parameter W_{ii} set to σ^2. The optimization problem to be solved can the be rewritten as minimizing the weighed sum of the squares of the residuals for the state vector x.

The objective is to minimize

$$\sum_{i=1}^{m} W_{ii} r_i^2 \tag{6.17}$$

where, for each measurement i=1...m

$$z_i = h_i(x) + r_i \tag{6.18}$$

A measurement model to be solved can be written as:

$$z = h\left(l_p, t_{p,} c_p\right) + e \tag{6.19}$$

where z is the measurement vector, $h(l_p, t_{p,} c_p)$ is the nonlinear function relating the measurements to the system parameters, consisting in the case under study of line parameters, topology and connection parameters, l_p is the vector containing network line parameters, t_p is the vector containing network topology and connection parameters, c_p is the vector of DG connection parameters, and e is the vector of measurement errors.

There are m measurements and n variables to be determined, with the over-specification constraint that n<m. The WLS parameter estimation can be formulated mathematically as an optimization problem with a quadratic objective function with additional equality constraints implemented as pseudo-measurements, the residual being defined as:

$$r = \ z - h\left(x, p\right) \tag{6.20}$$

The objective function to be minimized is:

$$J(x,p) = \sum_{i=1}^{m} \frac{(z_i - h_i(x))^2}{R_{ii}} \tag{6.21}$$

$$= [z - h(x,p)]^T R^{-1} [z - h(x,p)] \tag{6.22}$$

where R is the covariance matrix, related to the estimated accuracy of each measurement. The minimum of the objective function can be obtained if:

$$g(x) = \frac{dJ(x)}{dx} = -H^T(x) R^{-1} [z - h(x)] = 0 \tag{6.23}$$

$$H(x) = \left[\frac{dh}{dx}\right] \tag{6.24}$$

Expanding g(x) into its non-linear Taylor series, one obtains:

$$g(x) = g\left(x^k\right) + G\left(x^k\right)\left(x - x^k\right) + \ldots = 0 \tag{6.25}$$

and neglecting the higher order terms leads to an iterative solution scheme known as the Gauss-Newton method as shown below:

$$x^{k+1} = x^k - \left[G\left(x^k\right)\right]^{-1} \cdot g\left(x^k\right) \tag{6.26}$$

where k is the iteration index, x_k is the solution vector at iteration k.

$$G(x) = \frac{dg\left(x^k\right)}{dx} = H^T\left(x^k\right) \cdot R^{-1} \cdot H\left(x^k\right) \tag{6.27}$$

$$g\left(x^k\right) = -H^T\left(x^k\right) \cdot R^{-1} \cdot \left(z - h\left(x^k\right)\right) \tag{6.28}$$

The iterative process is usually stopped once convergence is assumed, that is for a threshold, once

$$\left|\Delta x^k\right| \leq \epsilon \tag{6.29}$$

Figure 6.3 provides a flowchart of the steps involved in the iterative WLS procedure.

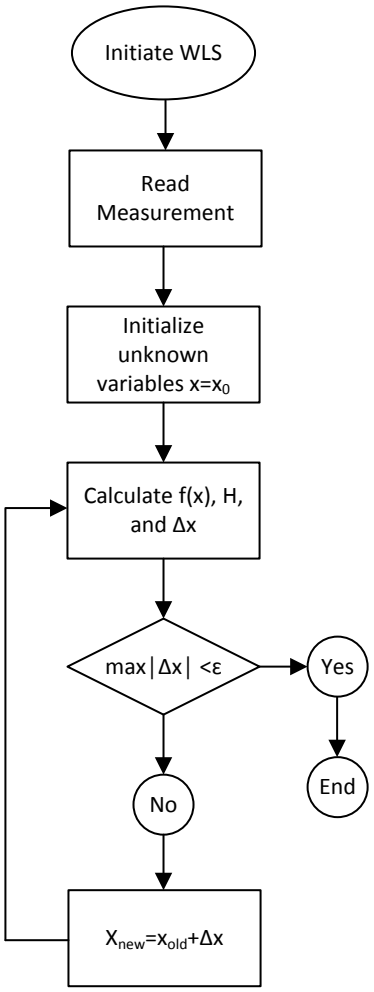

FIGURE 6.3: WLS flowchart

6.3.4 Application to Distribution Network

6.3.4.1 System Model

The distribution network topology depicted in Figure 6.4 is considered for the application of the parameter estimation algorithm. It consists of a high voltage network connected to a voltage transformer distributing power through two feeders. The feeders are branched twice to distribute power the loads. The electrical model of the network comprises three switches for topology reconfiguration, seven nodes, and six transmission lines. The complete network can be fed through feeder 1, feeder 2 or both depending on the status of the switches S1, S2 and S3. DG1, DG2, DG3, and DG4 are monitoring DGs. They inject periodically PRBS

sequences on the network. On top of the witch settings, the connection status of DG5 and DG6 is intermittent and not known by the operator. The electrical parameters of the system are described in Table 6.1. The intended frequency identification range is up to 2000 Hz, since the first forty harmonics are considered for power quality considerations in European grid codes [71].

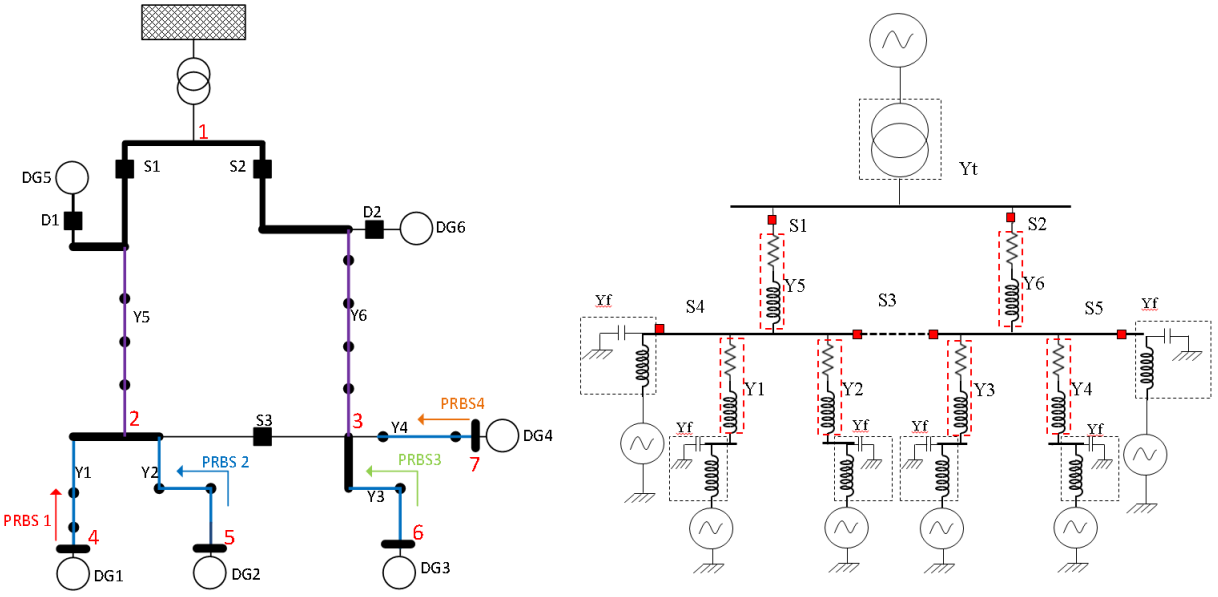

FIGURE 6.4: a. Distribution network model used for system identification b. Electrical model of network to be analyzed

The electrical model of the system under study is depicted in Figure 6.4b. The nodes with small loads can be discarded and only nodes with DG connections and switches are considered. The output filters of all DGs are LC filters and their admittances Yf are assumed to be all identical. The unknown parameters in the system are switch settings S1-S3, DG connection status connection status D1-D2 and the line impedances Y1-Y6, consisting of a resistive and inductive component. For the transmission line lengths considered and for the line parameters typically used in the Luxembourgish power network, the capacitive effect is negligible and will not be considered for line parameter estimation. The parameters to be characterized for each line are thus series resistance and series inductance represented by the complex parameter Y1-Y6. The admittance matrix of the network is shown

in 6.30:

$$Ymatrix = \begin{bmatrix} Y_{sum1} & -S1 \cdot Y5 & -S2 \cdot Y6 & 0 & 0 & 0 & 0 \\ -S1 \cdot Y5 & Y_{sum2} & -S3 \cdot Ys3 & -Y1 & -Y2 & 0 & 0 \\ -S2 \cdot Y6 & -S3 \cdot Ys3 & Y_{sum3} & 0 & 0 & -Y3 & -Y4 \\ 0 & -Y1 & 0 & Y_{sum4} & 0 & 0 & 0 \\ 0 & -Y2 & 0 & 0 & Y_{sum5} & 0 & 0 \\ 0 & 0 & -Y3 & 0 & 0 & Y_{sum6} & 0 \\ 0 & 0 & -Y4 & 0 & 0 & 0 & Y_{sum7} \end{bmatrix} \tag{6.30}$$

$$Y_{sum1} = Y_t + Y5 \cdot S1 + Y6 \cdot S2 \tag{6.31}$$

$$Y_{sum2} = Y5 \cdot S1 + Y1 + Y2 + Ys3 \cdot S3 + Yf \cdot D1 \tag{6.32}$$

$$Y_{sum3} = Y6 \cdot S2 + Y3 + Y4 + Ys3 \cdot S3 + Yf \cdot D2 \tag{6.33}$$

$$Y_{sum4} = Y1 + Yf \tag{6.34}$$

$$Y_{sum5} = Y2 + Yf \tag{6.35}$$

$$Y_{sum6} = Y3 + Yf \tag{6.36}$$

$$Y_{sum7} = Y4 + Yf \tag{6.37}$$

DG1-DG4 will be injecting PRBS patterns on the power network. The injections are orthogonal, thus their interference will be minimal if concurrent injections from two DGs happen. At DG1-DG4, and at the transformer substation, a receiver is correlating the incoming current with the PRBS codes of all senders. Upon arrival of the stimulation, a correlation peak is detected [20]. Using Equation 6.5, the transfer function between the emitter and the receiver can be established, for the frequency range stimulated by the PRBS.

The admittance matrix of the network is available for power networks for state estimation. It will serve as a basis for the proposed method, and it will be modified for our purpose of multi-frequency identification. Given that PRBS codes are orthogonal and that their cross-correlation with uncorrelated signals is very small, for the elaboration of the equations it will be assumed that during their injection, they are the only active injection present on the system for the considered frequencies. For the seven node system depicted in Figure 6.4, the relationship between Vsender and Ireceiver can be expressed based on methods such as the one

presented in [21]:

$$\begin{bmatrix} 0 \\ 0 \\ 0 \\ V_{snd4} \\ 0 \\ 0 \\ 0 \end{bmatrix} = Ymatrix^{-1} \cdot \begin{bmatrix} I_{rcv1-4} \\ 0 \\ 0 \\ I_{rcv4-4} \\ I_{rcv5-4} \\ I_{rcv6-4} \\ I_{rcv7-4} \end{bmatrix} \tag{6.38}$$

V_{snd4} corresponds to the voltage spectrum created at node 4, and $I_{rcv(1\text{-}4)}$ are the current harmonics measured at node 1 due to V_{snd4}. The current stimulations injected from each DG are detected at each of the monitored nodes in the network, corresponding to node 1, 4, 5, 6 and 7. V_{snd} is the pattern injected at the DG, and is known in advance for each DG. I_{rcv} is detected, measured and evaluated at the receiver when the PRBS pattern is incoming. Thus transposing V_{snd} and Ircv to the Fourier domain for each frequency provides 5 equations linking those parameters at nodes 1, 4, 5, 6, 7, using the unknown parameters of the admittance matrix, as shown in 6.38. The same operation can be performed with DG1, DG2, DG3 and DG4, thus a total set of 20 complex equations are obtained for each frequency. The complete matrix equation to be solved is shown in 6.39.

On the equation of the admittance matrix 6.30, the switch settings are modeled by a parameter S1-S3, and the DG connection status by a parameter D1-D2. These are binary values depending on the connection status of the switch/DG. When the switch S1 is open, the parameter S1 on the Ymatrix has the value 0, which represents an open connection between node 1 and node 2. For a closed connection, S1 takes the value 1, and the admittance of the line will be the parameter used in the admittance matrix.

$$\begin{bmatrix} 0 & 0 & 0 & 0 \\ 0 & 0 & 0 & 0 \\ 0 & 0 & 0 & 0 \\ Vsnd4 & 0 & 0 & 0 \\ 0 & Vsnd5 & 0 & 0 \\ 0 & 0 & Vsnd6 & 0 \\ 0 & 0 & 0 & Vsnd7 \end{bmatrix} = Ymatrix^{-1} \cdot \begin{bmatrix} Ircv_{1-4} & Ircv_{1-5} & Ircv_{1-6} & Ircv_{1-7} \\ 0 & 0 & 0 & 0 \\ 0 & 0 & 0 & 0 \\ Ircv_{4-4} & Ircv_{4-5} & Ircv_{4-6} & Ircv_{4-7} \\ Ircv_{5-4} & Ircv_{5-5} & Ircv_{5-6} & Ircv_{5-7} \\ Ircv_{6-4} & Ircv_{6-5} & Ircv_{6-6} & Ircv_{6-7} \\ Ircv_{7-4} & Ircv_{7-5} & Ircv_{7-6} & Ircv_{7-7} \end{bmatrix} \tag{6.39}$$

In the next sub-section, a Weighed-Least-Squares method based on the Gauss-Newton algorithm will be used to identify the unknown parameters. Subsequently, we will elaborate on how the WLS algorithm processes these values in order to estimate the connection/topology status.

6.3.4.2 WLS Execution on System Model

The system to be solved in equation 6.39 can be considered to be parameter estimation over multiple frequencies. The variables to be determined are partially binary (S1, S2, S3, D1, D2) and partially complex (Y1, Y2, Y3, Y4, Y5, Y6). The system is overdetermined and a unique solution can be obtained.

In the application of WLS to the system, the measured parameters are the resulting current signals, which provide the transfer function for each propagation path, through the application of Equations 6.1. The function relating measurements to system parameters is the modified admittance matrix which contains the following unknowns:

- Line parameters lp
- Switch settings tp
- DG connection status cp

$$h(l_p, t_p, c_p) = Ymatrix(l_p, t_p, c_p) \tag{6.40}$$

These parameters are being guessed initially, and the estimation is refined though the iterative process. The Jacobian of the inverse of the admittance matrix is computed for each parameter and the iterative process adjusts the unknown variables in order to minimize the residual. Thus, the objective function is minimized according to the Equations 6.20 - 6.29. The weights are an important factor, since all measurements don't have the same importance at each node. The weight (inverse of covariance) for each measurement is set based on the reliability of the measurement, which is related to the magnitude of the cross correlation peak, as determined in Chapter 5. The values for the weights are therefore dynamically computed for each measurement. Given the broadband nature of the PRBS, the parameter estimation can be operated for a wide range of frequencies. Thus the

WLS algorithm can be repeated for several frequencies, in order to provide additional data points for confirming the switch settings, and in order characterize the broad spectrum dynamics of the power network components.

In the system under study, there are four PRBS injectors, acting as senders, and five receivers, detecting and measuring each of the current harmonics produced by these senders. There are a total of 11 unknowns to be determined (5 connections settings, 6 line impedance values) and 20 equations linking those unknowns for each frequency.

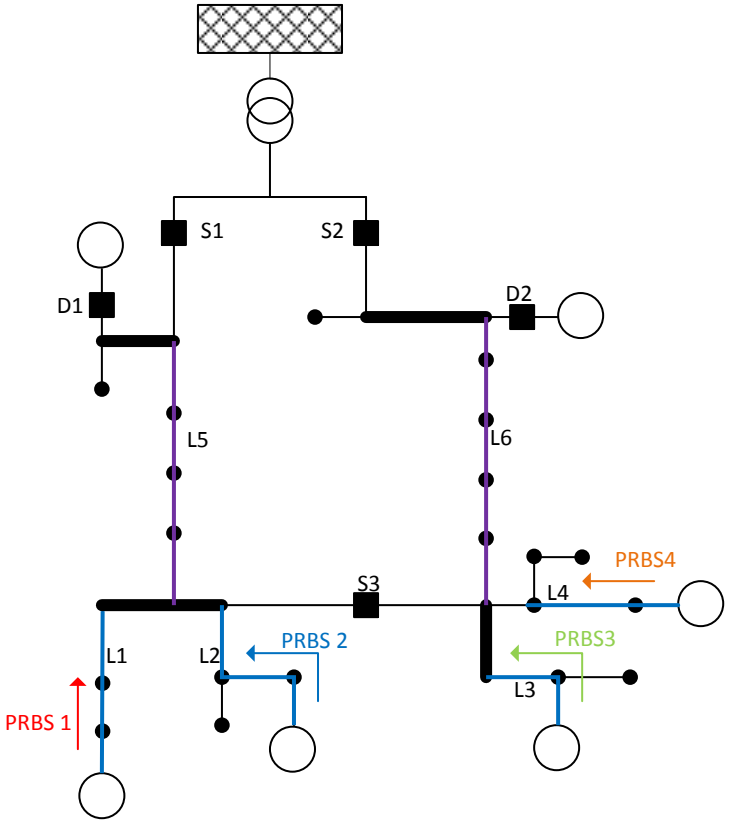

FIGURE 6.5: Distribution Network to be Characterized

Performing WLS on the system doesn't provide satisfactory results in all conditions. Instabilities might arise due to the binary nature of the switch setting parameters and the highly non-linear system may lead to inaccurate values due to local minima reached by the WLS algorithm, in conjunction with measurement noise caused by imperfect cancellation of existing interference and harmonics.

Several improvements are considered. The WLS algorithm is executed over a range of frequencies and the redundancy of these multiple WLS runs is exploited in order

to perform the identification sequentially and obtain the parameters serially. In addition, in order to enhance accuracy, in the first instance, line parameters are assumed to be known within their order of magnitude (within 40% of their actual value).The WLS equations are solved with the only unknown parameters being the switch settings and DG connection parameters. The algorithm is executed over the frequency range of 80 – 2000 Hz in 100 Hz intervals, and the average of the converged estimates, weighed with the final residual, are assumed to be accurate. In a second step, the line parameters (inductance and resistance of the lines) are determined. The resistive component becomes negligible beyond 200 Hz, compared to the inductive effect. Thus, once the switch settings are determined, the WLS algorithm is executed on the 80 – 2000 Hz range, in order to estimate the inductance for each line. The resistive parameters are finally computer assuming all other parameter known by running WLS for the low frequency range. Finally, the complete WLS algorithm is re-executed, with the previously obtained values used as an initial guess for unknown parameters, and a rapid convergence should be obtained if the previous estimates are accurate.

The flowchart in Figure 6.6 highlights the steps to be executed for topology and line parameter identification. Each receiver continuously scans for the injected stimulation codes as described in Chapter 5. When all codes are detected, the transfer functions of their propagation paths are estimated by applying equation 6.1. All the established transfer functions are then combined in Equation 6.39, linking the voltage stimulations to the corresponding current responses. Consequently, three WLS runs are executed determining first the topology and DG connection settings, then the inductive components of the lines, and finally the resistive components of the lines. The algorithm then returns to the initial step, looking for the new stimulation signals.

In the next sub-Section, the described model and the defined algorithm are executed on Simulink and Matlab, in order to illustrate the feasibility and performance of the proposed method.

6.3.5 Simulation Results

Simulations are based on the system described in the previous sub-Section. The model is executed on Simulink/Matlab for PRBS injection, correlation estimation and WLS algorithm. The characteristics of the system to be estimated, including

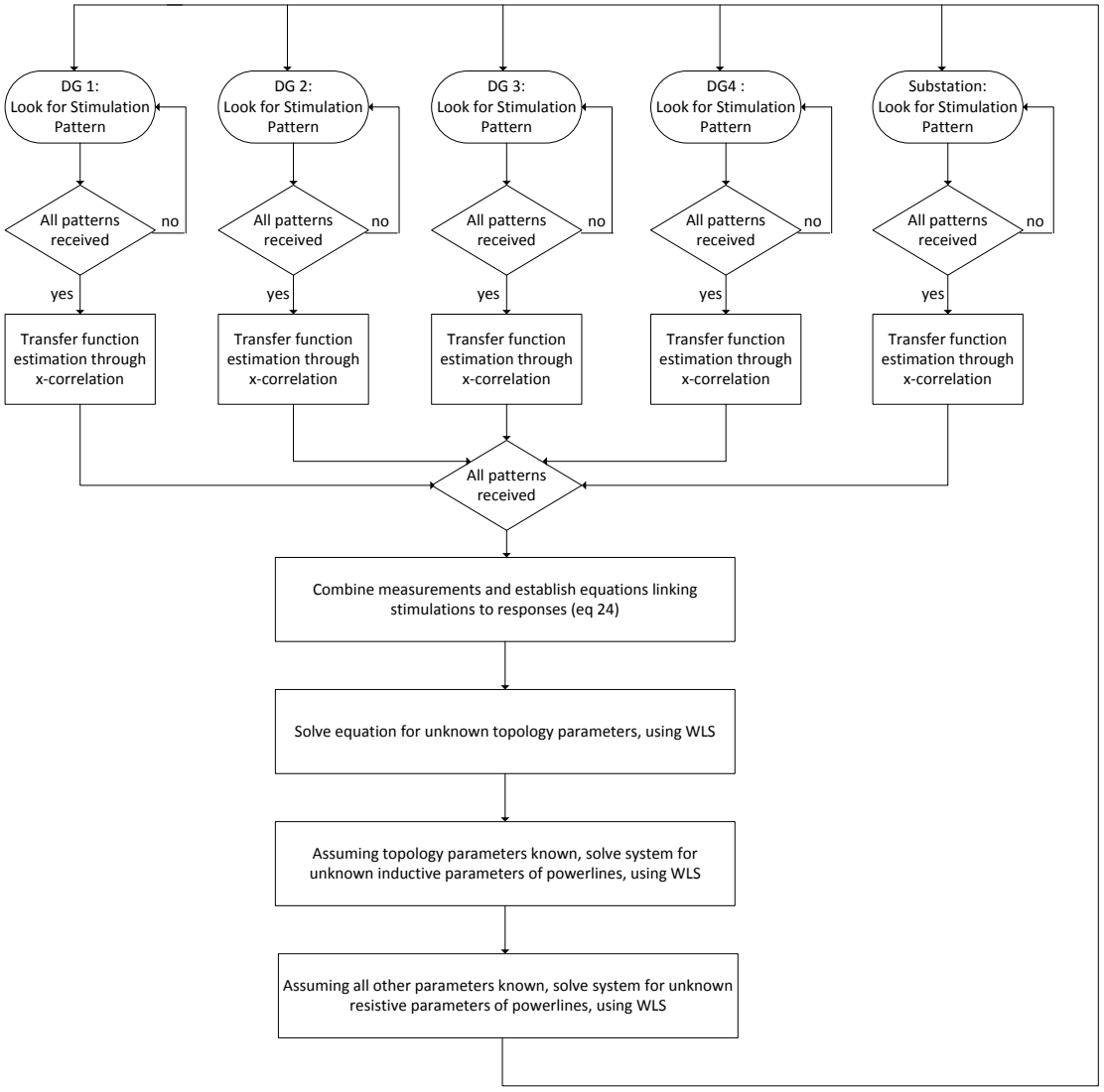

FIGURE 6.6: Proposed Algorithm Flowchart for System Identification

stimulation parameters and receiver settings are listed in Table 6.1. The network considered for the application of the algorithm is the one depicted in Figure 6.5. The output filters of all DGs are LC filters and their admittances Yf are assumed to be identical. The unknown parameters in the system are the switch settings S1- S3, DG connection status connection status D1-D2 and the line impedances Y1-Y6, consisting of a resistive and inductive component.

The polynomials of the PRBS codes emitted from each DG are shown in Table 6.1. They represent orthogonal 12-bit PRBS sequences and each generates a sequence of 4093 symbols before it repeats itself. In the simulation settings, the signals are

TABLE 6.1: System Parameters

Stimulation Parameters	
PRBS code length	4093
PRBS polynomial node 1	$x^{12} + x^8 + x^2 + x + 1$
PRBS polynomial node 2	$x^{12} + x^6 + x^4 + x + 1$
PRBS polynomial node 3	$x^{12} + x^6 + x^5 + x^3 + 1$
PRBS polynomial node 4	$x^{12} + x^7 + x^6 + x^2 + 1$
Sampling frequency	50 KHz
Carrier frequency	12800 Hz
Codes per fundamental cycle	256
PRBS duty cycle	5%
Electrical System Parameters	
Line 1 impedance Zl1	0.1 Ω , 2 mH
Line 2 impedance Zl2	0.3 Ω , 6 mH
Line 3 impedance Zl3	0.2 Ω , 1 mH
Line 4 impedance Zl4	0.1 Ω , 2 mH
Line 5 impedance Zl5	0.3 Ω , 3 mH
Line 6 impedance Zl6	0.1 Ω , 1 mH
Line 7 impedance Zl7	0.2 Ω , 2 mH
Inverter Output filter Zc – Zf	5 Ω , 9.45e1μF - 10 mH
Transformer Impedance Zt	0.12 Ω , 20 mH
Switch settings	SW1 = 1, SW2 = 0, SW 3= 1
DG connection setting	DG1=0, DG2 = 1

concurrent, thus, interference between signals is maximal. The current measurements are sampled at the receivers at 50 kHz, which is 25 times above the highest studied frequency. The inverter's carriers producing the stimulation have a switching frequency of 12800 Hz. Therefore each period of the fundamental takes 256 pulses, and 256 PRBS codes are transmitted during each fundamental. A PRBS sequence takes 16 50 HZ cycles to complete. The duty cycle for the PRBS is set to 5% in the simulation settings.

The first step of the algorithm is the estimation of the transfer functions correlating the PRBS injections, and measurements at various locations in the grid. The measurements are done in a noisy environment, with multiple generators running. Figure 6.7 shows the results of transfer function identification for PRBS from source DG1, DG2, DG3, and DG4. The straight line corresponds to the theoretical value to be obtained, based on the calculated value of the equivalent model. The noisy/colored lines are the results obtained through PRBS injection and correlation. The weights associated to these noisier measurements will be lower in

the WLS algorithm. The measurements close to the PRBS source will have higher impact during WLS, while measurements electrically far from the source provide low reliability data, associated with a small weight during WLS.

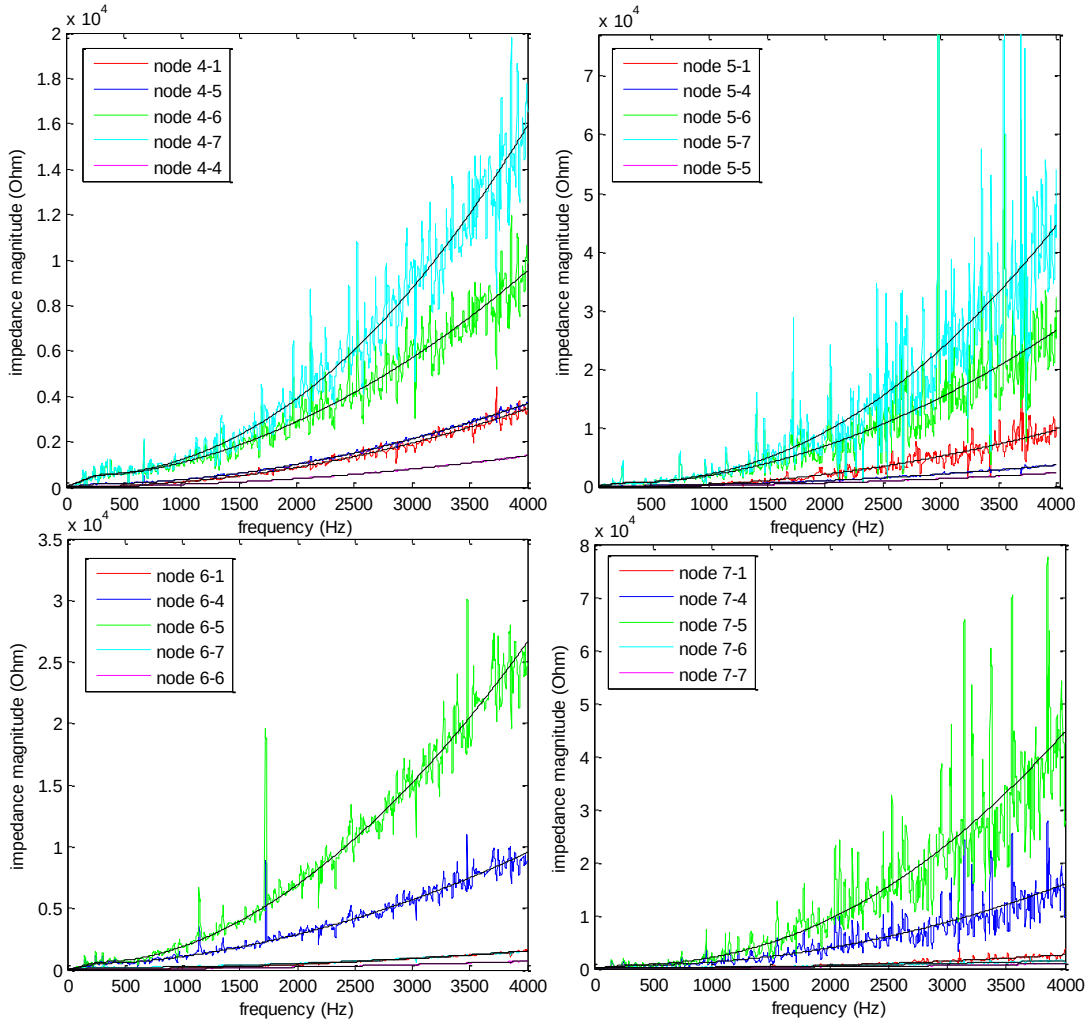

FIGURE 6.7: Theoretical and Estimated Transfer Function from Source to Destination Nodes

Equivalent data is collected and processed for all four PRBS sources, then evaluated. The second step of the algorithm is the estimation of the power network parameters. The data from the Simulink run, shown in Figure 6.7, is processed with the parameter identification algorithm, using the Ymatrix and the equations elaborated previously. The results of each of the two WLS runs is listed and analyzed below.

6.3.5.1 DG Connection and Switch Status Identification

The switch settings are set to '101', and the DG settings to '01': the complete network is powered by the left feeder, and the DG on node DG2 is disconnected. For the initial setting of the WLS algorithm, all parameters are set to '0.5'. The algorithm is executed on the 80-2000 Hz frequency range, with 100 Hz intervals. The results obtained by this procedure are shown in Table 6.2.

TABLE 6.2: Topology estimation through WLS for 80-2000 Hz

	S1	**S2**	**S3**	**D1**	**D2**		
	Topology values to be found						
	1	**0**	**1**	**0**	**1**		
	Initial WLS setting						
	0.5	**0.5**	**0.5**	**0.5**	**0.5**		
Frequency	**WLS result**					**residue**	**err %**
80	0.99	0.02	0.98	0.05	0.85	0.16	8%
180	*0.95*	*0.04*	*0.57*	*0.94*	*0.02*	*1.58*	*81%*
280	0.99	0.05	1	0.05	0.93	0.3	6%
380	0.78	0.03	1	0.05	0.96	0.24	13%
480	0.85	0.01	1	0.95	0.05	2.65	70%
580	0.98	0	0.99	0.01	0.95	0.22	7%
680	0.77	0.04	1	0.01	0.98	0.34	16%
780	*0.77*	*0.12*	*0.97*	*0.61*	*0.05*	*0.72*	*65%*
880	0.98	0.01	0.95	0	0.6	0.27	17%
980	0.86	0.05	0.72	0	0.93	0.4	19%
1080	*0.86*	*0.03*	*0.94*	*0.82*	*0.06*	*1.1*	*66%*
1180	0.88	0.04	0.95	0	0.99	0.36	22%
1280	0.75	0.04	0.85	0.17	0.92	0.43	23%
1380	0.99	0.05	0.95	0.05	0.95	0.07	8%
1480	0.89	0.06	0.99	0.05	0.94	2.29	7%
1580	0.81	0.03	0.87	0.11	0.99	0.94	17%
1680	0.68	0.02	0.95	0.28	0.99	0.92	24%
1780	*0.86*	*0.1*	*0.58*	*0.95*	*0.05*	*5.94*	*85%*
1880	0.79	0.04	0.82	0.27	0.66	0.64	34%
1980	0.64	0.11	0.91	0.05	0.99	0.58	22%
Weighted avg	**0.9**	**0.02**	**0.94**	**0.11**	**0.86**		**9%**

The weighted average of the result corresponds to the estimation of each parameter, associated with a weight inversely proportional to the residue at the end of the WLS run. In fact, erroneous runs typically are terminated with a high residue, and thus their contribution can be reduced without additional steps of data examination and processing. If the residues of the WLS result are above a certain

threshold, the convergence is assumed to have failed and the results discarded. This has been observed for 4 frequencies out of the 20 runs, marked in italics on Table 6.2. The results of the final weighted average show that the switch settings are estimated correctly, assuming that the final result will be rounded up/down. Simulations for various other settings have shown good results as well, and no additional result post processing or heuristics have been required in order to improve the WLS performance. It can be seen that for certain frequencies e.g. 1080 Hz, the WLS algorithm has converged to wrong values. This can be attributed to the highly non-linear nature of the system, since a parameter jump in the iterative procedure can lead the estimated value to an erroneous convergence. Nevertheless due the redundancy of the algorithm, this error can be tolerated, since the majority of the frequencies converge correctly and since the bad results typically end the WLS run with higher residues, making their contribution to the weighted average is less prevalent. The iteration limit was set to 15 and the tolerance to 1% of the value to be estimated. Typically, the WLS ran for the full 15 cycles, and increasing the iterations didn't improve the results considerably, mostly due to imperfect line parameter settings.

6.3.5.2 Impedance magnitude estimation

With the finalized switch and DG connection settings, the WLS procedure is executed with line impedances set to unknown parameters. The outcome of the WLS algorithm for both cases is shown in Table 6.3 and Table 6.4. Table 6.3 shows the inductance estimation for the powerline, and the results are generally accurate. The inaccuracies are minimal and are mostly to various effects, such as noise or interference. The criteria for acceptable runs are identical as for topology identification, runs with high residues are discarded, and the very low residue runs are given higher importance. The weighted average over the complete frequency range is very close to the actual value. Results with weaker stimulations have shown good results as well. In the settings of our simulation the peak of the stimulation is 5% of the fundamental at the DG. The results are less precise for resistance estimation. For higher frequencies the WLS doesn't operate quite well, given the relative importance of the inductive effect on those frequencies. Thus the algorithm was rerun only run for the 5-200 Hz range in 10 Hz intervals. The interferences are higher for these frequencies due to the fundamental and inverters noise frequencies around the fundamental show particularly bad results, due to

Table 6.3: Inductance estimation through WLS for 80-2000 Hz

	L1	**L2**	**L3**	**L4**	**L5**	**L6**		
			Real Parameter values to be found					
	2mH	**6mH**	**1mH**	**2mH**	**3mH**	**1mH**		
			Initial WLS parameter setting					
	0.5mH	**0.5mH**	**0.5mH**	**0.5mH**	**0.5mH**	**0.5mH**		
Freq				**WLS result**			**res.**	**err%**
80	0.0017	0.0056	0.0014	0.0017	0.0034	0.0021	1.2387	22%
180	0.0018	0.0058	0.0006	0.0018	0.0028	0.0019	0.8387	*10%*
280	0.0022	0.0062	0.0008	0.0015	0.0026	0.0011	0.2387	4%
380	0.0017	0.0055	0.001	0.0019	0.0034	0.0009	0.0813	4%
480	0.0014	0.0055	0.0007	0.0019	0.0033	0.001	0.2275	8%
580	0	0.0003	0	0	0.0018	0.0002	0.6502	89%
680	0.0018	0.006	0.0009	0.0019	0.0034	0.0012	0.1454	1%
780	0.0023	0.006	0.0007	0.0018	0.0029	0.0013	0.1233	*1%*
880	0.0021	0.0062	0.0004	0.0017	0.0031	0.0015	0.1565	1%
980	0.0023	0.006	0.001	0.002	0.0024	0.0009	0.1585	2%
1080	0.0018	0.0059	0.0009	0.0019	0.0031	0.0011	0.1078	*2%*
1180	0.0018	0.0059	0.0005	0.0016	0.0033	0.0014	0.2969	4%
1280	0.0018	0.0061	0.001	0.002	0.0033	0.001	0.0695	1%
1380	0.0015	0.0056	0.001	0.0019	0.0036	0.0012	0.2909	2%
1480	0.0015	0.0061	0.0008	0.0019	0.0044	0.0011	0.1647	5%
1580	0.0019	0.006	0.001	0.002	0.0031	0.001	0.0262	0%
1680	0.0015	0.006	0.0011	0.002	0.0043	0.0009	0.5047	5%
1780	0.0025	0.006	0.0011	0.0022	0.0025	0.0007	0.2573	*3%*
1880	0.0019	0.0061	0.001	0.002	0.003	0.001	0.0339	0%
1980	0.0018	0.0061	0.0014	0.0021	0.0033	0.0006	0.2197	10%
Wgt avg	**0.0018**	**0.0057**	**0.0008**	**0.0017**	**0.003**	**0.001**		**3%**

the strong effect of the 50 Hz signal on the signal processing algorithms. Nevertheless the weighed averaged provides results that are accurate within 24.4% of the correct value. The resistive component of the impedance is low compared to the other parameters of the system, and it is even proportionally lower at high frequencies. In ideal settings, this shouldn't have an impact on our methodology. But since the system is subjected to concurrent signal injections, additional white noise, prevalent inverter harmonics and fundamental, the identification signals are subjected to very strong interference. The resistive component of the lines being very small, its impact on the system behavior is limited. Thus, its influence is greatly masked by other signals in the system (fundamental, noise form other injections, white noise, inverter noise). The results can be improved by increasing stimulation strength on low frequencies, intelligent filtering of the signals before processing to remove fundamental and inverter noise, or advanced WLS heuristics to identify bad convergences. The outcome of the impedance estimation is

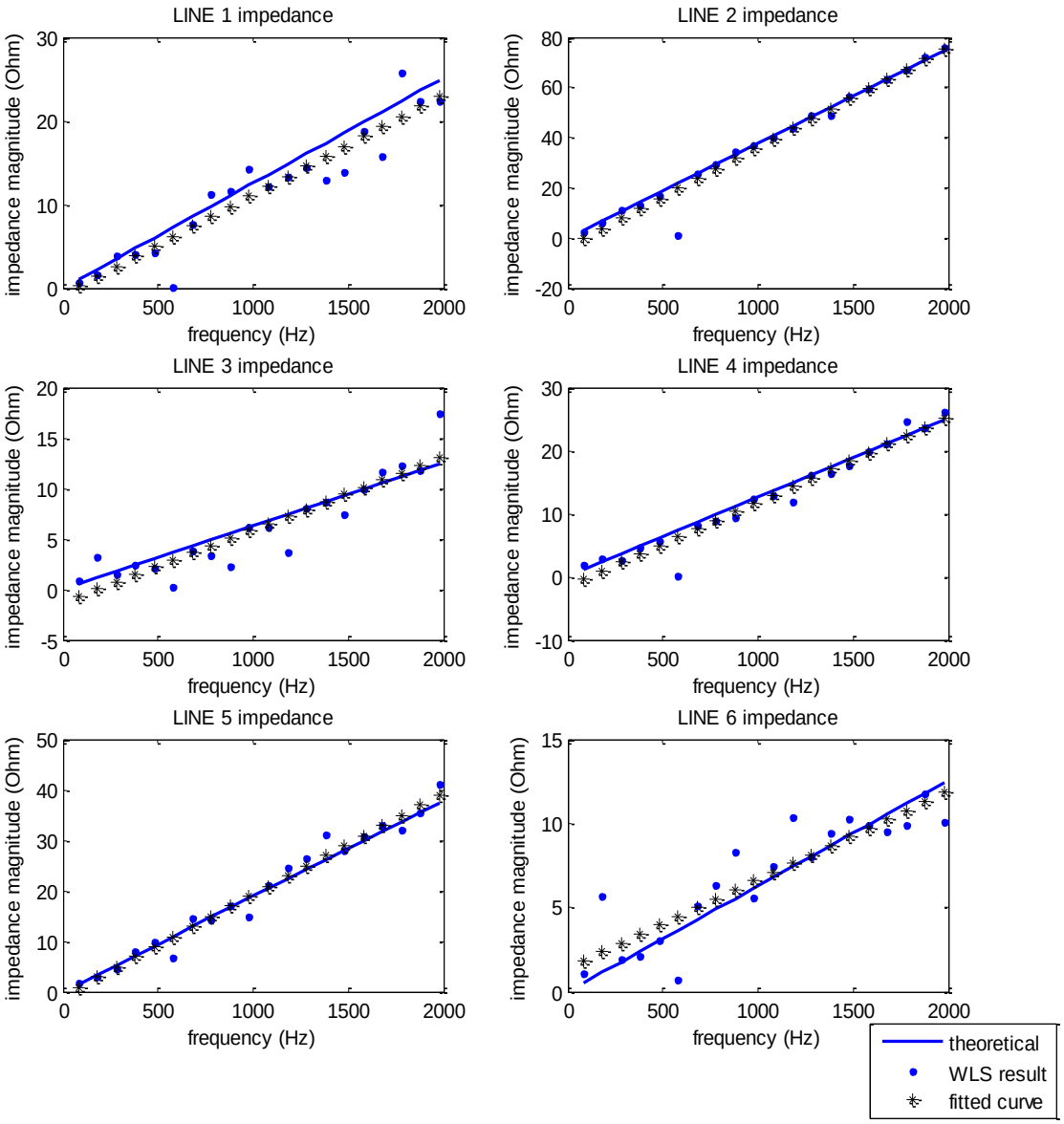

FIGURE 6.8: Line Impedance magnitudes obtained through parameter estimation

TABLE 6.4: Resistance estimation through WLS for 5-200 Hz

	R1	**R2**	**R3**	**R4**	**R5**	**R6**		
	Real Parameter values to be found							
	0.1Ω	**0.3Ω**	**0.2Ω**	**0.1Ω**	**0.3Ω**	**0.1Ω**		
	Initial WLS parameter setting							
	.01Ω	**0.01Ω**	**0.01Ω**	**0.01Ω**	**0.01Ω**	**0.01Ω**		
Frequency	**WLS result**						**residue**	**err %**
5	0.2434	0.6889	0.2456	0.1884	0.3796	0.0312	0.7112	52%
15	0.0003	0.5557	0.3197	0.3098	0.3204	0.0556	0.3892	*36%*
25	0.2047	0.3452	0.4141	0.0661	0.1089	0.0117	0.3946	4%
35	0.4077	0.4157	0.2482	0.0499	0.0151	0.1272	0.6147	13%
45	3.0928	5.1322	0	0	0.012	0.8609	0.9157	112%
55	1.61	3.4961	0	0.0385	0.0171	0.2625	0.8267	55%
65	0.2931	0.4048	0.4071	0.589	0.509	0.3587	0.6816	8%
75	0.1264	0.3687	0.1989	0.1135	0.385	0.1053	0.3439	*6%*
85	0.0571	0.6126	0.1247	0.0518	0.058	0.1968	0.252	24%
95	0.0877	0.3115	0.1204	0.1572	0.3407	0.0097	0.3006	16%
105	0.3129	0.6081	0.1218	0.1307	0.1671	0.0692	0.0892	*31%*
115	0.039	0.531	0.04	0.0905	0.1002	0.0908	0.1208	11%
125	0.1571	0.5481	0.1621	0.0969	0.1507	0.382	0.2921	104%
135	0.2084	0.5187	0.0054	0.11	0.0396	0.3595	0.3911	132%
145	0.1268	0.0359	0.2762	0.1894	1.3161	0.5118	1.0131	31%
155	0.0477	0.0052	0.3531	0.0708	1.5973	0.7439	1.0867	89%
165	0.0757	0.1451	0.0672	0.185	0.2613	0.3201	0.5551	41%
175	0.5545	0.2834	0	0.3286	0.0301	0.0508	0.9826	*52%*
185	0.427	1.2663	0.0405	0.1262	0.3372	0.0592	0.1522	36%
195	0.3202	0.4957	0.2833	0.1291	0.2667	0.1343	0.068	4%
Weighted avg	**0.1644**	**0.3621**	**0.2016**	**0.1461**	**0.3037**	**0.1598**		**24.4%**

summarized in Figure 6.8. In this Figure, the theoretical, estimated and averaged impedance magnitude is shown for each line and for each frequency. The continuous lines represent the theoretical value to be obtained, and the dots represent the results for the WLS algorithm for each frequency. The inaccuracies are minimal for most frequencies are mostly caused by noise and interference, while for some frequencies (e.g. 580 Hz) the convergence fails, and the result needs to be discarded. The weighed fitting line through the data, marked by the '*' dots in Figure 6.8 shows that the results aggregated over the complete frequency range exhibits results very close to theoretical values.

6.4 Conclusions and Contributions

In this Chapter, a novel method has been proposed to estimate topology and line parameters of the power network using online stimulations generated by grid-tie PWM based inverters. The method consists in injecting predefined coded stimulations from selected inverters on the grid, and measure the current response of these injections at several locations on the power network. The combination of these measurements can be exploited in order to compute the topology parameters and line parameters using WLS based algorithms. The proposed method can be applied to any parameters of the power system, as long as its effect on the stimulations current response can be materialized in equations related to the power systems admittance matrix.

A monitoring tool such as the one proposed in this paper can assist grid operators in supporting and accommodating modern and complex smart grid tools that are developed. For instance, the outcome of the research can help engineers to tune the parameters of the state estimator, and optimize line usage and improve reliability by providing a novel and complementary solution to traditional EMS tools.

Chapter 7

Summary, Contributions and Recommendations

The operation mode of European power systems is evolving, as highlighted by the steady increase of DG connected to distribution networks. The complexity of the power network is increasing, and in the long term, this might have an impact on grid infrastructure stability and reliability. The complications generated by this growth are highlighted in this thesis. While DGs do provide benefits in terms of voltage levels along the feeders, they have generated a new set of challenges regarding the protection mechanism, voltage stability and power quality in the distribution networks.

In future years, DG will most likely provide even a much higher share of the energy provided, and the challenge for the engineers will be to integrate them in a cost efficient manner without affecting the quality of the service. As it is expected for the cost of traditional energy fuels to increase, and the price of DG technologies to decrease, industries and private homeowners will be more and more likely to adopt these for electricity production. The formation of micro-grids or balanced sub-grids is a concept that has been of much interest as well. Thus while the grid of the future might look very different from the current one, the transition from the traditional paradigm needs to happen progressively and the problems incurred need to be solved in order to maintain successful operation.

In order to find solution to these new issues, the visibility in the distribution networks need to be increased. As of now, it is generally poorly monitored and controlled, since traditionally it only served as a power delivery network. This is

not the case anymore with the advent substantial DG connection. The powerflows in the distribution network are highly fluctuating and due to the presence of generators, faults in it have a larger impact than before. Thus, the system operators needs to have enhanced monitoring capabilities in order to have higher visibility and control of its status.

7.1 Thesis Contributions

The main contributions presented in this work with suggested future research will be provided in this Section.

7.1.1 Inverter Stimulation Injection

Impedance estimation has been considered an efficient and reliable islanding detection mechanism in power networks, and numerous scientific publications based on signal injection have been proposed. While these usually involve a dedicated signal injector attached to the DG, the developed method proposes to do islanding detection based on PRBS injection. This solution exhibits many advantages. The PRBS stimulate a broad range of frequencies, thus the impedance detection mechanism can be performed for several frequencies for enhanced reliability. The PRBS being a digital signal, it can be injected effortlessly, since the inverter's PWM is a pulse generating device. These pulses are jittered in order to overlap the PRBS on the fundamental. We designed an innovative and intelligent mechanism to superimpose the PRBS by allocating a duty cycle in the carrier to the Pulse Width Modulator. This method allows fine-tuning the PRBS strength, and avoids interference with the inverters control mechanisms given that is not impacting the reference signal used for frequency and voltage control.

7.1.2 Islanding Detection

Islanding protection is currently a major obstacle in DG integration, and this issue is therefore under much research. Nearly all utility standards require anti-islanding protection to be implemented in all DGs. Islanding detection is a main topic in power systems and a reliable and accurate detection is primordial in order

to enable significant DG penetration. The proposed method provides considerable advantages to existing methods in the state of the art. As a grid impedance based method, it is minimally prone to false detection or non-detection issues, since variations in powerflows have minimal impact on the measurements. Rather than providing methods based on standard impedance detection, we suggest to use a smart signal for islanding detection. Having a unique coded signal for each inverter allows us to know at other points in the system where this signal is coming form and use it as a pilot signal for system identification. This enables the monitoring of the distribution network through DG generated signals and permits the surveillance of broad distribution network, without having to implement and maintain a large number of measurement and ICT components. By proposing an impedance detection method based on a more elaborate signal, we enable the DG to participate implicitly in additional ancillary services.

A laboratory implementation of a PWM based inverter has been completed, and PWM based PRBS pattern have been injected in the prototype inverter built in the SnT RDES Laboratory. The LabVIEW based control has given some insight in the real life implementation of the system, and while it was not complete, the results obtained were convincing enough that future work in this area could be fruitful.

7.1.3 Line Parameter

The stimulation injected at the inverter can be measured at nearby locations on the power network, e.g. at the start of the feeder in the substation. A receiver located at the substation knowing the patterns in advance, can detect them and through correlation, estimate the transfer function of its propagation path. Through this reuse of the islanding stimulation signal, the electrical parameters of the line can be estimated. Since a wide frequency range is covered, the dynamics of the line up to 2 kHz can be established. This information can be gathered dynamically, while the line is in operation. In addition, the orthogonality of the PRBS patterns allows several measurements on several lines to be performed at once, since the interference of concurrent measurements is canceled effectively through correlation and SIC.

The data obtained through this procedure allows for instance to update the state estimation parameters dynamically, rather than using calculated and potentially

outdated values. This will improve efficiency of the network use. Through detected variations of the resistance, the temperature can be estimated, and the proposed tool can serve as a basis for dynamic thermal rating [144], where line capacity is adjusted based on its temperature. In addition the sag variations could be estimated based on this method.

The major advantage over other state of the art methods is that the line can remain operational during characterization, and no communication tools are required. In addition, assuming that the PRBS injection is necessary for islanding detection, this result is obtained without any infrastructure addition on the network.

7.1.4 System Parameter

Finally, to build on top of the solutions for islanding and line parameter estimation, a method is proposed where multiple injection from different inverters on a distribution grid are measured at various locations, and by combining all these measurements and processing them through a weighted least based squares method, an estimation of the power grid model is obtained including information on line impedances, switch settings and DG connection status.

Related methods in the state of the art are based on State Estimation. These methods are called generalized state estimation, since add an generalize SE to extract additional information. On the other hand, methods providing a broadband characterization and based on injections do not exist in the state of the art. Thus the research in this topic provides a very unique and original method for distribution network monitoring, by reusing inverter signals injected for other purposes.

7.2 Future Work

The proposed solution have proven to be innovative, useful and applicable in many cases. However improvements and additional work could expand it relevance and improve the concept.

7.2.1 Harmonic Analysis and Compensation

The grid tie inverter cause power quality degradation by feeding imperfect sines, due to the architecture of the PWM and inverter control. On the other hand, they can contribute to improving power quality by canceling harmonics through adjustments in the PWM control. In order to do so, the inverter needs to know which harmonics are prevalent and on which frequencies they tend to propagate most. The broad spectrum grid impedance measured at the inverter PCC for islanding detection would be the ideal tool for that purpose. Thus improving on the infrastructure proposed would be an inverter based harmonic compensator [145], that takes as an input the grid characterization proposed in Chapter 4.

7.2.2 Dynamic Thermal Rating

In Chapter 5, a powerline characterization methodology is showcased. That data can be used to infer real-time physical characteristics of the line, such as line temperature and line sag. In fact, in most distribution networks, it is the line temperature that limits the power that can be transmitted, and limits the capacity of the line. This value is normally estimated and a static-seasonal threshold is set for the capacity, which determines its thermal rating, and limits the maximum power to be transferred.

Having these ratings in real-time allows instantaneous control of power line, and adjust that limit dynamically, hence dynamic thermal rating [146]. Power utilities could use this feature in order to optimize powerflows, and obtain extra capacity out of existing infrastructure, rather than build additional lines. This would reduce infrastructure cost and delay creation of new transmission lines. Applying the developed methods for dynamic thermal rating would be a logical and interesting additional step to the proposed research.

7.2.3 State Estimation Analysis

The variation of system parameters in a distribution network are monitored in Chapter 6. Their impact on state estimation accuracy versus static parameters would be an relevant topic to investigate. For instance for a grid operator it would be information to know the variations of the system parameters, and the sensitivity

of state estimation to them. Thus, this subject would be a relevant and interesting topic to explore, building on the research in this paper.

7.2.4 System and Parameter Modeling

While complex line models exist, only simple line models have been used in the research. This is partly caused by the physical constraint of the distribution network, which is composed of short lines, partly to render calculations easy and manageable. For instance, the skin effect in the resistance has not been taken into account. In addition complex models for transformers and grid components would be relevant in the higher end of the analyzed spectrum.

7.2.5 Laboratory Implementation and Field Tests

An inverter has been built and PRBS sequences have been programmed to be injected by its PWM. In the laboratory setting, it powered an inductive load and the current signals were measured in order to deduce the load's impedance for up to 1 kHz. The laboratory tests didn't go as far as the research in simulations, and it would a valuable task to implement the proposed algorithm in grid inverters in a laboratory or in field tests with real power networks components.

7.2.6 Advanced Signal Injection through the Inverter

In the field of communication, more advanced signal injection techniques exist and also state of the art signal processing techniques could be applied in order to maximize the extracted information. While the SIC algorithm has been tested successfully, more options are availably to shape the spectrum of the stimulation, and to process the result and to exploit them. For instance processing through wavelets has been considered in the initial phase of this research. Also, techniques could be explored to improve the spectrum of the signal through small changes in the inverter hardware.

7.3 Final Remarks

The objective of the research presented in this thesis are the benefits of active identification in distribution grids. In order to describe the proposed methods, first the problems of large DG penetration in distribution grids are explained. Ancillary services from DG will be increasingly necessary. We have presented an innovative method for islanding detection and power system monitoring. The solution proposed is very simple and powerful and allows to have visibility on the distribution network without extensive component and sensor additions.

Bibliography

[1] Masoud Aliakbar Golkar. Distributed generation and competition in electric distribution market. In *EUROCON 2009, IEEE*, pages 558–563, May 2009. doi: 10.1109/EURCON.2009.5167687.

[2] Belmans R. Driesen J. Dhaeseleer W. Haeseldonckx D. Pepermans, G. Distributed generation: Definition, benefits, and issues. *Energy Policy*, 2006.

[3] A. Kumar, S. Chanana, V.N. Reddy, V. Goel, and A. Chaudhary. Distributed generation location based on fuel cost minimization in deregulated electricity markets. In *India Conference, 2008. INDICON 2008. Annual IEEE*, volume 1, pages 200–205, Dec 2008. doi: 10.1109/INDCON.2008.4768826.

[4] G. Celli, F. Pilo, G. Pisano, V. Allegranza, R. Cicoria, and A. Iaria. Meshed vs. radial mv distribution network in presence of large amount of dg. In *Power Systems Conference and Exposition, 2004. IEEE PES*, pages 709–714 vol.2, Oct 2004. doi: 10.1109/PSCE.2004.1397664.

[5] S. Twaha, Z. Al-Hamouz, and M.U. Mukhtiar. Optimal hybrid renewable-based distributed generation system with feed-in tariffs and ranking technique. In *Power Engineering and Optimization Conference (PEOCO), 2014 IEEE 8th International*, pages 115–120, March 2014. doi: 10.1109/PEOCO.2014.6814410.

[6] Julian D. Bayoumi D. Suter M. & Haederli C. Dondi, P. Network integration of distributed power generation. *Journal of Power Sources*, 2002.

[7] T. Hammons. International practices in distributed generation developments worldwide. In *Universities Power Engineering Conference*, 2007.

[8] S. Carley. Distributed generation: An empirical analysis of primary motivators. *Energy Policy*, 2009.

[9] H.E. Farag and E.F. El-Saadany. Voltage regulation in distribution feeders with high dg penetration: From traditional to smart. In *Power and Energy Society General Meeting, 2011 IEEE*, pages 1–8, July 2011. doi: 10.1109/PES.2011.6039262.

[10] J.G. Slootweg and W.L. Kling. Impacts of distributed generation on power system transient stability. In *Power Engineering Society Summer Meeting, 2002 IEEE*, volume 2, pages 862–867 vol.2, July 2002. doi: 10.1109/PESS.2002.1043465.

[11] N. Kyme and M.A. Redfern. Providing higher visibility of mv systems for smarter distribution networks. In *Developments in Power System Protection (DPSP 2014), 12th IET International Conference on*, pages 1–4, March 2014. doi: 10.1049/cp.2014.0067.

[12] P. Mahat, Zhe Chen, and B. Bak-Jensen. Review of islanding detection methods for distributed generation. In *Electric Utility Deregulation and Restructuring and Power Technologies, 2008. DRPT 2008. Third International Conference on*, pages 2743–2748, April 2008. doi: 10.1109/DRPT.2008.4523877.

[13] F. De Mango, M. Liserre, and A.D. Aquila. Overview of anti-islanding algorithms for pv systems. part ii: Activemethods. In *Power Electronics and Motion Control Conference, 2006. EPE-PEMC 2006. 12th International*, pages 1884–1889, Aug 2006. doi: 10.1109/EPEPEMC.2006.4778680.

[14] F. De Mango, M. Liserre, A.D. Aquila, and A. Pigazo. Overview of anti-islanding algorithms for pv systems. part i: Passive methods. In *Power Electronics and Motion Control Conference, 2006. EPE-PEMC 2006. 12th International*, pages 1878–1883, Aug 2006. doi: 10.1109/EPEPEMC.2006.4778679.

[15] J. Heckenbergerova and J. Hosek. Dynamic thermal rating of power transmission lines related to wind energy integration. In *Environment and Electrical Engineering (EEEIC), 2012 11th International Conference on*, pages 798–801, May 2012. doi: 10.1109/EEEIC.2012.6221484.

[16] Xu Jin. Photovoltaic grid-connected inverter harmonic compensation and grid-connected unified control. In *Power and Energy Engineering Conference, 2009. APPEEC 2009. Asia-Pacific*, pages 1–4, March 2009. doi: 10.1109/APPEEC.2009.4918598.

[17] O. Alsac, N. Vempati, B. Stott, and A. Monticelli. Generalized state estimation [power systems]. In *Power Industry Computer Applications., 1997. 20th International Conference on*, pages 90–96, May 1997. doi: 10.1109/PICA.1997.599382.

[18] P. Heskes. *Minimizing the Impact of Resonances in Low Voltage Grids by Power Electronics based distributed Generators*. PhD thesis, Technische Univerity Eindhoven, 2011.

[19] R.N. Mutagi. Pseudo noise sequences for engineers. *Electronics Communication Engineering Journal*, 8(2):79–87, Apr 1996. ISSN 0954-0695. doi: 10.1049/ecej:19960205.

[20] Glad T. Ljung L. Modeling of dynamic systems. *Prentice Hall*, 1994.

[21] Botao Miao, R. Zane, and D. Maksimovic. A modified cross-correlation method for system identification of power converters with digital control. In *Power Electronics Specialists Conference, 2004. PESC 04. 2004 IEEE 35th Annual*, volume 5, pages 3728–3733 Vol.5, June 2004. doi: 10.1109/PESC.2004.1355134.

[22] S. Neshvad, S. Chatzinotas, and J. Sachau. Online determination of grid impedance spectrum through pseudo-random excitation of a pulse width modulator. *International Conference on Renewable Energies and Power Quality*, 2014.

[23] S. Neshvad, S. Chatzinotas, and J. Sachau. Distribution grid monitoring through pilot injection and successive interference cancellation. *International Association for Energy Economics*, 2014.

[24] S. Neshvad, S. Chatzinotas, and J. Sachau. Wideband identification of power network parameters using pseudo-random binary sequences on power inverters. *IEEE Transactions on Smart Grid*, 6(5):2293–2301, Sept 2015. ISSN 1949-3053. doi: 10.1109/TSG.2015.2397552.

[25] U. Tewari, S. Neshvad, D. Goldbach, and J. Sachau. Verification and implementation of pseudo-random-binary-sequences for online determination of grid impedance spectrum. *International Conference on Renewable Energies and Power Quality*, 2015.

[26] S. Neshvad, Margossian H., and Sachau J. Topology and parameter estimation in power systems through inverter based broadband stimulations. *IET Generation, Transmission and Distribution*, 2016.

[27] S. Neshvad, Margossian H., and Sachau J. Estimation of power grid topology parameters through pilot signals. *International Conference on Renewable Energies and Power Quality*, 2016.

[28] G. T. Heydt. The next generation of power distribution systems. *IEEE Transactions on Smart Grid*, 1(3):225–235, Dec 2010. ISSN 1949-3053. doi: 10.1109/TSG.2010.2080328.

[29] IEEE. Ieee. *Power and Energy Standards*, 2016.

[30] IEC. Iec 61000-3-2,. *International Standard: Limits for harmonic current emissions*, 2005.

[31] Li Xuan, Song Qiang, Liu Wenhua, Rao Hong, Xu Shukai, and Li Xiaolin. Fault ride-through control and its impacts on wind generators in a vsc-hvdc system. In *Industrial Electronics (ISIE), 2013 IEEE International Symposium on*, pages 1–6, May 2013. doi: 10.1109/ISIE.2013.6563758.

[32] H. Hatta, M. Asari, and H. Kobayashi. Study of energy management for decreasing reverse power flow from photovoltaic power systems. In *Sustainable Alternative Energy (SAE), 2009 IEEE PES/IAS Conference on*, pages 1–5, Sept 2009. doi: 10.1109/SAE.2009.5534838.

[33] V. P. Mahadanaarachchi and R. Ramakuma. Impact of distributed generation on distance protection performance - a review. In *Power and Energy Society General Meeting - Conversion and Delivery of Electrical Energy in the 21st Century, 2008 IEEE*, pages 1–7, July 2008. doi: 10.1109/PES.2008.4596707.

[34] Wind in power: 2015 european statistics, 2016.

[35] Stephen Hendrickson Sandra Reategui. Economic development impact of 1,000 mw of wind energy in texas. *NREL Technical Report*, 2011.

[36] Keyuan Huang, Lang Dai, and Shoudao Huang. Wind prediction based on improved bp artificial neural network in wind farm. In *Electrical and Control Engineering (ICECE), 2010 International Conference on*, pages 2548–2551, June 2010. doi: 10.1109/iCECE.2010.630.

[37] H.S. Ullal, K. Zweibel, B.G. von Roedern, R. Noufi, and Peter Sheldon. Overview of the us doe/nrel polycrystalline thin-film photovoltaic technologies. In *Photovoltaic Energy Conversion, 1994., Conference Record of the Twenty Fourth. IEEE Photovoltaic Specialists Conference - 1994, 1994 IEEE First World Conference on*, volume 1, pages 266–270 vol.1, Dec 1994. doi: 10.1109/WCPEC.1994.519859.

[38] B. Bouneb, D.M. Grant, A. Cruden, and J.R. McDonald. Grid connected inverter suitable for economic residential fuel cell operation. In *Power Electronics and Applications, 2005 European Conference on*, pages 10 pp.–P.10, Sept 2005. doi: 10.1109/EPE.2005.219424.

[39] A. Rahimi, M. Zarghami, M. Vaziri, and S. Vadhva. A simple and effective approach for peak load shaving using battery storage systems. In *North American Power Symposium (NAPS), 2013*, pages 1–5, Sept 2013. doi: 10.1109/NAPS.2013.6666824.

[40] D. Kottick, M. Blau, and D. Edelstein. Battery energy storage for frequency regulation in an island power system. *Energy Conversion, IEEE Transactions on*, 8(3):455–459, Sep 1993. ISSN 0885-8969. doi: 10.1109/60.257059.

[41] M.P. Bahrman. Overview of hvdc transmission. In *Power Systems Conference and Exposition, 2006. PSCE '06. 2006 IEEE PES*, pages 18–23, Oct 2006. doi: 10.1109/PSCE.2006.296221.

[42] Manuel Reta-Hernandez. *Transmission Line Parameters*. Taylor and Francis Group, LLC, 2006.

[43] V. Cecchi, K. Miu, A. S. Leger, and C. Nwankpa. Study of the impacts of ambient temperature variations along a transmission line using temperature-dependent line models. In *Power and Energy Society General Meeting, 2011 IEEE*, pages 1–7, July 2011. doi: 10.1109/PES.2011.6039110.

[44] R. Adapa and D.A. Douglass. Dynamic thermal ratings: monitors and calculation methods. In *Power Engineering Society Inaugural Conference and Exposition in Africa, 2005 IEEE*, pages 163–167, July 2005. doi: 10.1109/PESAFR.2005.1611807.

[45] South Africa corriel@uj.ac.za JC Greeff Tshwane University of Technology greeffjc@tut.ac.za SV Joubert Tshwane University of Technology joubertsv@tut.ac.za CGJ Lock, University of Johannesburg. Modelling of telegraph equations in transmission lines. *Prentice Hall*, 2008.

[46] A.R.J. Araujo, R.C. Silva, and S. Kurokawa. Comparing lumped and distributed parameters models in transmission lines during transient conditions. In *T D Conference and Exposition, 2014 IEEE PES*, pages 1–5, April 2014. doi: 10.1109/TDC.2014.6863477.

[47] S. R. Bhide Paithankar Y. G. Fundamentals of power system protection. *PHI Learning*, 2010.

[48] Detlef Schulz Klaus Heuck, Klaus-Dieter Dettmann. *Elektriscke Energieversorgung*. Vieweg und Teubner, 2010.

[49] Wenjiao Yin and Yundong Ma. Research on three-phase pv grid-connected inverter based on lcl filter. In *Industrial Electronics and Applications (ICIEA), 2013 8th IEEE Conference on*, pages 1279–1283, June 2013. doi: 10.1109/ICIEA.2013.6566564.

[50] R. Stala, L. Stawiarski, and M. Szarek. Single phase grid-connected pv system with time-sharing modulation and pi-type regulators for dc-dc boost converter and full-bridge inverter. In *Power Electronics and Motion Control Conference (EPE/PEMC), 2010 14th International*, pages T12–68–T12–75, Sept 2010. doi: 10.1109/EPEPEMC.2010.5606849.

[51] J. H. R. Enslin and P. J. M. Heskes. Harmonic interaction between a large number of distributed power inverters and the distribution network. *IEEE Transactions on Power Electronics*, 19(6):1586–1593, Nov 2004. ISSN 0885-8993. doi: 10.1109/TPEL.2004.836615.

[52] C. Natesan, A. Devendiran, S. Chozhavendhan, D. Thaniga, and R. Revathi. Igbt and mosfet: A comparative study of power electronics inverter topology in distributed generation. In *Circuit, Power and Computing Technologies (ICCPCT), 2015 International Conference on*, pages 1–5, March 2015. doi: 10.1109/ICCPCT.2015.7159453.

[53] S. Moballegh, S. Madhusoodhanan, and S. Bhattacharya. Evaluation of high voltage 15 kv sic igbt and 10 kv sic mosfet for zvs and zcs high power dc

-dc converters. In *Power Electronics Conference (IPEC-Hiroshima 2014 - ECCE-ASIA), 2014 International*, pages 656–663, May 2014. doi: 10.1109/IPEC.2014.6869657.

[54] Jinming Xu, Shaojun Xie, and Jiarong Kan. Lcl-filter design for grid-connected inverter to suppress grid-induced low-order current harmonics. In *Energy Conversion Congress and Exposition (ECCE), 2015 IEEE*, pages 1178–1183, Sept 2015. doi: 10.1109/ECCE.2015.7309824.

[55] Ahmed Al-Durra S. M. Muyeen A. Reznik, M.Godoy Simoes. Lcl filter design and performance analysis for grid interconnected systems. *Colorado School of Mines*, 2012.

[56] S. V. Araujo, A. Engler, B. Sahan, and F. L. M. Antunes. Lcl filter design for grid-connected npc inverters in offshore wind turbines. In *Power Electronics, 2007. ICPE '07. 7th Internatonal Conference on*, pages 1133–1138, Oct 2007. doi: 10.1109/ICPE.2007.4692556.

[57] Hyosung Kim and Seung-Ki Sul. Analysis on output lc filters for pwm inverters. In *Power Electronics and Motion Control Conference, 2009. IPEMC '09. IEEE 6th International*, pages 384–389, May 2009. doi: 10.1109/IPEMC.2009.5157417.

[58] Petros Ramantanis-Badr Eddine Benkelfat Mohammed Feham Hadjira Badaoui, Yann Frignac. Prqs sequences characteristics analysis by auto-correlation function and statistical properties. *IJCSI International Journal of Computer Science Issues*, 2010.

[59] L. Hanzo, L. Yang, E. Kuan, and K. Yen. *CDMA Overview*, pages 35–80. Wiley-IEEE Press, 2004. ISBN 9780470863114. doi: 10.1002/0470863110.ch2. URL http://ieeexplore.ieee.org.proxy.bnl.lu/xpl/articleDetails.jsp?arnumber=5732958.

[60] Philip Koopman. Maximal length lfsr feedback terms. https://users.ece.cmu.edu/ koopman/lfsr/index.html.

[61] Botao Miao, R. Zane, and D. Maksimovic. System identification of power converters with digital control through cross-correlation methods. *Power Electronics, IEEE Transactions on*, 20(5):1093–1099, Sept 2005. ISSN 0885-8993. doi: 10.1109/TPEL.2005.854035.

[62] S. Milinkovic. Some applications of p-prbs signals in frequency domain measurements. In *Embedded Computing (MECO), 2013 2nd Mediterranean Conference on*, pages 204–207, June 2013. doi: 10.1109/MECO.2013.6601357.

[63] N. S. Abinaya and P. Prakasam. Performance analysis of maximum length lfsr and bbs method for cryptographic application. In *Electronics and Communication Systems (ICECS), 2014 International Conference on*, pages 1–5, Feb 2014. doi: 10.1109/ECS.2014.6892699.

[64] Abhijit Mitra. On pseudo-random and orthogonal binary spreading sequences. *International Journal of Communcation Engineering*, 2008.

[65] T.B. Norriss and P.S. Bodger. Ripple control signal interference due to a lightly loaded rural distribution line. *Generation, Transmission and Distribution, IEE Proceedings C*, 136(6):401–406, Nov 1989. ISSN 0143-7046. doi: 10.1049/ip-c.1989.0055.

[66] Using the binary maximum length sequence for the identification of system dynamics. *Electrical Engineers, Proceedings of the Institution of*, 114(10): 1582–1584, October 1967. ISSN 0020-3270. doi: 10.1049/piee.1967.0303.

[67] M. B. Mollah and M. R. Islam. Comparative analysis of gold codes with pn codes using correlation property in cdma technology. In *Computer Communication and Informatics (ICCCI), 2012 International Conference on*, pages 1–6, Jan 2012. doi: 10.1109/ICCCI.2012.6158894.

[68] Kimmo Kettunen. Code selection for cdma systems. *Licentiate Course on Signal Processing in Communications*, 1997.

[69] M. Cespedes and Jian Sun. Online grid impedance identification for adaptive control of grid-connected inverters. In *Energy Conversion Congress and Exposition (ECCE), 2012 IEEE*, pages 914–921, Sept 2012. doi: 10.1109/ECCE.2012.6342721.

[70] L. Asiminoaei, R. Teodorescu, F. Blaabjerg, and U. Borup. Implementation and test of an online embedded grid impedance estimation technique for pv inverters. *Industrial Electronics, IEEE Transactions on*, 52(4):1136–1144, Aug 2005. ISSN 0278-0046. doi: 10.1109/TIE.2005.851604.

[71] E.On Netz GmbH. German grid code. *Bayreuth Germany*, 2003.

[72] H. Jouybari-Moghaddam, S.H. Hosseinian, and B. Vahidi. Active distribution networks islanding issues: An introduction. In *Environment and Electrical Engineering (EEEIC), 2012 11th International Conference on*, pages 719–724, May 2012. doi: 10.1109/EEEIC.2012.6221471.

[73] Markus Jostock. *Stabilitat wechelrichtergefurhrter Inselnetze*. PhD thesis, University of Luxembourg, 2013.

[74] M. Liserre, R. Teodorescu, and F. Blaabjerg. Stability of photovoltaic and wind turbine grid-connected inverters for a large set of grid impedance values. *IEEE Transactions on Power Electronics*, 21(1):263–272, Jan 2006. ISSN 0885-8993. doi: 10.1109/TPEL.2005.861185.

[75] BC Hydro Systems Group. Distribution power generator islanding guidelines. *BC Hydro*, 2006.

[76] Komla Folly Priye Kenneth Ainah. Voltage rise issue with high penetration of grid connected pv. *19th world congress, International Federation of Automatic control, At Cape Town*, 2014.

[77] IEEE. Ieee guide for automatic reclosing of line circuit breakers for ac distribution and transmission lines,. *IEEE Std C37.104-2002*, 2002.

[78] F. De Mango, M. Liserre, and A. Dell'Aquila. Overview of anti-islanding algorithms for pv systems. part ii: Activemethods. In *Power Electronics and Motion Control Conference, 2006. EPE-PEMC 2006. 12th International*, pages 1884–1889, Aug 2006. doi: 10.1109/EPEPEMC.2006.4778680.

[79] F. De Mango, M. Liserre, A. Dell'Aquila, and A. Pigazo. Overview of anti-islanding algorithms for pv systems. part i: Passive methods. In *Power Electronics and Motion Control Conference, 2006. EPE-PEMC 2006. 12th International*, pages 1878–1883, Aug 2006. doi: 10.1109/EPEPEMC.2006.4778679.

[80] Qian Cao, Furong Liu, Guorong Zhu, and Wei Chen. Pmu based islanding detection method for large photovoltaic power station. In *Power Electronics and Drive Systems (PEDS), 2015 IEEE 11th International Conference on*, pages 126–131, June 2015. doi: 10.1109/PEDS.2015.7203417.

[81] Sachau J. Margossian H., Deconninck G. Distribution network protection considering grid code requirements for distributed generation. *Generation, Transmission & Distribution, IET*, 2015.

[82] H. Samet, F. Hashemi, and T. Ghanbari. Islanding detection method for inverter-based distributed generation with negligible non-detection zone using energy of rate of change of voltage phase angle. *Generation, Transmission Distribution, IET*, 9(15):2337–2350, 2015. ISSN 1751-8687. doi: 10.1049/iet-gtd.2015.0638.

[83] Jun Yin, Liuchen Chang, and C. Diduch. A new total frequency deviation algorithm for anti-islanding protection in inverter-based dg systems. In *Electrical and Computer Engineering, 2005. Canadian Conference on*, pages 570–573, May 2005. doi: 10.1109/CCECE.2005.1556995.

[84] B. Guha, R.J. Haddad, and Y. Kalaani. A passive islanding detection approach for inverter-based distributed generation using rate of change of frequency analysis. In *SoutheastCon 2015*, pages 1–6, April 2015. doi: 10.1109/SECON.2015.7133024.

[85] P. Zanchetta-M. Marinelli V. Diana, M. Sumner. Non-invasive power system impedance monitoring for improved power quality. *Institution of Electrical Engineers*, 2004.

[86] Soo-Hyoung Lee and Jung-Wook Park. New islanding detection method for inverter-based distributed generation considering its switching frequency. In *Industry Applications Society Annual Meeting, 2009. IAS 2009. IEEE*, pages 1–8, Oct 2009. doi: 10.1109/IAS.2009.5324872.

[87] Sung-Il Jang and Kwang-Ho Kim. An islanding detection method for distributed generations using voltage unbalance and total harmonic distortion of current. *Power Delivery, IEEE Transactions on*, 19(2):745–752, April 2004. ISSN 0885-8977. doi: 10.1109/TPWRD.2003.822964.

[88] Meiyi Hou, Houlei Gao, Yijun Lu, Yongwu Zhang, Huaming Cao, and Yong Lin. A composite method for islanding detection based on vector shift and frequency variation. In *Power and Energy Engineering Conference (APPEEC), 2010 Asia-Pacific*, pages 1–4, March 2010. doi: 10.1109/APPEEC.2010.5448252.

[89] d A. Rohatgi M. E. Ropp, M. Begovic. Prevention of islanding in grid-connected photovoltaic systems. *Progress in Photovoltaics: Research and Applications*, 1999.

[90] T. Funabashi, K. Koyanagi, and R. Yokoyama. A review of islanding detection methods for distributed resources. In *Power Tech Conference Proceedings, 2003 IEEE Bologna*, volume 2, pages 6 pp. Vol.2–, June 2003. doi: 10.1109/PTC.2003.1304617.

[91] A. Moallem, D. Yazdani, A. Bakhshai, and P. Jain. Frequency domain identification of the utility grid parameters for distributed power generation systems. In *Applied Power Electronics Conference and Exposition (APEC), 2011 Twenty-Sixth Annual IEEE*, pages 965–969, March 2011. doi: 10.1109/APEC.2011.5744711.

[92] Jian Sun. Impedance-based stability criterion for grid-connected inverters. *Power Electronics, IEEE Transactions on*, 26(11):3075–3078, Nov 2011. ISSN 0885-8993. doi: 10.1109/TPEL.2011.2136439.

[93] L. Asiminoaei, R. Teodorescu, F. Blaabjerg, and U. Borup. A digital controlled pv-inverter with grid impedance estimation for ens detection. *Power Electronics, IEEE Transactions on*, 20(6):1480–1490, Nov 2005. ISSN 0885-8993. doi: 10.1109/TPEL.2005.857506.

[94] M. Jordan, H. Langkowski, Trung Do Thanh, and D. Schulz. Frequency dependent grid-impedance determination with pulse-width-modulation-signals. In *Compatibility and Power Electronics (CPE), 2011 7th International Conference-Workshop*, pages 131–136, June 2011. doi: 10.1109/CPE.2011.5942220.

[95] M. Sumner, B. Palethorpe, D. W. P. Thomas, P. Zanchetta, and M. C. Di Piazza. A technique for power supply harmonic impedance estimation using a controlled voltage disturbance. *IEEE Transactions on Power Electronics*, 17(2):207–215, Mar 2002. ISSN 0885-8993. doi: 10.1109/63.988831.

[96] DELTA ELEKTONIKA. Dc power supplies. *http://www.delta-elektronika.nl/en/products/sm3300-series.html*, 2014.

[97] National Instruments. Ni single-board rio general purpose inverter controller (gpic). *http://www.ni.com/singleboard/gpic/*, 2014.

[98] En 50160 , merkmale der spannung in offentlichen elektrizitatsversorgungsnetzen.

[99] C. Yang, K. Liu, D. Wang, and Y. Su. Harmonic pollution and management measures. In *Sustainable Power Generation and Supply, 2009. SUPERGEN '09. International Conference on*, pages 1–4, April 2009. doi: 10.1109/SUPERGEN.2009.5347906.

[100] M. Kato, T. Hisakado, H. Takani, H. Umezaki, and K. Sekiguchi. Live line measurement of untransposed three phase transmission line parameters for relay settings. In *Power and Energy Society General Meeting, 2010 IEEE*, pages 1–8, July 2010. doi: 10.1109/PES.2010.5589579.

[101] A. Apostolov U. Klapper, D. Welton. Why we should measure impedance. *Omnicron electronics Technical Paper*, 2010.

[102] M. Bockarjova and G. Andersson. Transmission line conductor temperature impact on state estimation accuracy. In *Power Tech, 2007 IEEE Lausanne*, pages 701–706, July 2007. doi: 10.1109/PCT.2007.4538401.

[103] A. Garavaglia F. Zanellini R. Vailati P. Marannino, P. Breseti. Assessing the transmission transfer capability sensitivity to power system parameters. *4th PSCC Sevilla*, 2002.

[104] M. Qemali, R. Bualoti, A. Cukaj, and B. Cfarku. Increasing transfer capability of the transmission system using the meteorological data. In *Power Generation, Transmission, Distribution and Energy Conversion (MEDPOWER 2012), 8th Mediterranean Conference on*, pages 1–4, Oct 2012. doi: 10.1049/cp.2012.2047.

[105] B. Williams. *Electricity Networks and Generation Market Power*. PhD thesis, PhD Katholieke Universiteit Leuven, 2004.

[106] L. Ochoa S. Alnaser. Towards distribution energy management systems : Maximizing renewable dg. *CIRED*, 2013.

[107] S. Bahadoorsingh, L. Bhairosingh, M. Ganness, and C. Sharma. Improving overhead transmission line usage efficiency on a caribbean island power system. In *T D Conference and Exposition, 2014 IEEE PES*, pages 1–5, April 2014. doi: 10.1109/TDC.2014.6863215.

[108] F.S. Moreira, T. Ohishi, and J.I. Da Silva Filho. Influence of the thermal limits of transmission lines in the economic dispatch. In *Power Engineering Society General Meeting, 2006. IEEE*, pages 6 pp.–, 2006. doi: 10.1109/PES.2006.1709590.

[109] E. Ludwig, M. L. Crow, K. Erickson, and K. Shah. A feasibility study of on-line excitation system parameter estimation [of power networks]. In *Power Industry Computer Applications., 1997. 20th International Conference on*, pages 324–330, May 1997. doi: 10.1109/PICA.1997.599421.

[110] H.W. Dommel. Overhead line parameters from handbook formulas and computer programs. *Power Apparatus and Systems, IEEE Transactions on*, PAS-104(2):366–372, Feb 1985. ISSN 0018-9510. doi: 10.1109/TPAS.1985.319051.

[111] S. M. Chan. Computing overhead line parameters. *Computer Appl. Power, vol 6, num 1*, 1993.

[112] J.P. Rhode, A.W. Kelley, and M.E. Baran. Complete characterization of utilization-voltage power system impedance using wideband measurement. In *Industrial and Commercial Power Systems Technical Conference, 1996. Conference Record, Papers Presented at the 1996 Annual Meeting., IEEE 1996*, pages 123–130, May 1996. doi: 10.1109/ICPS.1996.533946.

[113] G. A. Asti, R. C. da Silva, S. Kurokawa, and E. C. M. da Costa. Identification of transmission line parameters from temporal measurements of currents and voltages in their terminals: Influence oh the length line. In *Power and Energy Society General Meeting, 2012 IEEE*, pages 1–7, July 2012. doi: 10.1109/PESGM.2012.6345270.

[114] W.-H.E. Liu, F.F. Wu, and Shau-Ming Lun. Estimation of parameter errors from measurement residuals in state estimation [power systems]. *Power Systems, IEEE Transactions on*, 7(1):81–89, Feb 1992. ISSN 0885-8950. doi: 10.1109/59.141690.

[115] Yan Du and Yuan Liao. Online estimation of power transmission line parameters, temperature and sag. In *North American Power Symposium (NAPS), 2011*, pages 1–6, Aug 2011. doi: 10.1109/NAPS.2011.6024854.

[116] V. Kekatos and G. B. Giannakis. Joint power system state estimation and breaker status identification. In *North American Power Symposium (NAPS), 2012*, pages 1–6, Sept 2012. doi: 10.1109/NAPS.2012.6336364.

[117] Tianshu Bil, Jinmeng Chen, Jingtao Wu, and Qixun Yang. Synchronized phasor based on-line parameter identification of overhead transmission line. In *Electric Utility Deregulation and Restructuring and Power Technologies, 2008. DRPT 2008. Third International Conference on*, pages 1657–1662, April 2008. doi: 10.1109/DRPT.2008.4523671.

[118] H. J. Vermeulen, J. M. Strauss, and V. Shikoana. Online estimation of synchronous generator parameters using prbs perturbations. *IEEE Transactions on Power Systems*, 17(3):694–700, Aug 2002. ISSN 0885-8950. doi: 10.1109/TPWRS.2002.800915.

[119] L.A. de S.Ribeiro, C.B. Jacobina, and A.M.N. Lima. Parameter estimation of induction machines under sinusoidal pwm excitation. *Energy Conversion, IEEE Transactions on*, 14(4):1218–1223, Dec 1999. ISSN 0885-8969. doi: 10.1109/60.815049.

[120] L.A. De Souza Ribeiro, C.B. Jacobina, A.M.N. Lima, and A.C. Oliveira. Real-time estimation of the electric parameters of an induction machine using sinusoidal pwm voltage waveforms. *Industry Applications, IEEE Transactions on*, 36(3):743–754, May 2000. ISSN 0093-9994. doi: 10.1109/28.845049.

[121] Jul-Ki Seok, Seung-Ill Moon, and Seung-Ki Sul. Induction machine parameter identification using pwm inverter at standstill. *Energy Conversion, IEEE Transactions on*, 12(2):127–132, Jun 1997. ISSN 0885-8969. doi: 10.1109/60.629694.

[122] ABB. Mv/lv transformer substations: theory and examples of short-circuit calculation. *Technical Application Papers*, 2008.

[123] T. Blackburn M. Bagheri, M. S. Naderi and T. Phung. Frequency response analysis and short-circuit impedance measurement in detection of winding. *ICHVE,*, 2008.

[124] D. Martin, I. Nam, J. Siegers, and E. Santi. Wide bandwidth three-phase impedance identification using existing power electronics inverter. In *Applied Power Electronics Conference and Exposition (APEC), 2013 Twenty-Eighth Annual IEEE*, pages 334–341, March 2013. doi: 10.1109/APEC.2013.6520230.

[125] Long Qu, Jiaming He, and C. Assi. Understanding the benefits of successive interference cancellation in multi-rate multi-hop wireless networks. *Communications, IEEE Transactions on*, 62(7):2465–2477, July 2014. ISSN 0090-6778. doi: 10.1109/TCOMM.2014.2315612.

[126] P. Patel and J. Holtzman. Analysis of a simple successive interference cancellation scheme in a ds/cdma system. *Selected Areas in Communications, IEEE Journal on*, 12(5):796–807, Jun 1994. ISSN 0733-8716. doi: 10.1109/49.298053.

[127] Pramod Viswanath David Tse. Fundamentals of wireless communication. *Cambridge University Press*, 2005.

[128] A. Monticelli. Electric power system state estimation. *Proceedings of the IEEE*, 88(2):262–282, Feb 2000. ISSN 0018-9219. doi: 10.1109/5.824004.

[129] Sachau J. Bilibin I., Capitanescu F. Overloads management in active radial distribution systems: An optimization approach including network switching. *PowerTech, IEEE, Grenoble*, 2013.

[130] H. Margossian, F. Capitanescu, and J. Sachau. Distributed generator status estimation for adaptive feeder protection in active distribution grids. In *Electricity Distribution (CIRED 2013), 22nd International Conference and Exhibition on*, pages 1–4, June 2013. doi: 10.1049/cp.2013.0874.

[131] P. Zarco and A. G. Exposito. Power system parameter estimation: a survey. *IEEE Transactions on Power Systems*, 15(1):216–222, Feb 2000. ISSN 0885-8950. doi: 10.1109/59.852124.

[132] J. C. Pereira, J. T. Saraiva, V. Miranda, A. S. Costa, E. M. Lourengo, and K. A. Clements. Comparison of approaches to identify topology errors in the scope of state estimation studies. In *Power Tech Proceedings, 2001 IEEE Porto*, volume 3, pages 6 pp. vol.3–, 2001. doi: 10.1109/PTC.2001.964921.

[133] T. Van Cutsem and V.H. Quintana. Network parameter estimation using online data with application to transformer tap position estimation. *Generation, Transmission and Distribution, IEE Proceedings C*, 135(1):31–40, Jan 1988. ISSN 0143-7046. doi: 10.1049/ip-c.1988.0004.

[134] E. Handschin and E. Kliokys. Transformer tap position estimation and bad data detection using dynamic signal modelling. *Power Systems, IEEE Transactions on*, 10(2):810–817, May 1995. ISSN 0885-8950. doi: 10.1109/59.387921.

[135] J.C.S. Souza, A.M. Leite da Silva, and A.P. Alves da Silva. Data visualisation and identification of anomalies in power system state estimation using artificial neural networks. *Generation, Transmission and Distribution, IEE Proceedings-*, 144(5):445–455, Sep 1997. ISSN 1350-2360. doi: 10.1049/ip-gtd:19971168.

[136] G. N. Korres and N. M. Manousakis. A state estimation algorithm for monitoring topology changes in distribution systems. In *Power and Energy Society General Meeting, 2012 IEEE*, pages 1–8, July 2012. doi: 10.1109/PESGM.2012.6345126.

[137] A. S. Debs. Parameter estimation for power systems in the steady-state. In *Decision and Control including the 13th Symposium on Adaptive Processes, 1974 IEEE Conference on*, pages 587–592, Nov 1974. doi: 10.1109/CDC.1974.270505.

[138] J.B.A. London, N.G. Bretas, and L.F.C. Alberto. Analysis of measurement set qualitative characteristics for state estimation purposes. In *Power Engineering Society General Meeting, 2005. IEEE*, pages 294–301 Vol. 1, June 2005. doi: 10.1109/PES.2005.1489206.

[139] Mokhtari S. Slutsker I. Comprehensive estimation in power systems: State, topology and parameter estimation. *Proceedings of American Power Conerence., Chicago, IL*, 1995.

[140] R. Singh, E. Manitsas, B.C. Pal, and G. Strbac. A recursive bayesian approach for identification of network configuration changes in distribution system state estimation. In *Power and Energy Society General Meeting, 2011 IEEE*, pages 1–1, July 2011. doi: 10.1109/PES.2011.6039000.

[141] P.N. Papadopoulos, T.A. Papadopoulos, P. Crolla, A.J. Roscoe, G.K. Papagiannis, and G.M. Burt. Measurement-based analysis of the dynamic performance of microgrids using system identification techniques. *Generation, Transmission Distribution, IET*, 9(1):90–103, 2015. ISSN 1751-8687. doi: 10.1049/iet-gtd.2014.0555.

[142] F. Garcia-Lagos, G. Joya, F.J. Marin, and F. Sandoval. Modular power system topology assessment using gaussian potential functions. *Generation, Transmission and Distribution, IEE Proceedings-*, 150(5):635–640, Sept 2003. ISSN 1350-2360. doi: 10.1049/ip-gtd:20030738.

[143] A. Abur and A. G. Exposito. Power system state estimation theory and implementation. *1st edn., New York:CRC Press*, 2004.

[144] D. A. Douglass and A. A. Edris. Real-time monitoring and dynamic thermal rating of power transmission circuits. *IEEE Transactions on Power Delivery*, 11(3):1407–1418, Jul 1996. ISSN 0885-8977. doi: 10.1109/61.517499.

[145] N. Hoffmann, F. W. Fuchs, and L. Asiminoaei. Online grid-adaptive control and active-filter functionality of pwm-converters to mitigate voltage-unbalances and voltage-harmonics - a control concept based on grid-impedance measurement. In *Energy Conversion Congress and Exposition (ECCE), 2011 IEEE*, pages 3067–3074, Sept 2011. doi: 10.1109/ECCE.2011.6064182.

[146] H. T. Yip, C. An, G. J. Lloyd, P. Taylor, A. Michiorri, S. Jupe, and M. Bartlett. Dynamic thermal rating and active control for improved distribution network utilisation. In *Developments in Power System Protection (DPSP 2010). Managing the Change, 10th IET International Conference on*, pages 1–5, March 2010. doi: 10.1049/cp.2010.0213.